National Library of Canada
Acquisitions and Bibliographic Services Branch
395 Wellington Street
Ottawa, Ontario
K1A 0N4

Bibliothèque nationale du Canada
Direction des acquisitions et des services bibliographiques
395, rue Wellington
Ottawa (Ontario)
K1A 0N4

Your file Votre référence

Our file Notre référence

NOTICE

The quality of this microform is heavily dependent upon the quality of the original thesis submitted for microfilming. Every effort has been made to ensure the highest quality of reproduction possible.

If pages are missing, contact the university which granted the degree.

Some pages may have indistinct print especially if the original pages were typed with a poor typewriter ribbon or if the university sent us an inferior photocopy.

Reproduction in full or in part of this microform is governed by the Canadian Copyright Act, R.S.C. 1970, c. C-30, and subsequent amendments.

AVIS

La qualité de cette microforme dépend grandement de la qualité de la thèse soumise au microfilmage. Nous avons tout fait pour assurer une qualité supérieure de reproduction.

S'il manque des pages, veuillez communiquer avec l'université qui a conféré le grade.

La qualité d'impression de certaines pages peut laisser à désirer, surtout si les pages originales ont été dactylographiées à l'aide d'un ruban usé ou si l'université nous a fait parvenir une photocopie de qualité inférieure.

La reproduction, même partielle, de cette microforme est soumise à la Loi canadienne sur le droit d'auteur, SRC 1970, c. C-30, et ses amendements subséquents.

Canada

UNIVERSITY OF ALBERTA

GLASS FIBRE AND NYLON 6: AN ADVANCED COMPOSITE MATERIAL

BY

APINYA DUANGCHAN

A thesis submitted to the Faculty of Graduate Studies and Research
in partial fulfillment of the requirements for the degree of **MASTER OF SCIENCE.**

DEPARTMENT OF CHEMICAL ENGINEERING

EDMONTON, ALBERTA

SPRING 1994

National Library
of Canada

Acquisitions and
Bibliographic Services Branch

395 Wellington Street
Ottawa, Ontario
K1A 0N4

Bibliothèque nationale
du Canada

Direction des acquisitions et
des services bibliographiques

395, rue Wellington
Ottawa (Ontario)
K1A 0N4

Your file Votre référence

Our file Notre référence

The author has granted an irrevocable non-exclusive licence allowing the National Library of Canada to reproduce, loan, distribute or sell copies of his/her thesis by any means and in any form or format, making this thesis available to interested persons.

L'auteur a accordé une licence irrévocable et non exclusive permettant à la Bibliothèque nationale du Canada de reproduire, prêter, distribuer ou vendre des copies de sa thèse de quelque manière et sous quelque forme que ce soit pour mettre des exemplaires de cette thèse à la disposition des personnes intéressées.

The author retains ownership of the copyright in his/her thesis. Neither the thesis nor substantial extracts from it may be printed or otherwise reproduced without his/her permission.

L'auteur conserve la propriété du droit d'auteur qui protège sa thèse. Ni la thèse ni des extraits substantiels de celle-ci ne doivent être imprimés ou autrement reproduits sans son autorisation.

ISBN 0-612-11192-X

Canada

UNIVERSITY OF ALBERTA

RELEASE FORM

NAME OF AUTHOR: Apinya Duangchan

TITLE OF THESIS: Glass Fibre and Nylon 6: An Advanced Composite Material

DEGREE: Master of Science

YEAR THIS DEGREE GRANTED: Spring 1994

Permission is hereby granted to the University of Alberta Library to reproduce single copies of this thesis and to lend or sell such copies for private, scholarly or scientific research purposes only.

The author reserves all other publication and other rights in association with the copyright in the thesis, and except as hereinbefore provided neither the thesis nor any substantial portion thereof may be printed or otherwise reproduced in any material form whatever without the author's prior written permission.

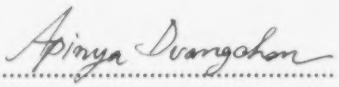

(Apinya Duangchan)
49/63 Soi Charoenkarn,
Sukhapiban 2 Rd., Bangkapi,
Bangkok, Thailand. 10240

January 31 , 1994

UNIVERSITY OF ALBERTA

FACULTY OF GRADUATE STUDIES AND RESEARCH

The undersigned certify that they have read, and recommend to the Faculty of Graduate Studies and Research for acceptance, a thesis entitled **GLASS FIBRE AND NYLON 6: AN ADVANCED COMPOSITE MATERIAL** submitted by **APINYA DUANGCHAN** in partial fulfillment of the requirements for the degree of **MASTER OF SCIENCE**.

M.C. Williams

Dr. M.C. Williams (Supervisor)

S.E. Wanke

Dr. S.E. Wanke

Reg Eadie

Dr. R.L. Eadie

January , 1994

ABSTRACT

Glass fibre/nylon 6 composites were made by *in-situ* anionic polymerization. Eight plies of heat-cleaned continuous-strand E-glass fibre mat were compressed in a mold 4 mm thick and flooded with a liquid mixture of ε-caprolactam, sodium hydride (NaH), and phenyl isocyanate (monomer, initiator, and activator, respectively) at 90-100°C. Raising the temperature to 150°C induced the polymerization, producing composite nylon 6 disks about 22 cm in diameter. Fibre/matrix surface bonding was varied, by applying to the glass fibres one of four different kinds of silane: 1,1,1,3,3,3,-hexamethyldisilazane, tert-butyldimethylsilyl chloride, chlorotrimethylsilane, and 3-aminopropyltriethoxysilane, designated as Silane I, Silane II, Silane III, and Silane IV, respectively. Composites with untreated and treated glass fibre then were characterized in terms of tensile properties (breaking stress σ_b and strain ε_b, modulus E, toughness), impact strength (E_s), and structural properties (density; volume fractions of fibre V_f and voids V_v).

Density and V_f were in the range from 1510 to 1600 kg/m^3, and 31.1 to 34.4% (except Silane IV, V_f = 25.4%), respectively. Voidage was reduced by silane treatment (0.7-4.9%, versus 3.6-8.9% for untreated glass). The tensile performance ranked as follows: Silane I gave properties even worse than Untreated; Silane II and III had almost the same performance--e.g., σ_b about 16% higher than Untreated; and Silane IV was the best. Silane IV improved σ_b by 136%, ε_b by 86%, E by 22%, and toughness by 271% over the Untreated.

Tensile properties varied inversely to impact properties--composites with high σ_b had low E_s and vice versa. All composites tremendously improved E_s over that of pure nylon 6 [e.g., $E_s(U)/E_s(N6)$ = 8, V_f = 32%]. Direct treatment of fibre surface with silane was found more effective in tensile properties (but of course, less in impact) than by adding silane directly into molten monomer solution. The harmful effect of moisture was demonstrated by testing deliberately water-soaked specimens and also by observing

ACKNOWLEDGEMENT

I would like to take this opportunity to express my gratitude and appreciation to Professor M.C. Williams for his great support, his valuable time, his encouragement, and academic guidance throughout my study. Observing his ways of doing research, his attitude and his academic devotion, encouraged me to work harder than ever and more cheerfully during enormously troubling times. His qualities were impressive and were imitated quietly. I also would like to extend my gratitude and appreciation to Dr. Naihong Li who gave me much valuable guidance and continual support.

I owe special thanks to my colleagues, in the Polymer and Rheology Group, who helped me to become familiar with these experiment: Yuqing Wu who kindly showed and helped me with the specimen testing, Dr. Joshua Otaigbe who demonstrated the composite preparation, Dr. Leigh Wardhaugh who served as a technical consultant whenever problems occurred in our laboratory, Nilesh N. Oak for DSC demonstration, Xiuguang Guo for DSC analysis and the assessment of some equipment, and to all in the group who are all nice and very good to me.

My sincere thanks to the Department of Mining, Metallurgical, and Petroleum Engineering for access to the Instron Machine and the furnace.

My earnest appreciation is to Dr. J.W. Foster, Head of Plastics Engineering and Mr. Ken Valen at NAIT for the access to the Lloyds L6000R Universal Testing Machine for tensile tests, and to the Tinius Olsen Izod Testing Machine for impact tests, respectively. Without their help this work could not have been successfully completed.

Special thanks to Walter Boddez and Richard Copper for the electrical instrument assistance and for being electronics consultants; and to Keith Faulder, Bob Scott, and Ron Van Den Heuvel for the specimens preparation and mold fixation.

My sincere thanks, for their love and encouragement, to my parents and relatives, Mr. Pipat Pichestapong, Ms. Fuenglarb Khambaratana, Ms. Orapin Stiramon, Ms. Panida

Asavapichayont, Mr. Suvit Pichayasathit, Mr. Edmond Gomes, and my colleagues at Kasetsart University in Bangkok, Thailand.

I acknowledge with gratitude my thesis committee members: Prof. S.E. Wanke and Prof. R.L. Eadie for their criticism and advice, and Prof. S.L. Shah for conducting my oral defense.

I would like to express my appreciation to the staff of the Department of Chemical Engineering, who are nice and very helpful, and to all my friends at U of A and in Edmonton who shared my difficulties and gave me big support, which is very meaningful to me.

I owe much gratitude to the Thailand-Canada Rattanakosin Scholarship Program for their financial support throughout my M.Sc. in Canada, and to the Department of Chemical Engineering, U of Alberta, which allowed me to continue my study here with a warm welcome.

property sensitivity to relative humidity (RH). Composites tested at high RH had inferior σ_b to those at lower RH, and in the wet composites (3% water gained) σ_b dropped enormously (84%).

TABLE OF CONTENTS

Page

Chapter 1 1

Introduction 1

Chapter 2 6

Materials Used in Composites 6

2.1. Glass Fibres 6

2.2. Nylon 6 8

Chapter 3 15

Interfaces 15

3.1. Wettability 15

3.2. Coupling Agents 17

Chapter 4 22

Morphology of Polymers 22

Chapter 5 27

Variables Affecting the Properties of Composites 27

5.1. Effects of Pressure and Thermal Processing Conditions 27

5.2. Effects of Fibre Diameter and Volume Fraction 30

5.3. Effects of Moisture on Properties of Thermoplastic Composites 31

5.4. Effects of Fibre Surface Treatment 33

5.4.1. Coupling Agent 33

5.4.2. Plasma Treatment 36

5.4.3. Other Chemical Treatment 37

5.4.4. Influence of Fibre/Matrix Interfacial Adhesion on Composite Fracture Behavior 38

5.5. Effect of Void Content 38

Chapter 6 40

Fabrication of Glassfibre/Nylon 6 Composites 40

6.1. Equipment 40

6.1.1. Mold 40

6.1.2. Temperature Inside Mold 43

6.1.3. Chemical Vessel 47

6.2. Polymerization Technique 47

6.2.1. Mold Preparation 49

6.2.2. Preparation of Activated Monomer in Vessel 50

6.2.3. Polymerization of Caprolactam and Removal of Disk 53

6.3. Fibre Surface Treatment 55

6.4. Treating by Adding Silane Directly into Monomer 57

Chapter 7 59

Structure and Composition of Composite Disks 59

7.1. Density 59

7.2. Volume Fraction of Fibre (V_f) 61

7.2.1. Reproducibility and Homogeneity of Disks 61

7.2.2. Masking Fibre Pretreatment Effects with Variations in V_f 63

7.3. Void Volume Fraction (V_v) 64

7.3.1. Correlation with Glass Fibre Treatment 64

7.3.2. Anomalous Voidage and ρ_n Uncertainty 65

7.3.3. Distribution of Local Voidage within Disks 67

7.4. Scanning Electron Microscope (SEM) Micrographs of Composites 74

Chapter 8 79

Mechanical Properties of Composite Specimens 79

8.1. Impact Properties 79

8.1.1. Improvement of E_s by Glass-Fibre Reinforcement 80

8.1.2. Effect of Silanes on E_s 81

8.1.3. Dependence of E_s on the Concentration of Silane Solutions Used for Treatment of Fibres in Composites. 83

8.1.4. The Role of Moisture 84

8.1.5. Reproducibility of Composite Disks 85

8.1.6. Comparison of Two Different Methods of Fibre Treatment 86

8.2. Tensile Properties 87

8.2.1. Nylon, and The Role of Glass Fibre Reinforcement 91

8.2.2. Silanes As Coupling Agents 101

8.2.3. Concentration Effects with Silanes 106

8.2.4. Further Study of Silane Type and Concentration 107

8.2.5. The Role of Humidity 108

8.2.6. Standardization and Assessment of The Lloyds Testing Machine Data 110

8.2.7. Tensile Properties of Composites Made with Silane IV 115

8.2.9. Alternate Method for Delivering Coupling Agent to Fibre Surface 116

8.2.10. Performance of a Wet Composite 117

8.3. Correlation of Impact Tests, Tensile Tests, and Humidity 118

Chapter 9 121

Conclusions and Recommendations 121

9.1. Conclusions 121

9.2. Recommendations 124

9.2.1. Mold Improvements 124

9.2.2. New Experiments 126

References 128

APPENDIX A Temperature Distribution Inside Mold 135
APPENDIX B Structural Properties and Mechanical Properties 137
APPENDIX C Samples of Calculation 154
APPENDIX D Stress-Strain Curves 161
APPENDIX E Calculation of Silane Saturated on Glass Fibre Surfaces 166
APPENDIX F Valve Redesign 169

LIST OF TABLES

Page

Table 2.1. Composition of glass used for fibre manufacture (all values in wt%) 6

Table 2.2. Properties of E-glass at 20°C; measured in fibre form with diameters in the range 8-14 μm 8

Table 2.3. Properties of nylon 6 and 30-35 wt% glass-fibre/nylon 6 composite 14

Table 4.1. Effect of thermal processing cycle on spherulite size and properties of PEEK resin 25

Table 8.1. Average mechanical properties from tensile tests 89

Table 8.1.I. Day I, RH = 53%, T = 25°C 89

Table 8.1.II. Day II, RH = 75%, T = 25°C 90

Table 8.1.III. Day III, RH = 40%, T = 22.5°C 90

Table 8.2. Comparison of commercial nylon 6 and our nylon 6 93

Table A-1. Temperature Upper Part of Mold (°C) 136

Table A-2. Temperature Lower Part of Mold (°C) 136

Table B-1. Density measurement 138

Table B-2. Volume fraction of fibre 140

Table B-3. Void volume fraction 142

Table B-4. Average breaking energies from Izod type impact tests 145

Table B-5. Izod impact tests on all specimens 145

Table B-5.0. Pure nylon 6 145

Table B-5.1. [1]Untreated 145

Table B-5.2. [1]Silane I (10%) 146

Table B-5.3. [1]Silane II (5%) 146

Table B-5.4. [1]Silane III (10%) 146

Table B-5.5. [1]Silane II (10%) 146

Table B-5.6. [1]Silane III (5%) 147

Table B-5.7. [2]Silane III (5%) 147
Table B-5.8. [2]Silane III (10%) 147
Table B-5.9. [1]Silane III (15%) 147
Table B-5.10. [1]Silane III (1.5%) 148
Table B-5.11. [1]Silane IV (10%) 148
Table B-5.12. [2]Untreated 148
Table B-6. Summary of tensile testing results 149
Table B-7. Mechanical properties from tensile tests of all specimens on Day I 149
Table B-7.0. Nylon 6 149
Table B-7.1. Untreated 150
Table B-7.2. Silane I (10%) 150
Table B-7.3. Silane II (5%) 150
Table B-7.4. Silane III (10%) 151
Table B-8. Mechanical properties from tensile tests on all specimens on Day II 151
Table B-8.1. Silane II (10%) 151
Table B-8.2. Silane III (5%) 151
Table B-9. Mechanical properties from tensile tests on all specimens on Day III 152
Table B-9.1. Untreated 152
Table B-9.2. Silane III (5%) 152
Table B-9.3. Silane III (10%) 152
Table B-9.4. Silane III (15%) 153
Table B-9.5. Silane III (1.5%) 153
Table B-9.6. Silane IV (10%) 153

LIST OF FIGURES

Page

Figure 1.1. Comparison between conventional monolithic materials and composite materials. 2

Figure 2.1. Amorphous structure of glass: (a) a two-dimensional representation of silica glass network and (b) a modified network that results when Na_2O is added to (a). Note that Na^+ is ionically linked with O^{2-} but does not join the network directly 7

Figure 3.1. A liquid drop on a solid surface making a contact angle (θ) between the solid and the liquid. 16

Figure 3.2. Function of coupling agent in aqueous environment. (a) Hydrolysis of organo-silane to corresponding silanol. (b) Hydrogen bonding between hydroxyl groups of silanol and glass surface. (c) Polysiloxane bonded to glass surface and laterally, to neighboring coupling molecule..... 19

Figure 3.3. Function of coupling agent in nonaqueous environment. (a) Reaction between silane and hydroxyl group at glass fibre surface in toluene solution (b) Organo-functional R group reacted with polymer matrix. 20

Figure 3.4. (a) Mechanisms of reversible bond formation associated with hydrolysis as proposed by Plueddemann. (b) Shear displacements without permanent damage of the interface bond..... 21

Figure 4.1. Tensile strength and toughness of PEEK neat resin as a function of degree of crystallinity..... 23

Figure 4.2. Tensile properties of PEEK as a function of degree of crystallinity 23

Figure 4.3. Degree of crystallinity of PEEK as a function of cooling rate (**17**) 24

Figure 4.4. Degree of crystallinity of PEEK as a function of cooling rate (**18**) 24

Figure 6.1. Diagram of experimental equipment ($H_1 \equiv 60$ mm, $H_2 \equiv 150$ mm)..... 41

Figure 6.2. Mold diagram (not to scale) unit: mm..... 42

Figure 6.3. Locations of thermocouples on the upper and lower surfaces of the mold cavity..... 45

Figure 6.4. Temperature distributions on mold surfaces when nominal set point is at 100°C 46

Figure 6.5. Temperature distributions on mold surfaces when nominal set point is at 150°C 46

Figure 6.6. Modification of reaction injection molding process and pultrusion process called RIM-Pultrusion process (a) Reaction injection molding process (b) Pultrusion process (c) RIM-Pultrusion process 49

Figure 6.7. Procedure to make nylon 6/glass fibre composite 51

Figure 7.1. Locations of regions from which specimens were taken for obtaining data on composition 60

Figure 7.2. Fibre volume fraction (V_f) of composite disks having different glass fibre treatment and molded on different days. 62

Figure 7.3. Void volume fraction (V_v) of composites treated with different kinds and concentrations of silane 64

Figure 7.4. Void volume fraction at different positions in composite disks (a) V_v values expressed as volume percents. (b) V_v ranking, as a scale of 6-1, with 6 highest. 69

Figure 7.5. Fibre volume fraction (V_f) vs. void volume fraction (V_v) of composite disks (a) local V_v vs. local V_f for all specimens of all disks (b) $\overline{V}_v$ vs. $\overline{V}_f$ for all disks 70

Figure 7.5 (continued). Fibre volume fraction (V_f) vs. void volume fraction (V_v) of composite disks (c) local V_v vs. local V_f for all specimens taken from disks ^2U, $^1II_5$, and $^1III_{15}$ 71

Figure 7.5 (continued). Fibre volume fraction (V_f) vs. void volume fraction (V_v) of composite disks (d) local V_v vs. local V_f for all specimens taken from disks ^1U, $^1II_{10}$, $^1III_5$, and $^2III_5$ 72

Figure 7.5 (continued). Fibre volume fraction (V_f) vs. void volume fraction (V_v) of composite disks (e) local V_v vs. local V_f for all specimens taken from disks $^1I_{10}$, $^1III_{10}$, $^2III_{10}$, and $^1III_{1.5}$ 73

Figure 7.6. SEM micrographs of glass fibre/nylon 6 composite specimen surfaces corresponding to different pretreatment of fibre. (a) Untreated: fracture in tensile test. (b) Silane I: fracture in tensile test. 75

Figure 7.6 (continued). SEM micrographs of glass fibre/nylon 6 composite specimen surfaces corresponding to different pretreatment of fibre. (c) Silane III: fracture in tensile test. (d) Untreated: top surface. 76

Figure 7.6 (continued). SEM micrographs of glass fibre/nylon 6 composite specimen surfaces corresponding to different pretreatment of fibre. (e) Silane II: top surface. (f) Silane III: top surface. 77

Figure 8.1. Impact strength (E_s) of composites using fibres treated with different silanes, and untreated fibres 81

Figure 8.2. Impact strength (E_s) of composites using fibres treated with Silane III and Silane II at different concentrations in toluene 83

Figure 8.3 (a) DSC scan for nylon 6 sample taken from pure-nylon disk (a full cycle)..... 94

Figure 8.3 (b) Expanded region of DSC heating trace, for pure nylon 6, near crystalline melting regime..... 96

Figure 8.3 (c) Expanded region of DSC heating trace, near glass transition regime..... 97

Figure 8.4 (a) DSC scan for composite sample taken from [1]Untreated disk (a full heating-cooling cycle)..... 98

Figure 8.4 (b) Expanded region of DSC heating trace, near the nylon 6 melting regime, for [1]Untreated composite. 99

Figure 8.4 (c) Expanded region of DSC heating trace, near T_g for nylon 6, for [1]Untreated composite. 100

Figure 8.5 (a) DSC scan for composite sample taken from specimen of Silane II (10%) disk (a full heating-cooling cycle). 102

Figure 8.5 (b) Expanded region of DSC heating trace near the nylon 6 melting regime, for Silane II (10%) composite disk. 103

Figure 8.5 (c) Expanded region of DSC heating trace, near the nylon 6 T_g, for Silane II (10%) composite disk. 104

Figure 8.6. Mechanical properties (σ_b, ε_b, τ, E) from tensile test of specimens made with glass fibres treated with Silane III at different concentrations (5, 10, and 15%) in toluene 114

Figure 8.7. σ_b vs. E_s for bonded composites (Silane II, III, and IV) at different relative humidities (RH). 119

Figure B-1. Dimensions of test specimens. (a) Tensile; (b) Izod type impact test 144

Figure D-1. Stress-strain curve of fibreglass/nylon 6 composites (Using Instron Machine) 161

Figure D-1.1. 1Untreated 162

Figure D-1.2. [1]Silane I (10%) 162

Figure D-1.3. [1]Silane II (5%) 163

Figure D-1.4. [1]Silane II (10%) 163

Figure D-1.5. [1]Silane III (5%) 164

Figure D-1.6. [1]Silane III (5%) 164

Figure D-2. Stress-strain curve of fibreglass/nylon 6 composites (Using Lloyds L6000R Universal Testing Machine) (a) Dry specimens (b) Wet specimens 165

Figure F-1. Valve redesign 170

CHAPTER 1

INTRODUCTION

In modern technology, especially, in aerospace technology, the need for high performance materials (high strength, high stiffness and light weight) is increasing. One of these materials is known as "polymer composite" which has been designed to replace metal parts, not only in aerospace technology but also in many other industries, such as car, boat, sports, etc.

Many researchers and engineers who work in the polymer industry believe that the future belongs to composites, and that by the end of this century, composites will replace half of the unfilled (non-composite) polymer finished products (**1**, p. 10).

Composite materials are materials composed of two or more components that have different physical and chemical properties. Those components are combined to give specific characteristics for particular uses (**2**, p. 1, **3**, p. 3).

Not only are there manmade composites, but also composites which occur naturally. For example, wood which comprises lignin as a matrix and cellulose fibre, bone which comprises mineral matrix called apatite and short and soft collagen fibres, etc. are all composites (**4**, p. 3).

Examples of manmade composites are carbon black filled rubber, Portland cement or asphalt mixed with sand, and fibreglass reinforced plastic.

Compared with aluminum and steel, composites have less weight and thermal expansion but higher specific stiffness, specific strength and fatigue resistance as shown in Figure 1.1.

It is generally believed that most materials are stronger and stiffer in fibrous form than in other forms. If strength and stiffness alone are considered, fibre reinforced

composite materials do not have many advantages compared to metals. But when we consider the modulus per unit weight (specific modulus) and strength per unit weight (specific strength), composite materials have higher specific modulus and specific strength than metals. These properties make possible energy savings and higher efficiency for transport industries (**3**, p. 4).

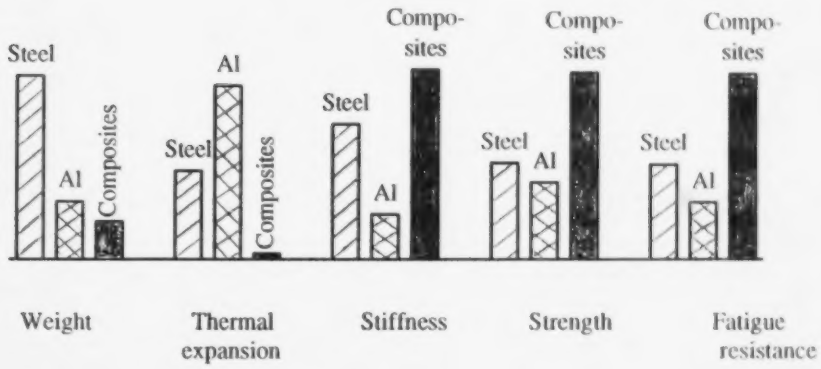

Figure 1.1. Comparison between conventional monolithic materials and composite materials (**4**, p. 4). The "stiffness" and "strength" parameters are on a unit weight basis e.g., stiffness/density.

Although thermoset composites have been successfully used to replace metals, they have some limitations compared to thermoplastic composites. Thermoplastic composites have some characteristics such as good thermal stability, high toughness and damage tolerance, short and simple processing cycles, and potential for significant reductions in manufacturing costs. In addition, thermoplastics can be remelted and reprocessed which is very useful for recycling and repairing considerations (**5**, p. 96). The voids or defects present in thermoplastic laminates, for example, can be reconsolidated and eliminated while the thermoset has to be rejected. Finally, there is no need for adhesive bonds and mechanical fasteners since composite parts can be thermally joined to form a

composite assembly.

The earliest thermoplastics were aliphatic based polymers (e.g., polyethylene) which have low elastic modulus and low glass transition temperature. The new thermoplastic composites developed for high-temperature structural applications are based on aromatic polymers which can surmount the major limitations of the earlier aliphatics. This has led to the increased replacement of metallic and fibre reinforced thermoset components with thermoplastic based composites. The materials which are considered as new thermoplastic polymers are polyketones, polyarylene sulfides, polyamides, polyimides, polysulfones, polybenzimidazoles, and polyphenylquinoxalines (**5**, p. 2-3).

One common polyamide (nylon 6) and one familiar reinforcing agent (fibreglass type E) are selected as matrix and fibre, respectively, to be studied here, because of their low cost and high performance as separate materials.

Fibreglass-reinforced plastic composites have been developed since 1940 (**6**, p. 1). These high performance composite materials consist of three regions: fibre, matrix, and the interface between the fibre and the matrix. The interfacial layers in polymer matrix composites play an extremely important role on the rheological and mechanical properties of composites since the stresses acting on the matrix are transmitted to the fibre across the interface (**1**, p. 3, **2**, p. 1, **3**, p. 37). As the adhesion between the fibre and the matrix is very important, the interface is being studied extensively nowadays by advanced analytical techniques of surface science. It has been found that the interface between fibre and matrix has some kind of discontinuity, such as crystal structure, atomic registry, elastic modulus, density, and coefficient of thermal expansion (**4**, p. 79).

In producing filled polymers, there is little interfacial interaction between the polymer and the filler particle surface since the surface of the filler is hydrophilic and the polymer generally hydrophobic. Therefore, the surface of the filler can adsorb water which

decreases the impact resistance tremendously (**7**). Even without such water adsorption however, it is clear that the hydrophobic/hydrophilic pair of materials would not be attracted to each other. In this case one possibility to improve the interfacial interaction between the polymer and the filler particle surface is to treat the latter with a coupling agent or surfactant (**7**).

It has also been found that the bonding between the matrix and the fibre depends on the degree of atomic and molecular surface ordering (e.g., crystal vs. glass) and chemical properties of the fibre, and the molecular conformation and chemical constitution of the polymer matrix (**4**, p. 37).

Hull (**3**, p. 39-40) explained why a strong physical bond is usually not achieved: (a) the fibre surface is contaminated so that the effective surface energy is much smaller than that of the base solid, (b) air and other gases are entrapped at the solid surface, and (c) large shrinkage stresses occur during the curing process (of thermosets, e.g., epoxy) which leads to displacements at the surface which cannot be healed.

If we can improve the bonding between the fibre and the matrix, we will be able to develop even better properties in a high performance composite material. There are many ways to improve the interfacial adhesion between the fibre surface and the matrix; e.g., etching, plasma treatment, coupling agent, copolymer, etc. One efficient method for glass fibres is treating the fibre surface with silane coupling agents.

Plueddemann has suggested several ways in which the silane agents may be effective: improvement of the filler-matrix adhesion, protection of the filler surfaces from microflaws which initiate failure, reinforcement of the interface layer, and improvement of filler wetting by the plastic (perhaps by increasing the hydrophobicity of the surface) (**1**, p. 94).

Even though the interfacial zone in a composite material is very complicated,

control of the nature of this region promises that the properties of the composite can be improved by ensuring efficient stress transfer between the matrix and the fibre (**8**).

Because experience in processing high performance thermoplastic composites is lacking, the utilization of these new materials is not progressing rapidly. The techniques to process thermoplastic composites are not as well-known as those developed for thermoset composite materials (**5**, p. 96).

The objectives of this study are to improve the interfacial adhesion of glass fibre and nylon 6 and examine whether material properties are thereby improved. Sample processing is a special form of RRIM (reinforced reaction injection molding). This study will therefore create some knowledge about a thermoplastic composite process for further development of the high performance thermoplastic composite materials.

CHAPTER 2

MATERIALS USED IN COMPOSITES

2.1. Glass fibres

Glass fibres were introduced in 1920's (**9**, p.129); since then, their high performance and low cost have resulted in increasing use. There are different types of glass fibres for different purposes, for example, type C (C for corrosion), E (E for electrical), and S (S for higher silica content). C-glass can resist chemical corrosion better than E-glass but is more expensive and has lower strength properties. S-glass has a higher Young's modulus and is more temperature resistant but is more expensive than E-glass. Because of the price advantage of E-glass, most continuous glass fibre (about 90%) produced is of the E-glass type; it also draws well and has good strength, stiffness, electrical and weathering properties.

Typical compositions of glasses of different types used for glass fibre in composite materials are shown in Table 2.1. Common glass fibres are based on silica (about 50-60% SiO_2) and oxides of calcium, boron, sodium, aluminum and iron.

Table 2.1. Composition of glass used for fibre manufacture (all values in wt%) (3, p. 16)

Components	C-glass	E-glass	S-glass
SiO_2	64.4	52.4	64.4
$Al_2O_3.Fe_2O_3$	4.1	14.4	25.0
CaO	13.4	17.2	-
MgO	3.3	4.6	10.3
Na_2O, K_2O	9.6	0.8	0.3
B_2O_3	4.7	10.6	-
BaO	0.9	-	-

The surface of glass consists of randomly distributed groups of oxides and is, like the bulk, amorphous. Some of the oxides, such as SiO_2, Fe_2O_3, and Al_2O_3, are non-hygroscopic. These non-hygroscopic oxides interact with water by forming hydroxyl groups such as –Si–OH, –Fe–OH and –Al–OH which then hold water molecules nearby through relatively weak hydrogen bonding; water never touchs or penetrates these surfaces. The hygroscopic oxides absorb water directly onto the surface which then becomes hydrated (**3**, p. 42) and can dissolve portions of the surface over long periods of time. Looking at the interior, we find that the two-dimensional view of the network of silica glass is shown in Figure 2.1(a). Oxygen atoms are bonded covalently to silicon. If Na_2O is added to this glass as represented in Figure 2.1(b), sodium ions will be linked ionically with oxygen but will not join the network directly. The addition of other metal oxides will change the network structure and the bonding, and as a result, the properties of this glass will be changed.

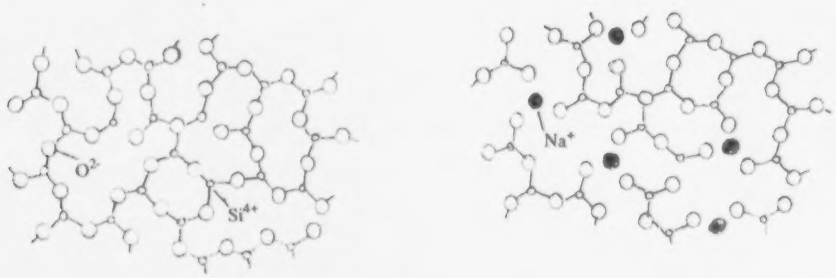

Figure 2.1. Amorphous structure of glass: (a) a two-dimensional representation of silica glass network and (b) a modified network that results when Na_2O is added to (a). Note that Na^+ is ionically linked with O^{2-} but does not join the network directly (**4**, p. 11)

The properties of glasses are quite isotropic. Young's modulus and thermal expansion coefficients are the same along the fibre axis and perpendicular to it because their three-dimensional network structure is isotropic (**4**, p. 11). The properties of E-glass

are shown in Table 2.2.

Furthermore, the strength of glass is sensitive to process conditions and the testing environment. For example, tensile strength decreases when the fibres are tested in humid air, due to absorption of water on the glass surface, and when the surfaces of the fibres are in contact with mineral acids (aqueous). It is significant that the presence of water also decreases the surface energy of glass fibre. As reported, glass fibre in the presence of water has a surface energy in the range of 10-20 mJm^{-2} while the dry virgin glass has the value of over 500 mJm^{-2} (**3**, p. 43).

Table 2.2. Properties of E-glass at 20°C; measured in fibre form with diameters in the range 8-14 μm (**3**, p. 14)

Properties	Units	E-glass
Density	$10^3\,kgm^{-3}$	2.56
Young's modulus (tensile, along fibre axis)	GNm^{-2}	76
Modulus (perpendicular to fibre axis)	GNm^{-2}	76
Tensile strength	GNm^{-2}	1.4-2.5 (typical) 3.5 (freshly drawn)
Elongation to fracture	%	1.8-3.2 (typical)
Coefficient of thermal expansion (0 to 100°C)	$10^{-6}K^{-1}$	4.9
Thermal conductivity (parallel to fibre axis)	$Wm^{-1}K^{-1}$	1.04

2.2. Nylon 6 (**10**, p. 536-541, **11**, p. 429-430, **12**, p. 23-24)

Nylon 6, a polyamide, is a melt-processable thermoplastic whose chain structure is composed of repeating amide groups separated by five $-CH_2-$ groups. In this study nylon 6 is made by polymerization of ε-caprolactam. Caprolactam is widely used because nylon 6 has excellent fibre properties and this monomer is cheaply made from phenol.

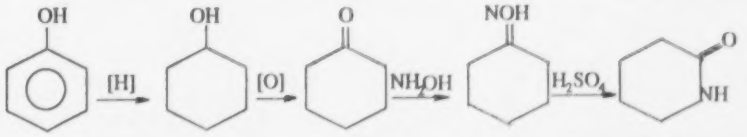

(2.1)

ε-caprolactam

The polymerization of lactams is a ring-opening process, using cationic or anionic initiators . In this experiment the reaction is anionic.

The structure of ε-caprolactam monomer is 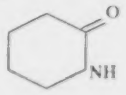 , which can also be written in the form 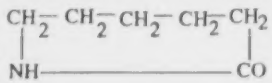 . This monomer contains both acid ($\overset{O}{\overset{\|}{C}}$) and amine (NH) groups which are divided during the ring-opening initiation but are found together in the amide bond ($-\underset{H}{\overset{|}{N}}-\overset{O}{\overset{\|}{C}}-$) when polymerized. The polymer is therefore a polycaproamide or polycaprolactam (nylon 6) which can be written as

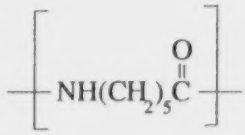

(2.2)

Details of this anionic polymerization are as follows.

Sodium hydride (NaH) was selected as a strong base to initiate the polymerization of a lactam by forming the lactam anion. Besides sodium hydride (one of the metal hydrides), one can use any other strong base such as alkali metals, metal amides, and organometallic compounds.

For ε-caprolactam with a metal derivative,

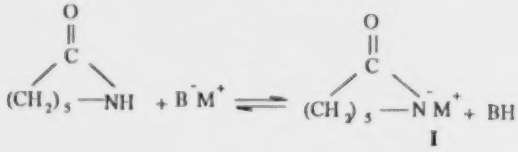

(2.3)

BM = metal derivative, for example, sodium hydride (NaH, B = H, M = Na, BH = $H_2\uparrow$)

Weaker bases such as hydroxides and alkoxides cannot be used satisfactorily, because a high concentration of the anion **I** would usually be obtained only if the product H_2 is removed to push the equilibrium to the right.

The lactam anion **I** then reacts with monomer in the second step of the initiation process by a ring-opening transamidation.

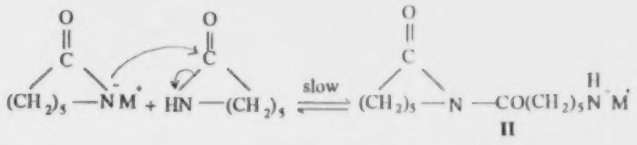

(2.4)

The primary amine anion **II** is not stabilized by conjugation with a carbonyl group. It is highly reactive and rapidly abstracts a proton from monomer

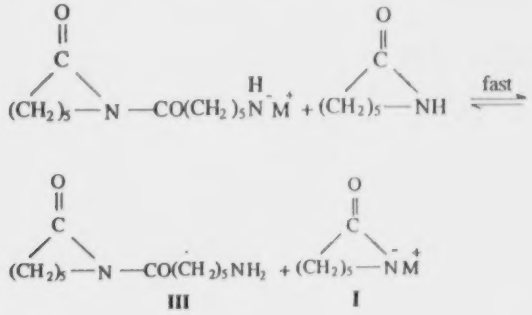

(2.5)

to form the imide dimer **III**, N-(ε-aminocaproyl)caprolactam, and regenerate the lactam anion.

The imide dimer **III** is the actual initiating species necessary for the onset of polymerization. The initial induction period of lactam polymerization is slow because the imide dimer builds up slowly. Propagation is the reaction between a propagating N-acyllactam species and the lactam anion

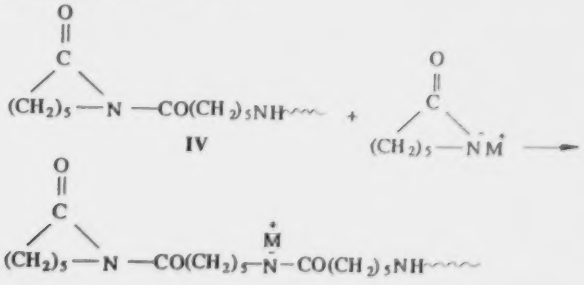

(2.6)

followed by fast proton-exchange with monomer.

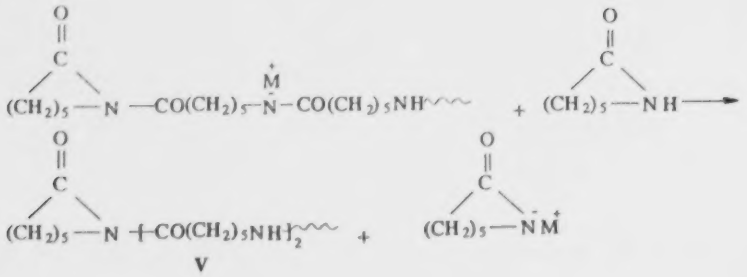

(2.7)

The anionic polymerization of lactams is different from other polymerizations. First, the propagating center is the cyclic amide linkage of the N-acyllactam instead of a radical, carbanion, or carbenium ion. Second, it is the monomer anion called "activated monomer" instead of monomer that adds to the propagating chain.

The concentrations of both the propagating species and the activated monomer are determined by the concentration of base.

Since the induction of lactam polymerization by using a strong base alone is very slow, we can increase the rate of polymerization by adding acylating agents in the monomer. The acylation agents such as isocyanates (used in this experiment), acid chlorides and hydrides, inorganic anhydrides, and others, will form an amide when reacting with monomer.

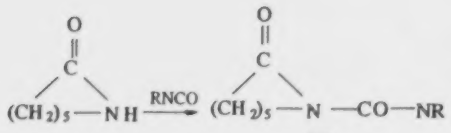

(2.8)

By reaction in the presence of an isocyanate, ε-caprolactam can be converted rapidly to an N-acylcaprolactam (**VI**).

Initiation period in this acceleration case refers to the reaction of the N-acylcaprolactam with activated monomer followed by a fast proton-exchange with monomer.

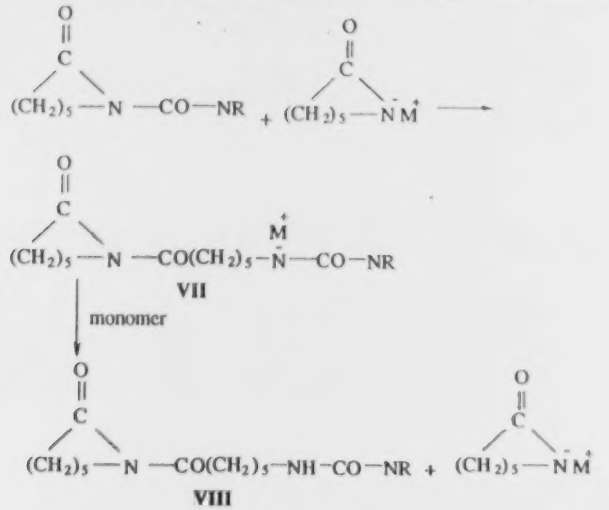

(2.9)

The species **VII** and **VIII** correspond to species **II** and **III** in polymerization without adding acylating agent. The use of acylating agents is advantageous because the induction periods are absent, the polymerization rates increased, and the polymerization can be conducted at lower temperature. Propagation follows in the same manner as for propagation of species **IV**

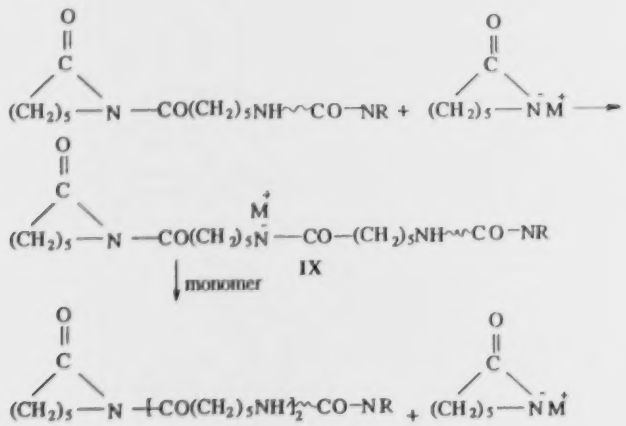

(2.10)

The base is referred to as the initiator and the acylating agent as the activator. The polymerization rate depends on the concentrations of base and activator. It is observed

that the rate initially increases with increasing base concentration but, after reaching the maximum, it decreases at higher base concentrations.

One of the problems in anionic lactam polymerization is that proton transfer can occur with the polymer chain, especially near completion of the reaction when monomer concentration is very low and side reactions are more probable. This results in chain branching and a polydisperse polymer.

Nylon 6, a semi-crystalline polymer, has a melting point of 223°C (**13**, p. 68) which is rather high compared to other thermoplastic polymers. But one of the disadvantages of nylon 6 is, like all nylons, it absorbs moisture from its immediate environment. Eventually, equilibrium with the relative humidity of the atmosphere is achieved, which generally has a plasticizing effect that increases flexibility and impact resistance. The rate of moisture absorption depends on temperature (nylon 6 absorbs moisture very quickly when immersed in warm water), crystallinity, humidity, and thickness of samples.

Nylon 6 has a good chemical resistance to hydrocarbons, aromatic and aliphatic solvents, such as automotive oils and fuels, and refrigerants, but it is attacked by strong acids, bases and phenol or even hot water. The properties of nylon 6 and 30-35 wt% glass fibre (chopped)-reinforced composite are shown in Table 2.3.

Table 2.3. Properties of nylon 6 and 30-35 wt% glass-fibre/nylon 6 composite (**12**, p. 391, **13**, p. 68)

Properties	Units	Nylon 6 [a]	Nylon 6 [b]	30-35 wt% glass fibre-reinforced [b]
Melting temperature, T_m (crystalline)	°C	223	210-220	210-220
Glass temperature, T_g (amorphous)		49	-	-
Density	g/cm^3	1.12-1.15	1.12-1.14	1.35-1.42
Tensile strength at break	MPa	48-83	41-165	165-179[c], 110[d]
Elongation at break	%	25-400	30-100[c], 300[d]	2.2-3.6[c], 6-7[d]
Tensile yield strength	MPa	-	81[c], 51[d]	-
Tensile modulus	GPa	1.0	2.6[c], 0.7[d]	8.6-10[c], 5.5[d]
Compressive strength	MPa	48-97	90-110	131-165[c]
Compressive modulus	GPa	1.7-2.4	1.7	-
Flexural strength (rupture or yield)	MPa	-	108[c], 40[d]	234-248[c], 145[d]
Flexural modulus, 23°C	GPa	2.7-2.8[c]	2.7[c], 1.0[d]	8.6-9.7[c], 5.5-6.5[d]
Izod impact (1/8-in. thick specimen)	J/m	-	32-117[c], 160[d]	112-181[c], 198-294[d]
(Izod, 0.5 in. notch)	J/m	53-294	-	-
Water absorption at saturation, 20°C	%	9-11	8.5-10.0	6.5-7.0
Thermal expansion	10^{-5}/°C	8.3	8.0-8.3	1.6-8.0

Note: Units in both references were converted to SI unit as following:
1 psi = 6894.7238 Pa;
1 ft-lb./in. of notch = 53.3784 J/m of notch

a data from reference **13**, p. 68

b data from reference **12**, p. 391

c Dry, as molded (approximately 0.2% moisture content)

d As conditioned to equilibrium with 50% relative humidity

CHAPTER 3

INTERFACES

3.1. Wettability

The properties of composites depend on the types of matrix, fibre, and their interface structure (**2**, p. 283). To choose polymer and fibre to make composite materials one has to consider their properties separately and also their interfacial adhesions. With glass fibres, the adhesion is usually the strongest in polar polymers and those with carbonyl oxygens (epoxy resins, polyesters, nylon, etc.), which are able to form hydrogen bonds with the hydroxyls on the glass fibre surface. By using coupling agents, it is possible to increase the adhesion between fibres and hydrophobic polymers (**1**, p. 15). Zisman (**6**, p. 20) concluded that good wetting of the solid surface by the liquid resin was of major importance in preparation of composites. Physical adsorption of resin on high-energy fibre surfaces could provide greater adhesive strength than the cohesive strength of organic resins, if complete wetting were obtained-i.e., localized failure would not occur at weakened interface locations, but rather within the bulk material.

Wettability is defined as the extent to which a liquid would spread on a solid surface (**4**, p. 80). If the net free energy of the system is reduced by liquid coverage of the solid surface, the liquid drop will spread and wet the surface completely. Wettability is most often characterized in terms of surface forces arising from surface tension. For example, for a drop of liquid resting on a plane solid surface, wettability can be measured by considering the equilibrium of forces in a system.

For complete wettability (**4**, p. 80),

$$\gamma_{LS} + \gamma_{LV} < \gamma_{SV}$$

where γ_{ij} represents the specific surface energy (energy/interfacial area) or

specific surface tension (force/length of contact line) and LS, LV, SV designate the various surfaces (or interfaces) between bulk phases of solid (S), liquid (L), and vapor (V).

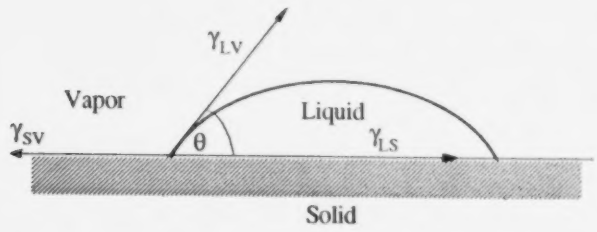

Figure 3.1. A liquid drop on a solid surface making a contact angle (θ) between the solid and the liquid. The terms γ_{LS}, γ_{LV} and γ_{SV} denote the surface energies of solid-liquid, liquid-vapor, and solid-vapor interfaces, respectively (4, p. 80).

From the equilibrium of forces (Young's equation) (**3**, p. 39, **4**, p. 80-81), as shown in Figure 3.1 ,

$$\gamma_{LS} + \gamma_{LV}\cos\theta = \gamma_{SV} \qquad (3.1)$$

or $$\theta = \cos^{-1}\frac{(\gamma_{SV} - \gamma_{LS})}{\gamma_{LV}}$$

where θ represents contact angle.

The Dupre equation for the thermodynamic work of adhesion, W_A, of a liquid to a solid states that (**3**, p. 39)

$$W_A = \gamma_1 + \gamma_2 - \gamma_{12} \qquad (3.2)$$

where γ_1 and γ_2 are the surface free energies of the liquid and solid respectively,

and γ_{12} is the free energy of the liquid-solid interface.

By putting $\gamma_1 = \gamma_{LV}$, $\gamma_2 = \gamma_{SV}$ and $\gamma_{12} = \gamma_{LS}$,

$$W_A = \gamma_{LV} + \gamma_{SV} - \gamma_{LS} \qquad (3.3)$$

Zisman introduced the idea of critical surface tension of wetting, γ_C, such that only liquids with $\gamma_{LV} < \gamma_C$ will spontaneously spread on the solid. This parameter is used to evaluate the wetting of fibres by resins (**3**, p. 39).

Theoretical calculations (**14**) indicate that a typical silicate glass fibre has a surface energy 560 mJm^{-2} and can be wetted by liquid polyester and epoxy resin with surface energies of 35 mJm^{-2} and 43 mJm^{-2}, respectively. But these resins cannot wet solid polyethylene with critical surface energy (γ_C) of 31 mJm^{-2} (**3**, p. 39).

In order to obtain complete wetting of a surface, the adhesive must initially be of low viscosity and have a surface tension lower than the critical surface tension (γ_c)of the mineral surface (**6**, p. 20).

Figure 3.1 shows a liquid drop on a solid surface making a contact angle between the solid and the liquid. No wetting occurs at an angle of 180° while partial wetting occurs at $0° < \theta < 180°$, and perfect wetting occurs at 0°. The contact angle depends on the nature of the surfaces; for example, the surface roughness would diminish the contact angle if the smooth surface had $\theta < 90°$ but increase it if the smooth surface had $\theta > 90°$, while adsorbed gases would increase it. Any impurities in or deliberate additions to the solid or liquid phase or a chemical reaction between the phases would affect the wettability (**4**, p. 80).

Fortunately, the wettability of glass can be controlled and made more compatible with liquid organic materials (polymers and monomers) by treating the glass surface with the proper coupling agents, such as, hydrolyzable silanes (**6**, p. 21).

3.2. Coupling agents

In general, inorganic materials (e.g., glass) have high surface free energy which is opposite to organic materials that have a low surface energy. Since the affinity is low, they

cannot adhere to each other very well. It is possible to use coupling agents to reduce the critical surface free energy of the inorganic materials to a low critical surface free energy in a range near that of polymers (**2**, p. 4).

Coupling agents are materials that improve the practical adhesive bond of polymer to the material (**6**, p. 2). They contain chemical functional groups that can react with silanol groups on glass, attached to the glass by covalent bonds. And the other different functional groups could react with the matrix during polymerization (**6**, p. 17). The main function of coupling agents is to provide strong chemical links between the hydroxyl groups on the fibre surfaces and the polymer molecules of the resin (**3**, p. 43).

The coupling agents used for glass fibre are organofunctional silanes which are hybrid organic-inorganic compounds that have been used as coupling agents across the organic-inorganic interface. The general chemical formula for the silane coupling agents is R_{4-n}-Si-X_n where R is an organofunctional group which must be compatible with the resin and X is capable of reaction with -OH groups on the glass (perhaps mediated with water). When n = 1, each molecule bonds singly with the glass, and when n = 3 there can exist lateral silane-silane bonds (networks) as well (**3**, p. 43). For example, for aqueous-media treatment X represents hydrolyzable groups (e.g., $-OC_2H_5$) which first yield the corresponding silanol groups (Figures 3.2 a, b). When water is removed, a reversible condensation reaction occurs between the silanol and the surface, and (when n = 3) between adjacent silanol molecules on the surface. The result is a polysiloxane layer bonded to the glass surface (Figure 3.2 c). Therefore, the silane coated fibre presents a surface of R groups to the surrounding monomer. During polymerization, specific groups on the monomer (e.g., $\overset{|}{\underset{|}{C}}{=}O$) react with R groups, establishing covalent bonds to the polymerized resin (Figure 3.2 d).

For treating glass from organic solvents, X-groups need not be hydrolysable. In our work, the solvent was toluene and X was usually Cl (with n = 1; see Figure 3.3) but

sometimes OC_2H_5 (with n = 3).

In a case with no application of silane to the glass surface, water can diffuse through the resin and attack the fibre by the hydration processes, which results in rapid deterioration of the glass-resin interface. This will reduce the ability of the fibres to accept a transfer of stress from the polymer matrix. To explain how a silane coupling agent leads to a strong water-resistant bond, Plueddemann (**15**) proposed that movement or displacement at the interface was able to relax the local stresses and maintain the chemical bond if a reversible bond breakage mechanism possibly occurred (**3**, p. 43-45).

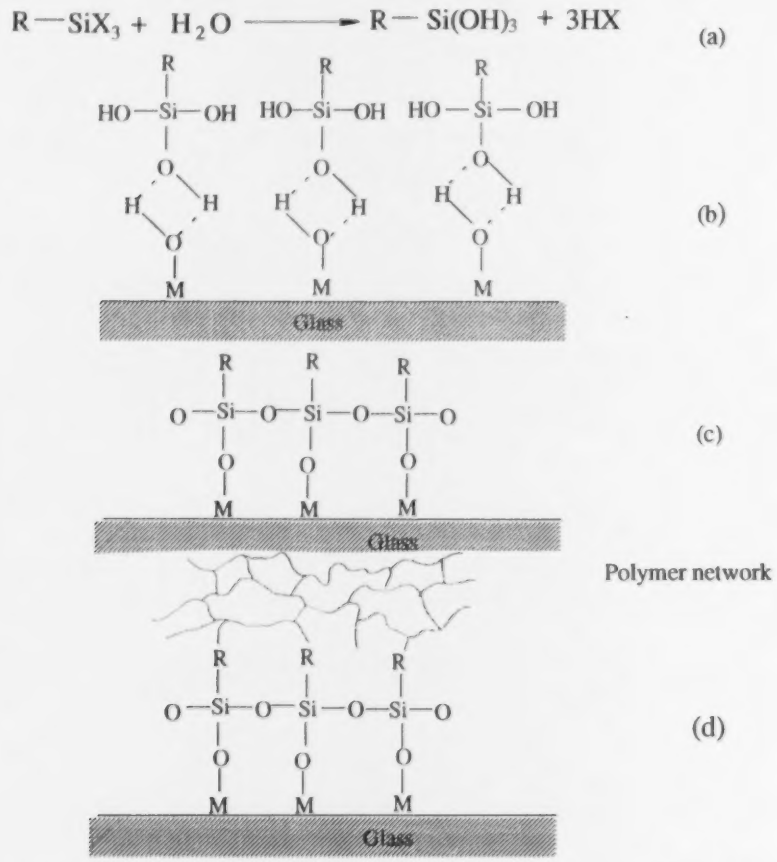

Figure 3.2. Function of coupling agent (a) Hydrolysis of organo-silane to corresponding silanol. (b) Hydrogen bonding between hydroxyl groups of silanol and glass surface. (c) Polysiloxane bonded to glass surface and laterally, to neighboring coupling molecules, to form a network structure surrounding the fibre. (d) Organo-functional R group reacted with polymer matrix. (**3**, p. 44)

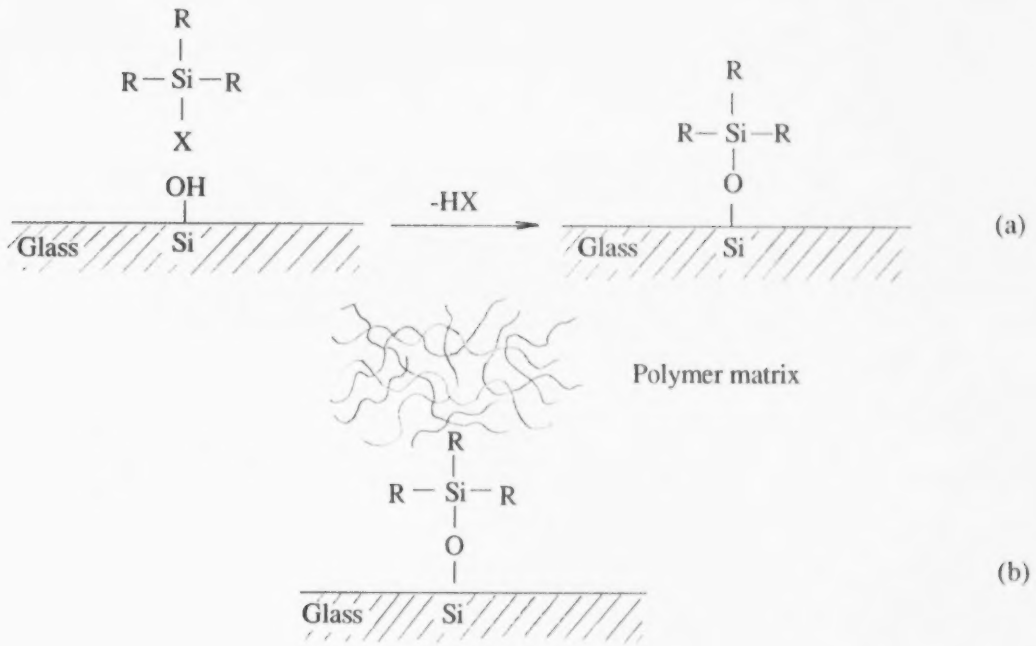

Figure 3.3. Function of coupling agent (a) Reaction between silane and hydroxyl group at glass fibre surface in toluene solution (non aqueous) (b) Organo-functional R group reacted with polymer matrix.

He proposed a mechanism wherein water may diffuse through the resin to the interface, after which the covalent M-O bond hydrolyses as shown in Figure 3.4. Because this process is reversible, therefore, the covalent bond can reform when the water diffuses away. If there is a simple shear stress parallel to the interface, the surfaces can slide past each other without permanent bond failure (**3**, p. 45-46). This reversible bond process has been verified by Fourier transform infra-red spectroscopy (**16**).

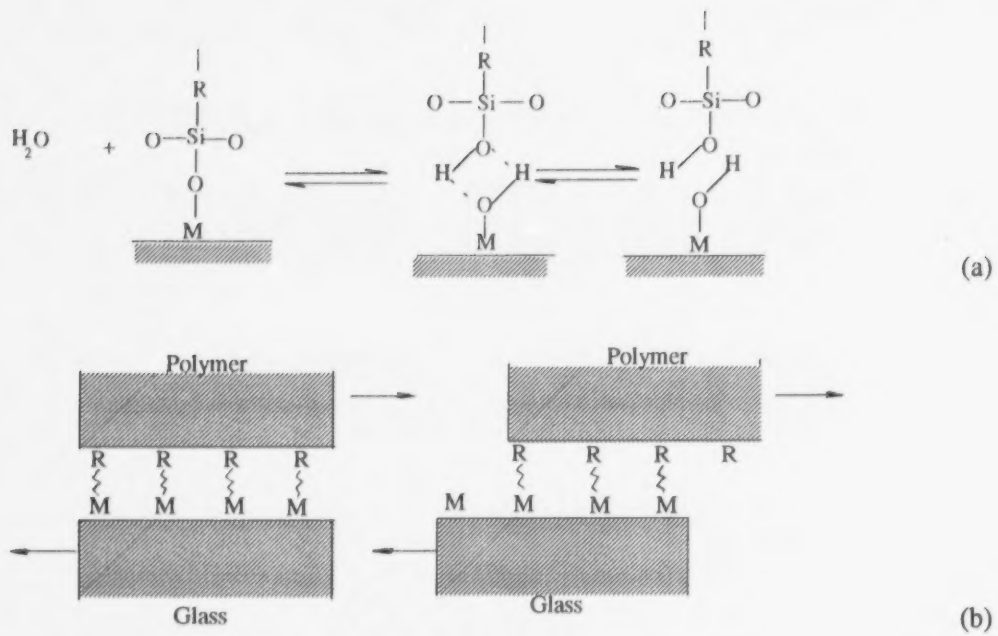

Figure 3.4. (a) Mechanisms of reversible bond formation associated with hydrolysis as proposed by Plueddemann (15). (b) Shear displacements without permanent damage of the interface bond. (3, p. 45)

CHAPTER 4

MORPHOLOGY OF POLYMERS*

It is well recognized that the mechanical properties of semi-crystalline thermoplastics depend on their morphology e.g., the degree of crystallinity (mass fraction), the number/volume and size of spherulites, the crystalline structure and the crystalline orientation. In general, a lower crystallinity will produce higher elongation and better toughness but lower strength, thermal stability and chemical resistance. Illustrations of these trends, for toughness and tensile strength, are given for poly(etheretherketone) (PEEK) in Figure 4.1 and 4.2.

The morphology of semi-crystalline thermoplastics is influenced by the processing conditions and the presence of foreign surfaces. The processing conditions are the temperature to which the polymer is heated and the time it is held there, cool-down rate, character of shear flow (if such exists), etc. For example, crystallinity is lower at higher processing temperature, long annealing times, and high cooling rate; and large spherulites are formed at low cooling rate while smaller spherulites can be formed by fast cooling (see Table 4.1). It has been reported that for composites with a PEEK matrix, at cooling rates greater than 700°C/minute, spherulites did not grow completely, and the optimum level of crystallinity (25-30%) was not obtained. And at cooling rates greater than 2000°C/min, a PEEK matrix will be amorphous. Blundell et al. (**17**) found that the degree of crystallinity of neat PEEK resin is a function of cooling rate as shown in Figure 4.3. Figure 4.4 shows similar results obtained by Talbott et al. (**18**) and Velisaris and Seferis (**19**). Crystallinity achieved with any given cooling rate can usually be increased by subsequent annealing at elevated temperature, leading to improvement of mechanical properties (see Figure 4.2).

* This chapter was summarized from chapter 3 of reference 5 from which further details can be obtained.

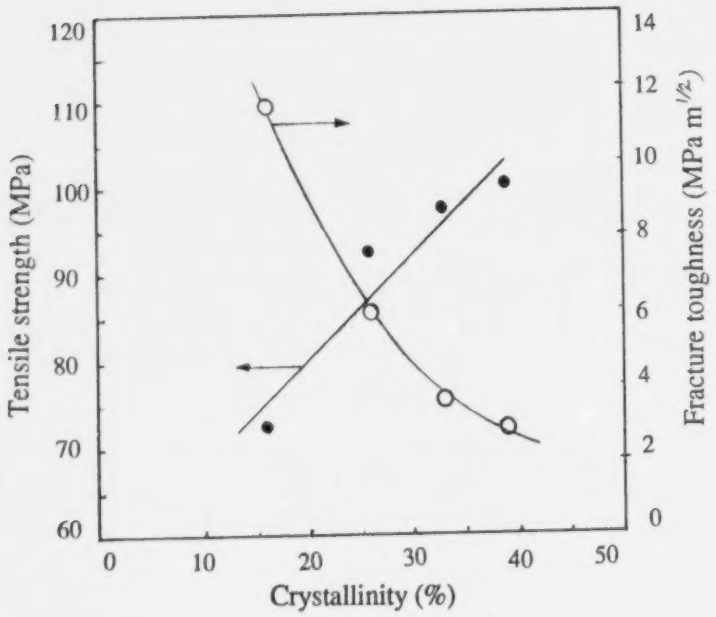

Figure 4.1. Tensile strength and toughness of PEEK neat resin as a function of degree of crystallinity (**18**)

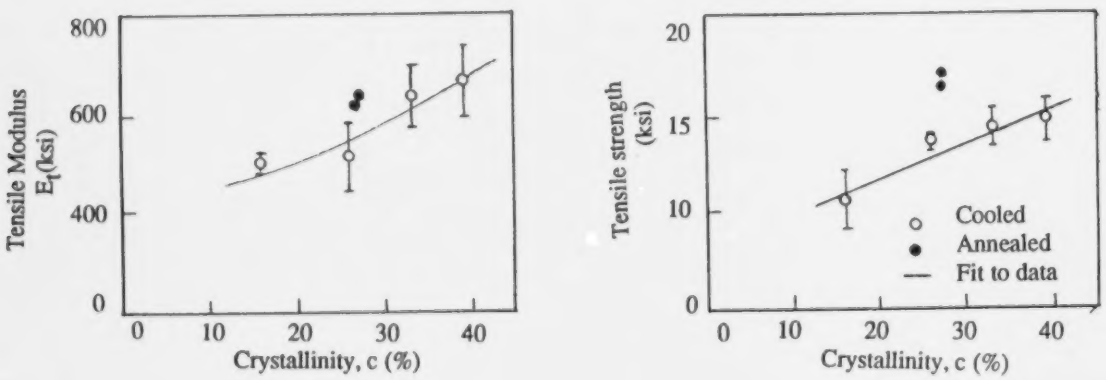

Figure 4.2. Tensile properties of PEEK as a function of degree of crystallinity (**18**)

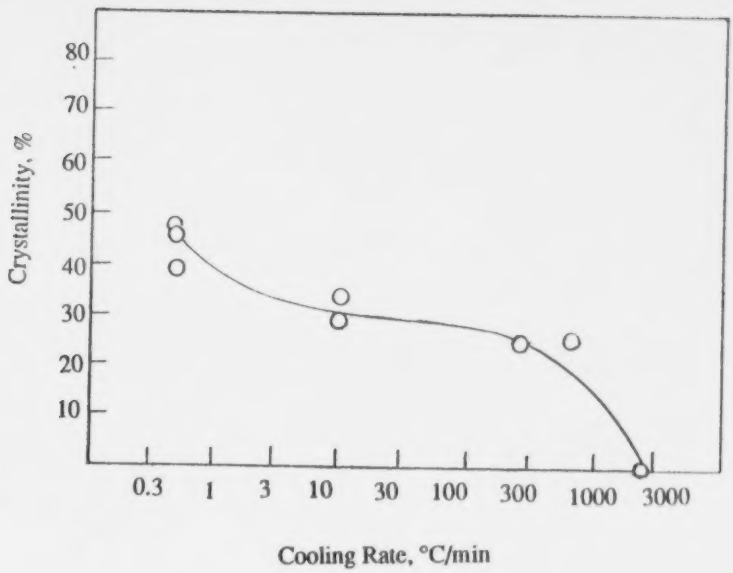

Figure 4.3. Degree of crystallinity of PEEK as a function of cooling rate (17)

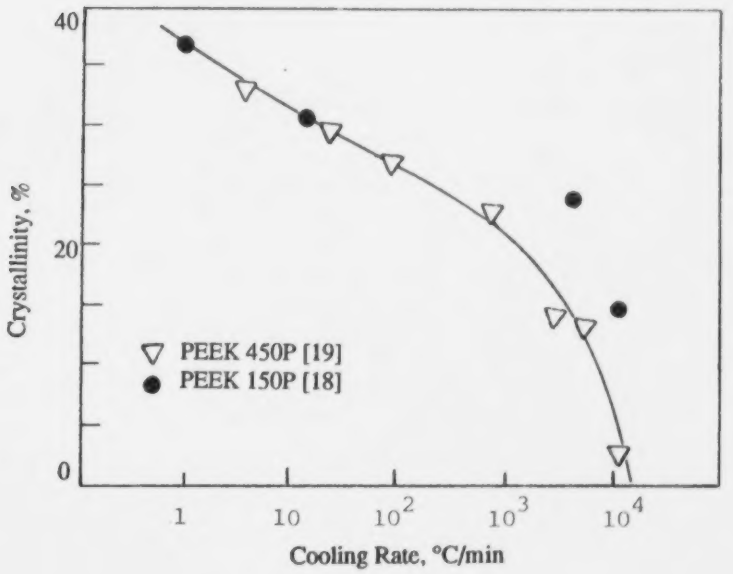

Figure 4.4. Degree of crystallinity of PEEK as a function of cooling rate (18)

Table 4.1. Effect of thermal processing cycle on spherulite size and properties of PEEK resin (**20**)

Process cooling rate	Effect on PEEK morphology	Effect on composite mechanical performance
Quench	Low percent crystallinity	Tough, but lower matrix modulus causes reduced compression strength
Slow cool to nonoptimum crystallization temperature	Large spherulites	Decreased toughness
Fast cool to optimum crystallization temperature	Small spherulites	Increased fracture toughness

Some systems may exhibit trends that differ from the generalities cited above. For example, Beever et al. (**21**) have varied the total mold residence time of the carbon/PPS (polyphenylene sulfide) composite from 7 to 20 minutes and varied the molding temperature from 291°C to 360°C and found no effect on mechanical properties. However, Ma et al. (**22**) have shown different results for PPS alone: long annealing times lead to lower ultimate crystallinity and may change the molecular structure, mechanical properties and thermal stability.

If higher melt temperature and long heating times lead to lower crystallinity, this should be of great concern during a repair process using welding techniques, as heating is localized at the damage area while the surrounding areas have lower temperature. This would result in undesired changes in degree of crystallinity and then mechanical properties in those surrounding areas.

The presence of foreign surfaces (e.g., fibres in a composite) affects morphology of a polymer because the fibre surfaces act as nucleating sites. For carbon/PEEK composites, PEEK was found to crystallize at higher temperatures with higher nucleation densities (higher carbon fibre content of the composite) (**23**, **24**). Blundell et al. (**25**) also observed that nucleation from a PEEK matrix (without fibre) is relatively rare.

Lee et al. (**26**) have found that while the strength and stiffness in both tension and shear increase with crystalline content (as also shown by others, Figure 4.2) compressive strength remains relatively unaffected and fracture energies and toughness decrease significantly with increasing crystalline content (see also Figure 4.1). They also observed that tensile and compressive properties of the polymer were sensitive to processing history, even while having the same degree of crystallinity. This observation was supported by Cebe et al. (**27**) who studied mechanical properties and morphology of PEEK specimens which had different thermal histories. They found that the degree of crystallinity is not as important as processing history. Samples with the same degree of crystallinity could have different tensile properties, depending on rate of cooling. This was the result of the differences in crystal size and size distribution.

CHAPTER 5

VARIABLES AFFECTING THE PROPERTIES OF COMPOSITES

The properties of semi-crystalline thermoplastic-based fibre composites are influenced by different factors as follows.

5.1. Effects of pressure and thermal processing conditions

The processing conditions of pressure, molding temperature, and cooling rate can affect the crystalline and fibre morphology of the polymer, resulting in different properties.

Adams *et al.* (**28**) made and tested single-fibre composites (a dumbbell shaped specimen, containing a single carbon fibre embedded along its axis). They used high modulus graphite fibres and three matrix materials: polycarbonate, polyetherimide and polyester. From experiments, they found that the adhesion of matrix to fibres was improved when specimen fabrication (molding) was changed by increasing the mold pressure and decreasing the cooling rate. They explained that slow cooling rates allowed the material to relax, and resulted in lower residual tensile stresses in the center of the sample. (The higher pressures may have been effective in maintaining good physical contact between surfaces when cooling would normally cause volume shrinkage).

Verdeau and Bunsell (**29**) studied effects of processing conditions on the fibre-matrix interfacial zone. Two polymers were employed with carbon fibre, PEEK (Polyetheretherketone) and PPS (Polyphenylene sulphide), and both are known to be semicrystalline under most conditions but also amorphous if cooling from the melt is sufficiently fast. Specimens were initially made in unidirectional crystalline composite sheets reinforced with carbon fibres by using prepregs obtained directly from the

manufacturers. The volume fractions of the fibres in the PEEK/carbon composite and PPS/carbon composite were 61% and 57%, respectively. Then, three types of thermal treatments were applied to alter the polymer matrix crystallinity: nearly-amorphous, and two semi-crystalline matrices of different crystal morphology were therefore available for study.

The nearly-amorphous matrices (crystallinity, W_c: PEEK = 10 ± 3%, PPS = 5 ± 3%) were obtained by heating composite specimens to the PEEK or the PPS melting point (350°C and 300°C, respectively) or above and then cooling rapidly in a metal press to retard crystal development. Highly developed crystalline matrices (W_c: PEEK = 34 ± 3%, PPS = 51 ± 3%) were obtained by cooling the specimens at slow rates, about 5°C/min. For the third heat treatment, the PEEK/carbon composite specimens and the PPS/carbon composite specimens were heated to T_m + 20° or 30° (380°C and 320°C respectively), held for periods of 120 minutes and then slowly cooled by letting the furnace cool by itself in the room air. The crystallinities of the matrices from the third heat treatment were: PEEK, $W_c = 30 \pm 3\%$ and PPS, $W_c = 58 \pm 3\%$.

Static mechanical tests (including tensile, shear, and bending) were performed and results explained or correlated in terms of the crystal phases and compatibility with the fibre surface. We will highlight only a few of their findings, since most of them were expected--e.g., the low-crystal (LC)/nearly amorphous forms were generally weaker than the two high-crystal (HC) forms, for both PEEK and PPS composites, and the special air-cooled heat treatment (HC*) generally gave better properties than the constant-rate cooling (HC_1). However, the two polymers produced different results in several ways. The transverse tensile modulus increased monotonically with W_c for PEEK, but dropped slightly at the highest W_c (HC*) for PPS. The tensile strength behaved similarly, although for PPS strength of the highest-W_c sample simply did not increase, whereas for PEEK it did. The shear strength for both of the two HC-forms were ranked according to $HC^* > HC_1$ regardless of W_c value, for both polymer systems. However, for PPS the

strength dropped so greatly for the HC_1 case that it was less than the LC case (unlike PEEK).

The authors explained these different behaviors, and particularly the inferior performance of PPS, in terms of delamination during cooling. They proposed that for PPS, during crystallization, a shrinkage of the matrix occurred which led to "weakening" of the interface. And from photomicrographs of fracture surfaces of the amorphous and high-crystallinity composites, the PPS/carbon system showed clean fibres (delamination) while the PEEK/carbon composite showed fibres well coated with a layer of PEEK. This demonstrated that PPS/carbon had a very poor adhesion at the interface and PEEK/carbon much better, but the authors did not explain why the shrinkage of PEEK matrix did not cause loss of adhesion and corresponding decrease of the mechanical properties of the PEEK/carbon composite. But, clearly, the ability to maintain interfacial contact and a tight grip by the matrix on the fibre was important.

Two secondary results emerged, to help explain differences between the quality of PEEK and PPS composite properties. The superior PEEK performance for HC* (with only $W_C = 0.30$, vs. $W_C = 0.34$ for HC_1) was attributed to the presence of transcrystallinity (monodimensional crystal growth perpendicular to the fibre axis) in the PEEK/carbon composite, which was absent in the PPS/carbon composite. This transcrystallinity was believed to increase the rigidity of the PEEK/carbon composite. And, the inferior PPS performance might have been induced by thermal degradation. The increase of the treatment temperature, or of the treatment time, in PPS/carbon composite apparently caused a decreased molecular weight of the PPS. The reduced molecular weight might explain the increased crystallinity (to 58%), since the shorter chains would have greater mobility in the melt and more capability to settle into a well-organized crystal lattice than their longer counterparts. However, the reduced molecular weight must damage other aspects of the PPS mechanical properties, as thermal degradation is rarely

desirable, and this may have been more important than the W_c increase in determining the composite performance.

5.2. Effects of fibre diameter and volume fraction

Nair *et al.* (**30**) studied the mechanical properties (plane-strain fracture toughness, K_{IC}, using a three point bend method on pre-cracked 6.35 mm thick bend bars) of composites composed of nylon 6,6 reinforced with short glass fibres at various fibre concentrations. Composites were made by dry-blending fragments of nylon 6,6-based fibre-reinforced composites (supplied by Monsanto Chemical Company) with pure nylon 6,6 followed by melt injection molding. E-glass fibre with nominal 13 μm diameter and G-glass fibre with nominal 9.5 μm diameter were used. Eight concentrations of glass fibres (0%, 1%, 5%, 10%, 20%, 25%, 30% and 40% by weight of the matrix) were made by a dilution process; concentrations below 40% were made by diluting the 40 wt% glass composite with additional nylon 6,6. It was found that, for identical volume fractions of fibre, the composite with the smaller-diameter fibre had the higher tensile strength but the lower ductility.

Fibre concentration effects show some complexity. The addition of small amounts of glass fibres (up to 10 wt%) increased material stiffness and tensile strength, as expected, but obviously reduced the fracture toughness of the composite. Moreover, at these low concentrations (only), the reduction of fibre diameter further reduced the fracture toughness. The authors suggested that the fracture behaviour of nylon 6,6 composites is controlled by the competition between two matrix phenomena at the fibre ends: fibre-induced load embrittlement and matrix plasticity. The reduction of fracture toughness at low fibre concentrations was found to result from an increased nylon embrittlement at fibre ends for the smaller fibre diameter. For a composite with high glass fibre content (beyond 10 wt%), a reversal of fibre diameter effects on fracture toughness

was found. For these cases, the reduction of fibre diameter increased the fracture toughness of the composite, apparently due to local ductilization of the matrix at the fibre ends and consequent increased plasticity in front of the crack tip. They also found, for these higher fiber concentrations, that an increase of glass fibre content caused higher values of the tensile strength and the fracture toughness (a reversal of the $V_f < 10\%$ case).

Otaigbe and Harland (**31**) used mats of continuous-glass-fibre (diameter 15 μm, from Vetrotex (U.K.) Ltd.) to make nylon 6 composites with glass volume fractions of 0.17, 0.22, 0.26, and 0.33; this work is the closest to ours of any in the literature, and the present project is an outgrowth of theirs (made possible by Dr. Otaigbe's recent activity in our research group as a Postdoctoral Fellow). They found that composite modulus and strength increased with V_f steadily but nonlinearly and with different rates. For example, they measured pure nylon 6 to have σ_b = 43.6 MPa and E = 1.45 GPa, and a composite with V_f = 0.17 to have σ_b = 52.3 MPa (20% increase) and E = 2.90 GPa (100% increase); a doubling of V_f (to 0.33) produced σ_b = 65.3 MPa (total of 50% increase, more than a doubling) but only E = 3.74 GPa (total of 158% increase, less than a doubling). Moisture effects were absent, as samples were dried in a vacuum oven maintained at 100°C, to constant weight, and stored in a desiccator until testing began .

5.3. Effects of moisture on properties of thermoplastic composites

Otaigbe (**32**) studied the effect of moisture (equilibrium hygroscopic state at 20°C) on the tensile stress-strain behavior of the same type of composite (no coupling agent) at 33 vol% fibre. Specimens were cut from the molded composite sheet and dried as described above (**31**) for "dry samples". Wet samples were prepared by immersing the dried samples in boiling water until constant weight and then immersed in cold water at room temperature for at least 2 weeks. The wet samples contained 10.0 and 6.9 weight percent water for the nylon 6 and composite, respectively. Results showed that the dry

composites displayed failure in an unambiguous and obvious way, while the wet materials underwent gross yielding, with stress passing through a maximum before decreasing, and with no precise fracture point. He observed from photomicrographs, using optical and scanning electron microscope, that in wet materials most of the failure occurred at the fibre-matrix interface. He included in this study the effect of moisture on composites with coupling agent, γ-amino propyl triethoxy silane, which is described further in the following section.

His data revealed that moisture decreased tensile strength from 65.3 MPa (dry uncoupled) to 23.9 MPa (wet uncoupled), and from 95.4 MPa (dry coupled) to 36.8 MPa (wet coupled), decreased modulus from 3.74 GPa (dry uncoupled) to 1.41 GPa (wet uncoupled), and from 4.68 GPa (dry coupled) to 3.54 (wet coupled), decreased tensile breaking-strain from 3.38% (dry uncoupled) to 2.52% (wet uncoupled), and from 3.71% (dry coupled) to 1.26% (wet coupled). He explained that the large moisture-induced reduction in tensile strength was due to moisture-induced dewetting or debonding of the fibre surfaces from the adjacent nylon 6. Because the wet materials showed no precise fracture point, but rather a maximum in $\sigma(\varepsilon)$ followed by a gradual drop in σ (as ε increased greatly) until near-zero values were reached, the breaking stress was taken as the maximum point in the $\sigma(\varepsilon)$ curves of the wet materials in his study and ε_b from that $\sigma_{max}(\varepsilon)$ point too. This is the reason why his ε_b values were lower than those reported by others; the true ε_b values were higher than $\varepsilon = \varepsilon\ (\sigma_{max})$.

Moisture sensitivity with nylon 6 and its composites has been reported often. For example, the mechanical properties of nylon 6 and 30-35 wt% glass fibre-reinforced nylon 6, listed in "Modern Plastics Encyclopedia' 92" (**12**), show for moist environments (different from Otaigbe's) a decrease of tensile strength, and tensile modulus (as did Otaigbe) but <u>increase</u> of elongation at break (opposite to Otaigbe's result, surely due to his measuring $\varepsilon_b = \varepsilon\ (\sigma_{max})$ which is lower than ε at true ε_b).

5.4. Effects of fibre surface treatment

5.4.1. Coupling agent

As we know, adhesion between a silicate glass fibre surface and a hydrocarbon polymer matrix is not very strong, so that coupling agents are widely used to improve the interfacial adhesion.

Jenneskens *et al.* (**33**) studied the evidence for interfacial amide formation between surface-bound poly(3-aminopropyltrisiloxane) and nylon 6 in composites reinforced with glass beads at 30 wt%. The glass beads were pretreated by immersing 0.5 g glass beads in a mixture of toluene, water (molar concentration three times that of the coupling agent), and 3-aminopropyltriethoxysilane (10 wt%) with the end carbon (bonded to the amine nitrogen) being either ^{13}C or natural-abundance $^{12}C/^{13}C$. The mixture was stirred for 1 hour at room temperature and the glass beads filtered off and dried under vacuum at 100°C for 1 hour. During the pretreatment, ethoxy groups of 3-aminopropyltriethoxysilane were hydrolyzed in aqueous solution to yield silanol groups which reacted with the hydroxyl groups on glass surface and between adjacent silanol molecules on the surface, resulting in a poly(3-aminopropyltrisiloxane) network layer bonded to the glass surface (see detail of reaction in p. 18 and Figure 3.2). These glass beads were later isolated from the composites by dissolving the matrix in trifluoroethanol. The amount of surface-bound organic on the glass beads, determined with thermogravimetry, was far greater than a mere monolayer of the glass-bonded silane molecule could account for. The analysis revealed that there had been formation of covalent chemical bonds in the polymer melt between some of the amine groups of the surface-bound poly(3-aminopropyltrisiloxane) and nylon 6 carboxylic endgroups in the interface region during composite preparation.

Hamada *et al.* (**34**) studied the "crushing performance" (the specific energy absorption value) of glass cloth/epoxy composite tubes with different glass surface treatments. (In this work the author did not study the untreated-glass-surface composite to compare those properties with the treated ones). The composite tubes were fabricated from woven glass cloth/epoxy prepreg sheets. Two types of prepreg were used: prepreg that contained glass surface-treated with acryl silane (which gives poor interface bonding) and prepreg that contained glass surface-treated with amino silane (to give good interface bonding; the author did not give the name of amino silane used). Tubes used in the axial crushing experiments were made by mandrel wrapping of prepreg sheets (43 vol% of glass cloth) with the warp and weft directions parallel to the hoop and axial directions of the tubes.

From axial compression tests, the amino-silane-treated material was found to have specific energy absorption approximately 25% higher than that of acryl-silane-treated material. Tensile strength, bending modulus, interlaminar shear strength (ILSS), and Mode I fracture toughness were also tested. Those tests employed flat specimens, made from 10 plies of prepreg sheet, fabricated by a hot pressing method. It was found that the tensile modulus was almost the same for amino-silane-treated materials and acryl-silane-treated materials (as one might expect, since no debonding occurs in the low-strain E measurement). But for other properties, the amino-silane-treated glass/epoxy composites showed a 28% higher tensile strength, 23% higher bending modulus, 44% higher bending strength, 29% higher ILSS, and 19% higher fracture toughness, than the corresponding properties of the acryl-silane-treated specimens. Fibre/matrix debonding was observed on both the compression and tensile sides of the bending specimen, with the stress-whitened regions being wider in the acryl-treated material (hence, more delamination) than in the amino-treated one.

Otaigbe (**32**) studied the effect of γ-amino propyl triethoxy silane coupling agent on the properties of his glass/nylon composites (described in Sec. 5.2). He added to

the pre-reaction mixture of ε-caprolactam an amount of the coupling agent equal to 1.5 wt% of the glass mat used. The low-viscosity 100°C caprolactam solution then entered the glass-filled mold, and the silane contacted the glass as the temperature was raised to 150°C and polymerization occurred. This use of silane, with a glass loading of $V_f = 33\%$, increased the composite tensile strength from 65.3 MPa (uncoupled) to 95.4 MPa (coupled), tensile modulus from 3.74 GPa (uncoupled) to 4.68 (coupled), and the ultimate strain from 3.38% to 3.71%. This increment of mechanical properties of coupled composites demonstrated that this coupling agent successfully improved the interfacial adhesion between the fibres and the matrix. It also provided some protection from moisture (see Figure 3.3); although the wet samples lost considerable strength (σ_b reduced from 95.4 to 36.8 MPa), the result was still better than when no coupling agent was used (σ_b reduced from 65.3 to 23.9 MPa). Interestingly, the fractional reduction was about the same in both the uncoupled (-63.3%) and coupled (-61.5%) cases.

Karian *et al.* (**35**) dry-blended polypropylene homopolymer with 30 wt% of type E fibreglass (13 μm fibre diameter, 4.76 mm fibre length and approximately 3450 MPa fibre tensile strength) and added an acrylic-acid-grafted polypropylene (AA-g-PP) coupling agent at concentrations ranging from 0 to 15 wt%. Each dry blend was compounded into pellets via a 63.5 mm single screw extruder, and the pellets were converted by injection molding into ASTM tensile bars for testing. They found that the interfacial shear strength increased by 90% as the level of AA-g-PP increased from 0% to 15% of AA-g-PP. The tensile strength increased by 17% as the AA-g-PP concentration increased to 10%, but it then reached a constant plateau for higher concentrations.

Borden *et al.* (**36**) used maleic anhydride modified polypropylene (thus containing polar functionality) as a coupling agent, blending it in a mica-filled polypropylene. They found improvement of the physical-mechanical properties with the increase of polymeric coupling agent. With a 30% mica-filled system, addition of 10%

coupling agent resulted in an increase in tensile strength by 9%, in flex modulus by 29%, and in flex strength by 10%.

5.4.2. Plasma treatment

"A plasma is a system of gaseous ions and radicals formed by radio-frequency (megahertz) induction across a gas at low pressure" (**37**).

Chang and Jang (**38**) found that pretreatment of carbon fibres with oxygen plasmas effectively improved the interfacial adhesion between the carbon fibre and bis maleimide matrix. Increase of oxygen content and polarity induced in the modified carbon fibre surface were observed. The composite transverse tensile strength increased from 2.20 MPa (untreated) to 4.71 MPa (20-minute treatment). However, exposure of fibres to the plasmas degraded the tensile strength of the fibre from 3.8 GPa (untreated) to 3.0 GPa (20-minute treatment). Therefore, an optimal treatment time was needed. They found that for short exposure time (less than half a minute) the fibre surface remained smooth (hence no external physical damage) and acquired an increase of surface free energy; this promoted wettability of fibre by matrix and produced stronger van der Waals forces. Longer exposure time caused the fibre surface to become rougher which would promote a desirable physical interlocking mechanism between the fibre and the matrix.

Hinkley *et al.* (**39**) found improvements in adhesion of polycarbonate and carbon fibre composites made from unsized fibre treated in a continuous plasma treatment. (The authors did not give detail what kind of gases were used in their plasma treatment)

Gaur and Davidson (**40**) treated aramid fibre (Kevlar) with different types of plasmas: oxidizing plasma, reducing plasma, neutral plasma, and hydrophilic plasma. A small amount of epoxy resin was applied to the surface of each treated fibre, and the interfacial shear strength of these fibres tested by microbond technique. They found increments of interfacial adhesion for all the plasma-treated fibres, up to 7.9 times

(interfacial shear strength of plasma-treated/untreated), irrespective of the chemical nature of the ionized gas. The adhesive bond strength was believed to be improved due to texturing of the fibre surface.

Yuan *et al.* (**41**) etched carbon fibres by an oxygen or an argon plasma and found large improvements of interfacial shear strength (IFSS) with etched carbon/PPS composites, up to 2.5 times (IFSS of plasma-treated/untreated). They observed that higher plasma powers resulted in higher IFSS values.

5.4.3. Other chemical treatment

Yip and Lin (**42**) treated surfaces of five different kinds of carbon fibres with three different oxidizing chemical reagents (60% concentrated nitric acid, 15% hydrogen peroxide, and concentrated phosphoric acid) to modify surface characteristics. Scanning electron microscope (SEM), scanning Auger microprobe (SAM), and X-ray photoelectron spectroscopy (XPS or ESCA) techniques were used to characterize surface morphology and chemistry of these treated fibres. The chemical treatments increased both the oxygen surface concentration and surface roughness ("etching"). They found that the extent of oxidation on the carbon fibre surface depended on the chemical reagents rather than on the surface structures and the precursors of the fibres. The adhesion of carbon fibre to the epoxy resin was not promoted by the amount of oxygen or carbon-oxygen functional groups on the fibre surface but by the roughness at the surface which enhanced the mechanical interlocking and physical mating of carbon fibre and epoxy resin. The transverse tensile strength of fibre composites was improved up to 2.9 times (transverse tensile strength of treated/untreated).

5.4.4. Influence of fibre/matrix interfacial adhesion on composite fracture behavior

Lee (**43**) studied the effect of fibre/matrix interface strength on various composite properties, employing explicitly carbon fibre/epoxy composites. Unidirectional composites were made of toughened epoxy and carbon fibres, with and without surface treatment. In this case carbon fibres were treated with a release agent to yield a poor fibre/matrix interface. The specimens of good interface strength (using untreated carbon fibre) and poor interface strength (using treated carbon fibre) were carefully made, with good-quality prepregs prepared by controlling fibre spacing, alignment, and resin content of the laminates so that the effect of the fibre/matrix interface could be observed without being affected by other processing parameters. These composites were then subjected to a number of tests, divided into two modes. One mode consisted of tests involving propagating pre-existing delamination cracks, such as double cantilever beam (DCB), end-notched flexural (ENF) and crack lap shear (CLS) methods. The other mode was testing that had to initiate cracks in specimens without pre-introduced cracks, such as impact and edge delamination. He reported that the material properties of the first mode were not appreciably affected by surface treatment, whereas the test of materials of the second mode were highly sensitive to the fibre/matrix interface.

5.5. Effect of void content

It is found generally that composites tend to contain voids which reduce their maximum possible strength and diminish the advantages sought by the strategies of composite manufacture.

Fan (**44**) studied the effect of void content on composite flexural strength and modulus of elasticity, because these are the major properties in any structural design. Using the rule of mixtures, he derived an engineering formula to estimate the degradation

of mechanical properties as functions of void content. The formula fitted the flexure data of Ghirose (**45**), on carbon fibre/epoxy composites, within ± 5%, as long as the voidage did not change appreciably during the test. In the one example displayed by Fan ($\overline{V}_f$ unknown), a void fraction of 2.0% in the composite reduced the flexural strength by 10%, and increasing V_v to 5.0% led to a total drop in strength of 20%. The paper by Ghirose (**45**), which can serve as a rare but excellent review of this topic, states that the highest quality composites should have $V_v \leq 1\%$ but that voidage up to 5% can be tolerated (or cannot be reduced any further) in some lower-quality products.

CHAPTER 6

FABRICATION OF GLASSFIBRE/NYLON 6 COMPOSITES

6.1. Equipment

The equipment consists of two parts: mold, where the polymerization takes place, and chemical vessel (from which the nylon monomer and other ingredients flow into the mold). The overall arrangement is shown in Figure 6.1.

6.1.1. Mold

The mold consisted of a male and a female part. Major dimension are given directly on Figure 6.2. The male part was fitted with a Viton o-ring to ensure vacuum tight conditions in the mold. A tapered hole was drilled through the centerline of the male part to allow the reaction mixture to fill the mold from above. The female part was drilled from the side with a hole of diameter 3.6 mm (9/64"), connecting to a valve leading to a vacuum pump to evacuate the mold. The mold was machined from rectangular slabs of aluminum alloy, selected to ensure good thermal conductivity, and heated by 8 cartridge heaters. Four of the heaters (400 W each) were in the male part of the mold, placed vertically and spaced at 90° intervals around the mold centerline; the other four heaters (250 W each) were in the female part of the mold, placed horizontally along radii at 90° intervals that were spaced about 22.5° to the vertical heaters above. A thermocouple was inserted into the female part, closely below the recess containing the polymerizing fluid and glass fibres (shown in Figure 6.1) and connected to a digital temperature readout and on-off controller which activated all 8 heaters simultaneously. The mold, pre-loaded with

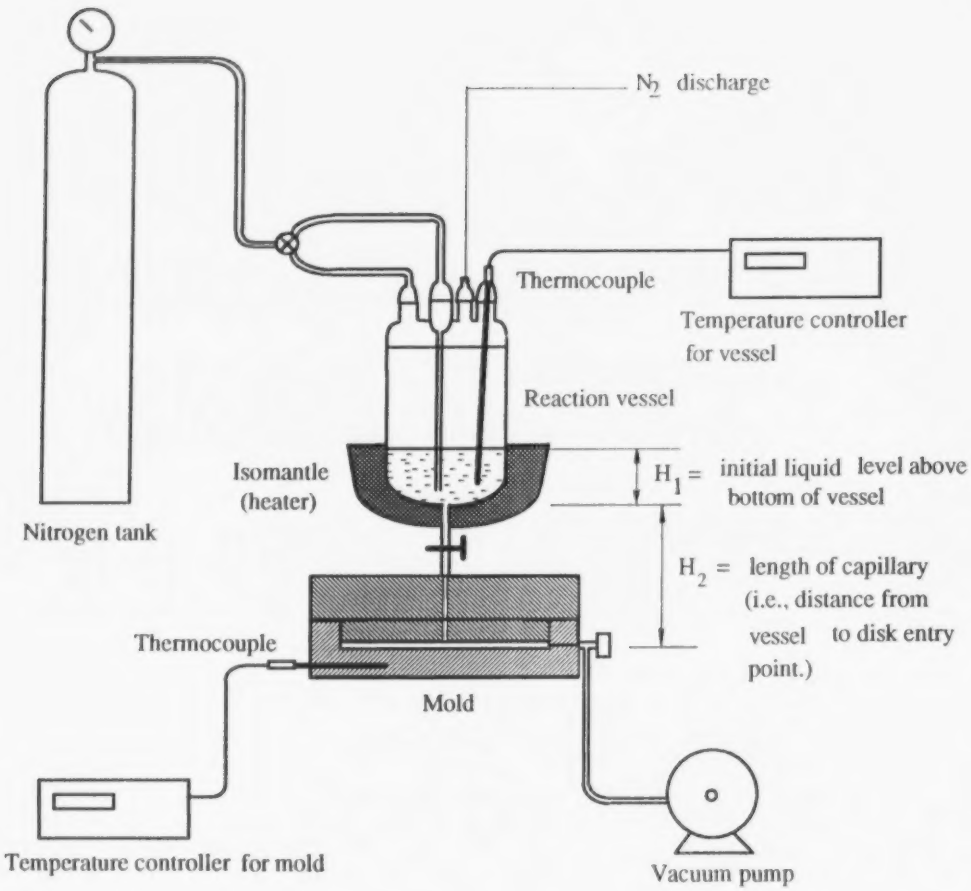

Figure 6.1. Diagram of experimental equipment ($H_1 \cong 60$ mm, $H_2 \cong 150$ mm)

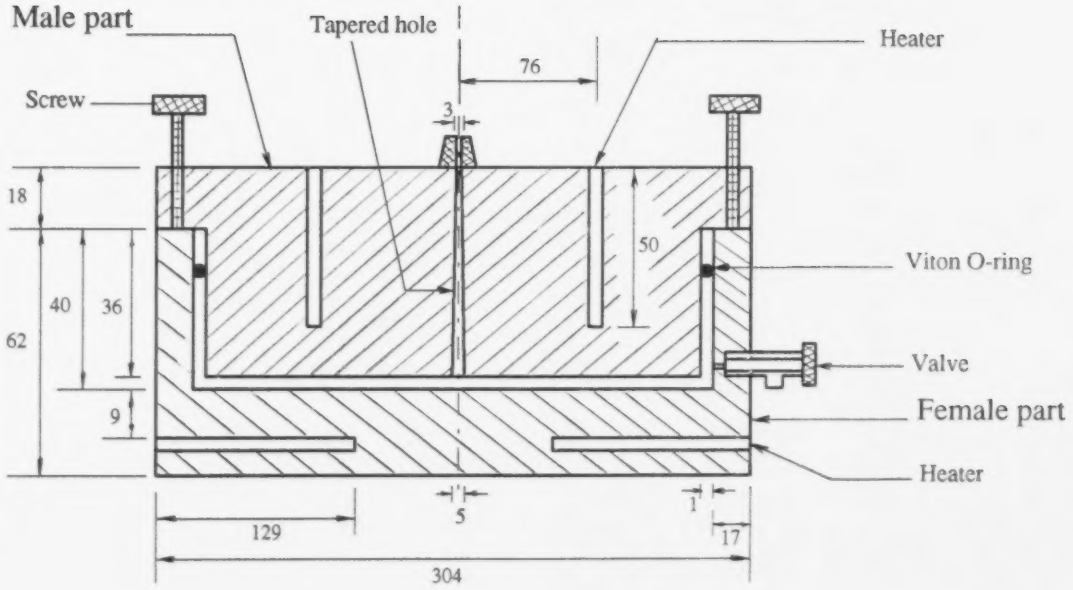

Figure 6.2. Mold diagram (not to scale) unit: mm

compressed glass-fibre mats for encapsulation by polymer, was held tightly shut by 4 C-clamps. Its outer surface was insulated by fibreglass cloth tape and Kaowool blanket to minimize heat loss and temperature gradients within the polymerizing caprolactam. To open the mold, after polymerization had occurred, the 4 screws in the top of the male part were turned to exert force against the female part, breaking any polymer seal and lifting the male part up for manual removal.

6.1.2. Temperature inside mold

The metal surface temperature inside the mold was measured (Appendix A) along upper and the lower surfaces, at different radii and angular positions of the mold as shown in Figure 6.3. Both radial and vertical temperature gradients were found. The steady-state temperature of the upper part was always slightly higher than that of the lower part, a $\Delta T(z)$ ranging from about 2° to 5° (near rim) when the target was around 150°C (Figures 6.4 and 6.5). The mold had higher temperature near the center and lower temperature toward the edge of the mold, the total radial gradient $\Delta T(r)$ being about 1°C across the upper surface and 4°C across the bottom surface when the overall level was 150°C. The temperature along a path directly above a lower heater position was higher than that along the path equidistant between two heaters by about 1°C. The only puzzling feature of the data in Figure 6.4 and 6.5 is the apparent drop in temperature on the lower surface at position L_{30}, which is seen in both Figures 6.4 and 6.5. This is probably due to an inadequate thermal contact between the aluminum surface and the thermocouple. Contact was secured in all cases by strips of fibreglass tape, but these could become loose; it was noted that thermocouples were occasionally displaced and had to be repositioned. Therefore, the reason for low temperature readings at L_{30} might be the loose contact of the thermocouple at this position. All these spatial temperature variations were regarded

Caption for Figure 6.3

Locations of thermocouples on the upper and lower surfaces of the mold cavity. Their proximity to the electric heating rods, embedded in the aluminum upper and lower parts, is also given.

(a) Upper surface, seen from below. Positions are designated as "NU_n" where n is radial distance in millimeters, U refers to the upper surface, and N = 1 or 2 to indicate alignment along a radial path that passes either (1) under one of the upper vertical heaters or over one of the lower horizontal heaters, or (2) halfway between two such positions. At position $1HU_{76}$ we use N = 1H to highlight its placement directly under one of the vertical heaters, a location which has the greatest likelihood of being a "hot spot" on the upper surface.

(b) Lower surface, seen from above. Positions are designated as either "L_n" or "HL_n", where n is the same as in (a), L refers to the lower surface, and H indicates alignment on a radial path that passes directly along and above one of the lower horizontal heaters, thus possibly being a "hot line" and containing a local hot spot at r = 76 mm. The unprefixed L_n locations lie on a radius halfway between two of the HL trajectories. The dashed line represents the position of the horizontal thermocouple well beneath the surface, for insertion of the sensing control thermocouple which was always pushed to the end of the well.

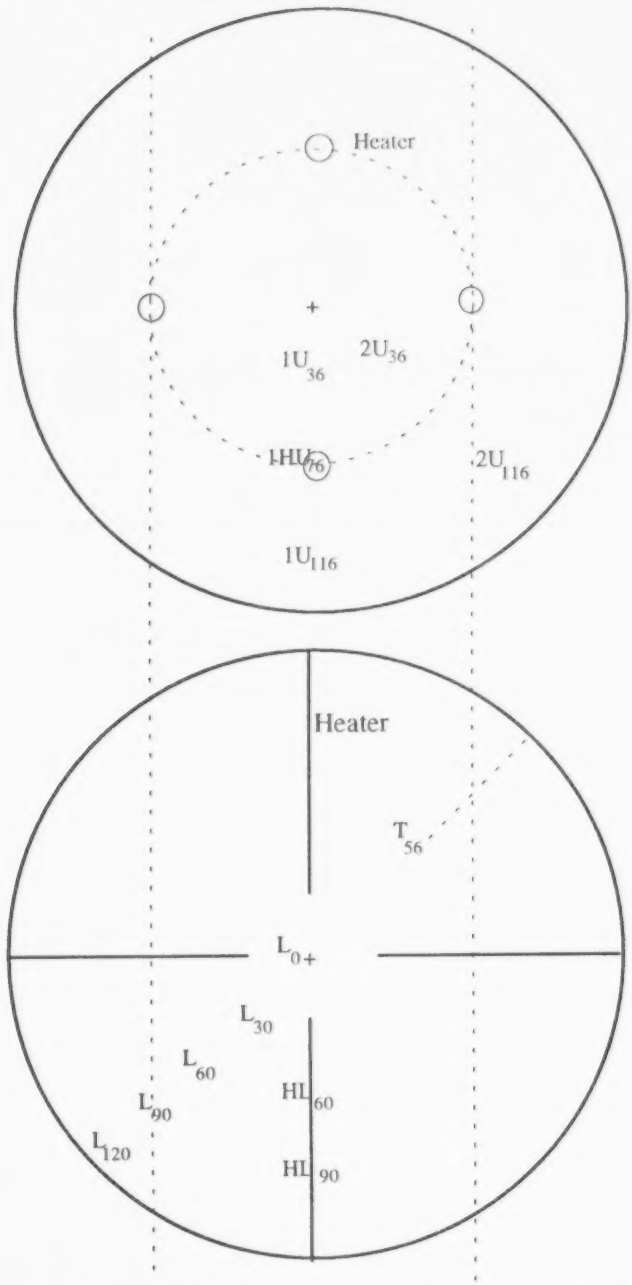

Figure 6.3. Locations of thermocouples on the upper and lower surfaces of the mold cavity.

NU_n	:	U	=	Upper surface
		N	=	Radial path, (N = 1, 1H (below heater), 2)
		n	=	Radial distance, mm
L_n	:	L	=	lower surface
HL_n	:		=	Lower surface above heater
T_n	:		=	Thermocouple

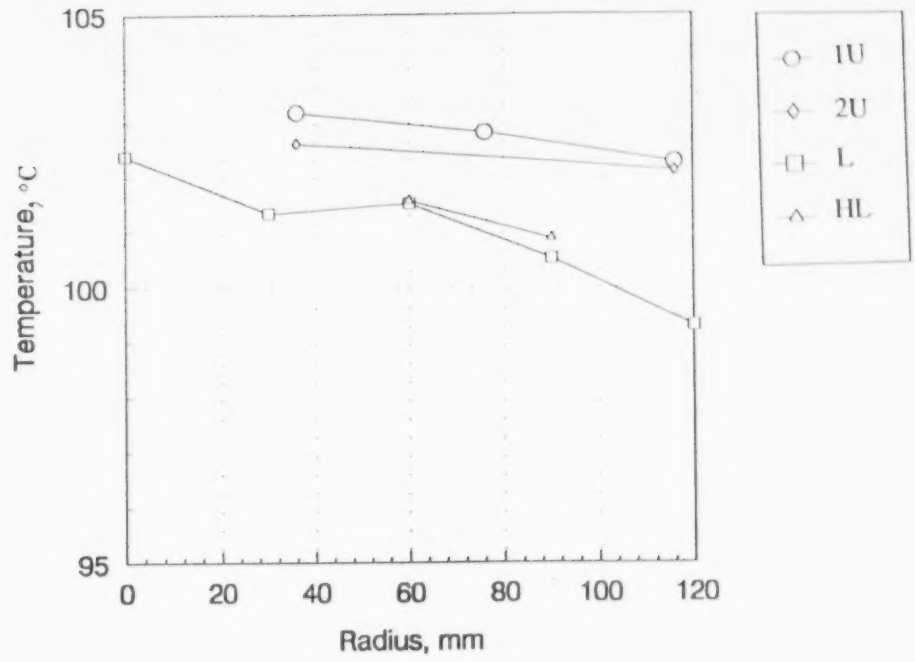

Figure 6.4. Temperature distributions on mold surfaces when nominal set point is at 100°C

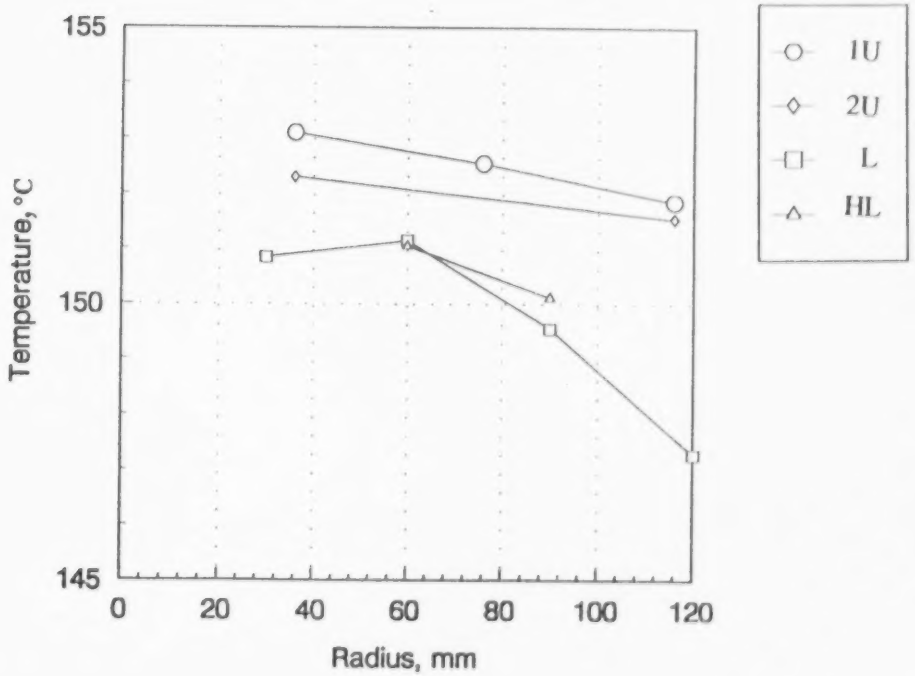

Figure 6.5. Temperature distributions on mold surfaces when nominal set point is at 150°C

small enough to neglect, in the sense of being unable to cause major localized variation in the polymerization process or in final product properties. Therefore, the mold was assumed to have a uniform temperature at whatever steady-state level was set (e.g., 100°C or 150°C) .

6.1.3. Chemical vessel

The chemical vessel (Figure 6.1) was a cylindrical-shaped glass flask with round bottom to which was attached a long glass tube (inside diameter 5 mm., length 40 mm) used for delivering the flask contents to the mold below, through a short silicone rubber tube. The temperature of the vessel liquid was maintained by a temperature controller, which received a signal from a thermocouple inserted inside the vessel and regulated power to an isomantle (heater) around the vessel to achieve the desired set point. A small screw clamp on the silicone rubber tube was used to prevent molten caprolactam from flowing down into the mold until some later desired time. Two nitrogen lines entered the vessel, one through a long tube extending to the flask bottom and the other entering the vapor space above the liquid; the N_2 exit for both was a vent to atmosphere atop the flask, which could also be closed as desired. When degassing was performed, the N_2 exit was connected to the vacuum pump instead and disconnected when atmospheric pressure was needed.

6.2. Polymerization technique

The formation of a reinforced thermoplastic sheet, followed by thermoforming to a desired shape, is a frequent procedure in the pressing operations of the automobile industry. Presently, the glass-fibre reinforced thermoplastic sheet (**46, 47**) is produced by extruding molten polymer in one of two ways: (a) mixed with short glass fibres extruded

into rectangular slabs and then rolled to sheet dimensions, or (b) as a pure but highly viscous liquid onto a continuous glass (swirl) mat or chopped strand mat, then forced under high pressure (and perhaps with heating) to permeate the mat. The problems of this latter method are related to (i) nonuniformity of penetration of the mat, (ii) the difficulty of coating all surfaces of the glass fibres, and (iii) the need for high pressures (due to high viscosity of the polymer). Problems of the former method arise from undesired and non uniform orientation of the short fibres in shear flow and associated nonuniform distribution of the glass fibres in the composite sheet (as well as high extrusion pressure). Because of these problems, there is considerable incentive to design new methods for producing long-fibre (or continuous fibre) composites.

Ishida and Rotter (**48**) have developed a new processing method, a combination of RIM (Reaction Injection Moulding) and a pultrusion process, called RIM-Pultrusion (Figure 6.6), to produce composites in a continuous manner. Polyurethane was used to verify the viability of this modified process for thermosets, and nylon 6 was used for thermoplastics. The reaction for nylon 6 is ring-opening anionic polymerization; ε-caprolactam, phenyl isocyanate and sodium hydride were used as monomer, catalyst and initiator, respectively (see Chap. 2). It was found that the nylon 6/glassfibre (rovings) composite was successfully produced by RIM-Pultrusion. The products represented good surface quality and substantial mechanical integrity.

Otaigbe and Harland (**31**) made nylon 6 and glass fibre composites by placing a continuous strand (swirl) glass fibre mat in a mold similar to ours and then injecting under vacuum the reactive liquid mixture containing caprolactam monomer, sodium hydride, and phenyl isocyanate. The fibre volume fraction distribution across the diameter of the composite seemed to be uniform; the crystallization of the matrix was over 50% . This technique ("*in-situ* polymerization") produced a sheet of material that could be thermoformed and had uniform distribution of glassfibre in the composite.

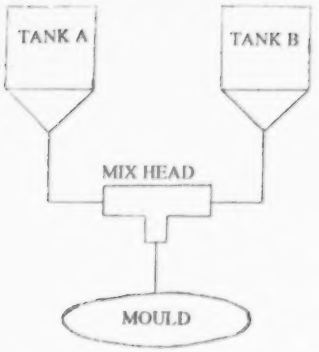

(a) Reaction injection molding process

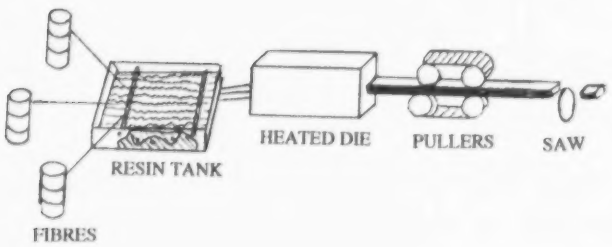

(b) Pultrusion process

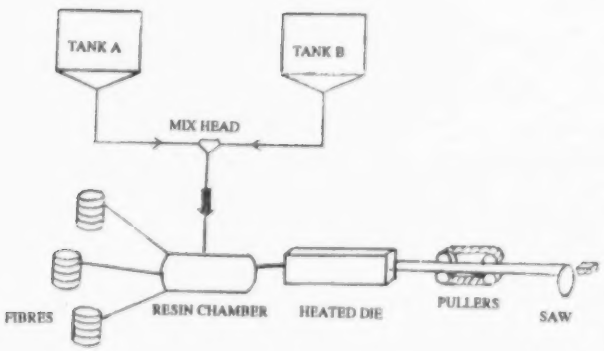

(c) RIM-Pultrusion process

Figure 6.6. Modification of reaction injection molding process and pultrusion process called RIM-Pultrusion process (a) Reaction injection molding process (b) Pultrusion process (c) RIM-Pultrusion process(46)

The process used by Otaigbe and Harland had a number of advantages. The low-viscosity injected caprolactam permeated the mat easily, without application of pressure, and easily wet the glassfibre. The temperature for liquid processing of the caprolactam monomer was lower than that needed to process nylon 6, since T_m = 72°C for the monomer and 225°C for the polymer*; moreover, the highest temperature used was the post-flow polymerization temperature 150°C that was set in the mold. Reduction in operating cost was also achieved, because of the accumulation of all the advantages cited above. For these reasons, it was decided that the composites in this study would be made by the same technique (see Figure 6.7), with some mold modifications applied to overcome operational problems and some fibre surface modifications to enhance composite properties. These will be detailed below.

6.2.1. Mold preparation

First, silicone grease and silicone release spray (Dow Corning Corp.) were applied inside the mold to ensure easy post-polymerization removal of specimen disks. The grease was applied around the cylindrical surface inside the mold (female part) and around the o-ring rubber (male part), while the release spray was applied at the flat surface of both female and male parts and also in the tapered hole at the centre of the male part.

Continuous-strand glass "E"-fibre mat, non-woven and planar-random (grade M8608), was obtained in rolls from Fibreglass, Canada. Characterization data

* Rodriquez points out (**49**) that unreacted monomer which would remain as about 10% of an equilibrium mixture with molten nylon 6 can be minimized in the final product if the reaction takes place at T<225°C (presumably because removing the polymer by immediate crystallization drives the equilibrium toward full consumption of caprolactam).

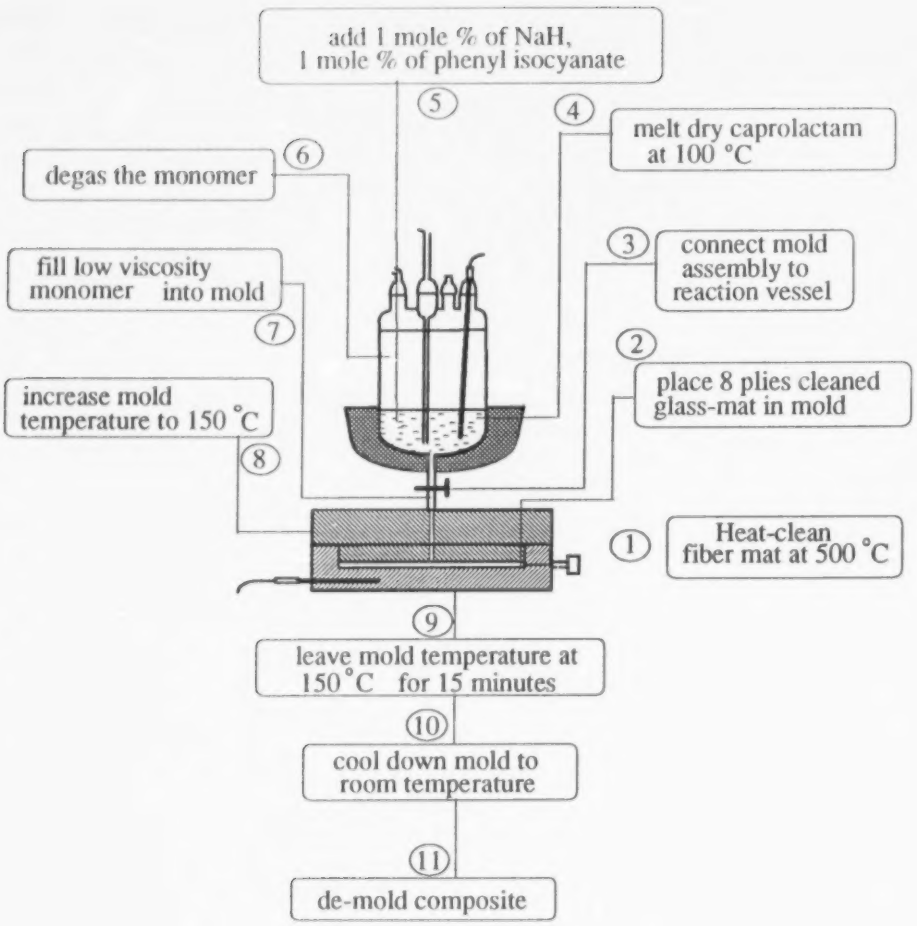

Figure 6.7. Procedure to make nylon 6/glassfibre composite

supplied by the manufacturer are: filament diameter = 20 μm, filaments/strand = 36-37, textile (strand) weight = 25 g/km, mat rest thickness = 1.02 mm, mat areal weight = 450 g/m^2, σ_b = 1.86-2.0 MPa, ε_b = 4.5-4.9%, E = 69.0-72.4 GPa. From these rolls, mat disks were cut with a scissors to a diameter of 22 cm. In most commercial glass-fibre mats, chemical agents called sizing are applied to the glass surface to prevent breakage of fibres and promote fibre/matrix adhesion. The size is usually an aqueous emulsion containing processing aids, such as an anti-static agent, a lubricant, a wetting agent, a binder, and adhesion promotors. If these sizing agents are compatible with nylon 6 and it would not be necessary to clean the glass-fibre mat. In this work, an attempt was made to use directly the glass-fibre mat with its as-received sizing to make a glass-fibre/nylon 6 composite. The resulting composite was brown due to the color of burnt sizing compound, and the composite was so brittle that it could be broken by hand.

This showed that this sizing was not compatible with our nylon 6, and the glass-fibre mat had to be cleaned before use. Glass-fibre mat (already cut) was heated in a muffle furnace, in air, at 500°C about 1 hour to remove the sizing (coated onto fibres by the manufacturer as a coupling agent for use with epoxy matrix). The color of the glassfibres turned from white to dark brown (due to color of the burnt sizing) and then turned to white again when there was no more sizing.

Eight of the heat-cleaned glass fibre mats were placed inside the lubricated mold. This 8-ply stack, rising above the desired sheet height of the mold, was then compressed as the mold was closed firmly by 4 C-clamps (the 8-ply specimens thus all have a fibre volume fraction V_f of about 0.33). Next, the insulator (Kaowool), which was cut in two circular-shaped pieces to cover the top and bottom part and a rectangular piece to wrap around the edge of the mold, was installed with tape. The vacuum pump was turned on, with the pinch-cock on the silicone tubing closed, to evacuate the fibre-filled mold to a pressure of about P = 5 kPa, after which the vacuum was sealed by closing the

valve at the side of the mold. The temperature of the mold was raised and maintained at 100°C by appropriate setting of the controller.

6.2.2. Preparation of activated monomer in vessel

The polymerization of caprolactam in this experiment is anionic, using sodium hydride (Aldrich 60% dispersion in mineral oil) and phenyl isocyanate (Aldrich 98% pure) as initiator and activator, respectively. The dry caprolactam (Aldrich 99+% pure) was charged into the chemical vessel, then was heated to about 90-100°C by the isomantle in order to liquefy ($T_m \approx 72°C$, $T_b = 136\text{-}138°C$) throughout the vessel. Dry nitrogen gas was bubbled through the liquid in order to remove oxygen and moisture from the vessel. Equimolar concentrations (1 mol% based on the weight of caprolactam used) of sodium hydride and phenyl isocyanate were added to the molten caprolactam. For example, 0.43 gram of sodium hydride (powder form) were first added into 200 gram of ε-caprolactam. Hydrogen bubbles occurring from the reaction of sodium hydride and caprolactam were observed. After about 10 minutes (or until no hydrogen bubbles could be seen), 1.92 cc. of phenyl isocyanate (liquid form, using a syringe to transfer into the vessel) was added into the hydrogen-free monomer solution. Introducing the nitrogen gas to the other inlet tube, which was above the monomer solution, provided an inert gas blanket but maintained atmospheric pressure in the vessel during the remainder of the discharge process. At this step the polymerization will not occur due to the low rate of reaction at this temperature; the catalyst mixture is not sufficiently active.

6.2.3. Polymerization of caprolactam and removal of disk

Since nitrogen gas was bubbled through the monomer, it was certain that some nitrogen gas dissolved in the solution (probably saturated, at 100°C, in melted caprolactam). Therefore, N_2 flow was stopped and the chemical vessel was evacuated via

vacuum pump to degas the monomer solution. If there had been some gases dissolved in the monomer feed, these gases would be released in the mold under vacuum and create some voids in composite. Following degassing, a N_2 blanket at 1 atm was restored to the vapor space above the liquid, but no more bubbling of N_2 through the liquid occurred.

Mold-filling was initiated by opening the valve at the connection between the chemical vessel and the mold while closing the valve that connected the mold and vacuum pump. The activated monomer then filled the evacuated mold, by a flow driven by atmospheric pressure (1 atm, approximately 93 kPa in Edmonton, less the residual pressure in the nearly-evacuated mold--here, 5 kPa--for $\Delta P \cong 88$ kPa in this work) plus gravitational pressure, $\rho g(H_1 + H_2) \approx 2$ kPa (see Figure 6.1)). As the mold filled, H_1 was reduced approximately from 6 cm to 1.5 cm, while $\Delta P \rightarrow 0$ as atmospheric pressure was restored to the mold. In a typical case, a total time of only about 10-20 seconds was needed to fill the mold, but usually an extra 10 minutes was provided to ensure that the filling operation was complete (the difference of monomer level in the reaction vessel could not be observed).

After the mold was filled, the pinch-valve on the silicone tube was closed before beginning to heat the mold. If the pinch-valve had been left open, the monomer inside mold would not have been affected by atmosphere (O_2 and H_2O); and only some layer of the upper surface of monomer solution in the reaction vessel would have been affected. In this work, the pinch-valve was usually closed before heating the monomer inside the mold so that the reaction vessel could be removed and disassembled after filling the monomer into mold. A small amount of water was also poured into the reaction vessel after completion of filling the monomer into mold and the pinch-valve was closed, for ease of cleaning the reaction vessel. After the monomer solution in the silicone tube solidified (freezing at about 75°C), scissors were used to cut the tube to disconnect the mold and the reaction vessel. Then, the reaction vessel could be removed in anticipation of the need for space to open the mold later.

Polymerization was initiated by increasing the temperature of the mold to 150°C, which took about 8 minutes, and this temperature was maintained for 15 minutes to ensure complete polymerization. Then the heater was turned off and the mold allowed to air-cool. The composite disk was removed some time after the mold had cooled to room temperature, commonly about 24 hours. Removal was easy as long as the mold had been pre-treated with a release agent, and no damage ever occurred to any disk surface during removal. However, it was always true that some bubbles or voids could be seen by casual inspection. Most of these were on the top disk surface, and rarely on the bottom. In retrospect, we can presume that these probably originated from the air remaining in the mold, following incomplete evacuation (to ~ 5 kPa). As the mold was filled by a rising pool of low viscosity caprolactam, the residual air would have been either entrapped in fibre-fibre crevices or pushed to the top surface of the mold. Later measurements (Chap. 7) confirmed that appreciable voidage (over 1%) existed in almost all samples.

6.3. Fibre surface treatment

Glass fibre surfaces were treated with four kinds of silane which were designated as Silane I, Silane II, Silane III, and Silane IV as following:

Silane I: 1,1,1,3,3,3,-Hexamethyldisilazane (98%, from Aldrich)

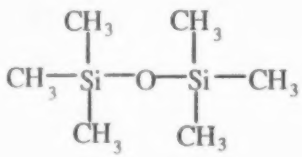

Silane II: tert-Butyldimethylsilyl chloride (1.0 M solution in tetrahydrofuran from Aldrich)

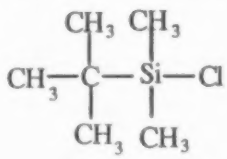

Silane III: Chlorotrimethylsilane (98%, from Aldrich)

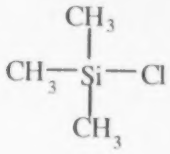

Silane IV: 3-Aminopropyltriethoxysilane (98%, reacts with porous glass to form the aminopropyl derivative of glass, and adsorbent for affinity chromatography, from Aldrich)

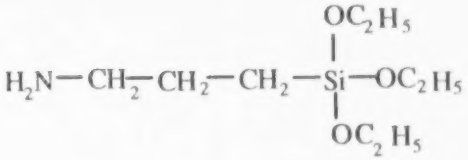

These four silanes were chosen for the following reasons: Silane I, because it had -Si-O- bonds which might have some affinity for the Si-O bonds in glass and thus have some tendency toward physical adsorption on the glass surface, even though it had no groups which should react with hydroxyls on the glass surface; Silane III, because it had a chloride group which should react with hydroxyls on glass to form a strong covalent bond (Chap. 3), while being the smallest silane molecule that could reasonably be used in this way and have the least steric hindrance effect; Silane II, because it had the same bonding potential as Silane III but additional length which might help it to be more capable of physical intermingling with the chains of the nylon matrix, or (using its length in a different way) the additional length might interfere with neighbor molecules in gaining access to the hydroxyls on glass surface (hindrance effect); and Silane IV because it had several desirable structural features--three reactive sites (ethoxy) for bonding to either glass or to a local cross-linked network of neighbors on the glass, a backbone length of three carbons extending beyond the Si whereas Silane II had only two, and an amino tail that provided -

NH bonds that resembled those in the amide group of nylon 6. Additional motivating factors for using Silane IV were that recent literature (**33**) indicates it actually reacts with nylon 6, thereby anchoring the coupling agent chemically to the matrix, and also that the use of this agent (**32,33**) and possibly other amino silanes (**34**) have produced good results with nylon as well as epoxy matrices.

Fibre surfaces were treated with these silanes in four steps:

1. Heat -cleaned fibreglass mats (circular disk, 22 cm dia) was dried at 150°C for 4 hours in order to eliminate water at the fibre surface.

2. Fibreglass mat was immersed in a room-temperature solution of toluene and silane agent (concentration by vol% e.g., 5% = silane 100 ml in 2000 ml of toluene), contained overnight in a good sealed container (silane is very sensitive to water), to allow complete interaction of silane and glass fibre surface.

3. These fibreglass mats were washed in dichloromethane and then in methanol to get rid of all excess silane.

It is very important to do the silane-surface treatment under well ventilated conditions since silane is very toxic.

4. Fibreglass mats were dried in an oven at 60°C overnight and used the next morning.

6.4. Treating by adding silane directly into monomer

This composite was made with clean (untreated) glass mats loaded into the mold, as when beginning to make the regular "untreated" composites. However, before introduction of monomer into the mold, Silane III was poured into the hot monomer solution in the chemical vessel. the intention was that the silane would interact with glass

fibre inside the mold, after the mold was filled with liquid caprolactam but before polymerization had occurred at still higher temperature. No extra time was allowed during the procedures for such an interaction to take place; after monomer loading at 100°C, the mold temperature was increased toward 150°C at the usual pace.

The amount of Silane III added (about 2.2 g) to the caprolactam liquid (itself weighing about 200 g) was based on the weight of fibre in the mold (about 148 g). Following one earlier report of a similar coating (**32**), the amount selected was 1.5% of the fibre weight. This corresponded to a concentration of about 1.1 wt% in the caprolactam solution.

CHAPTER 7

STRUCTURE AND COMPOSITION OF COMPOSITE DISKS

A specialized notation will hereafter be used to identify the disks and disk types, for which results will be reported in Chapter 8 and in the Appendices. Each disk will be uniquely coded to indicate the chemical agent used to treat the glass fibre mat (e.g., Silane II), the concentration of that agent in the treating solution [e.g., Silane II (5%)] and, for nominally replicated disks molded at different times, also the sequence of those two [e.g., 2Silane III (5%)]. The one exception to these rules comes with the concentration of Silane III (1.5%): the concentration 1.5% was wt of silane/wt of fibreglass (i.e., 1.5 g of Silane III used per 100 g of fibreglass mat).

7.1. Density (ρ)

The densities of specimens of composites (ρ_c) and nylon 6 (ρ_n) were measured, following ASTM standard: D792 (described in Appendix C). Five samples at different positions (random positions) of a nylon 6 disk produced here and six samples at different fixed positions of each composite disk (shown in Figure 7.1) were measured and averaged ($\overline{\rho}$).

The average density of all composites made (all contained 8 plies of glass fibre mat) was 1.56 g/cm^3, in the range from 1.51 to 1.60 g/cm^3. From Table B-1 (Appendix B) we see for each composite disk that $\rho_c > \rho_n$ (= 1.125 g/cm^3) because the density of glass fibre (ρ_g = 2.54 g/cm^3) is higher than that of ρ_n. The measured ρ_n was found to be in the range of typical nylon 6 (1.12-1.15 g/cm^3) (**13**) shown in Table 2.3. This ρ_n was used as

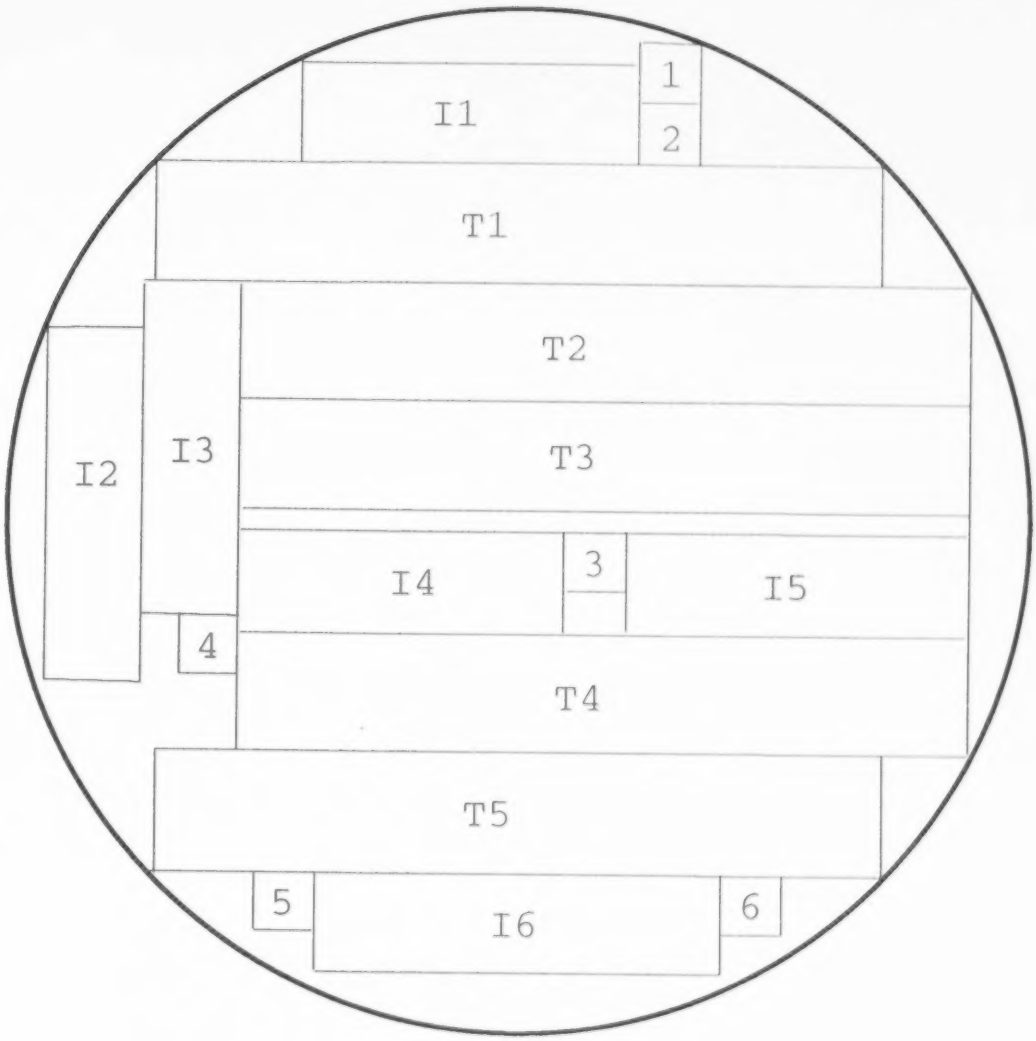

Figure 7.1. Locations of regions from which specimens were taken for obtaining data on composition (numbered 1-6), impact strength (I1-I6), and tensile behaviour (T1-T5)

the standard for this study. Values of ρ_c for all specimens taken from all composite disks and values of ρ_n from the nylon 6 disk are shown in Table B-1 (Appendix B).

7.2. Volume fraction of fibre (V_f)

7.2.1. Reproducibility and homogeneity of disks

Although the number of plies of glass fibre mat was fixed to 8 plies for each composite preparation, we were not sure how much the fibre contents in each composite varied. The method of measuring V_f is described in Appendix C. Figure 7.2 shows $\overline{V}_f$ of all composite disks. Values of $\overline{V}_f$ for all composites, excluding the Silane IV (10%) composite, were in the range of 31.1-34.4% (average value = 32.9%). There is a trend (Figure 7.2) for the "Day 1" results to be higher than the nominally replicate "Day 2" results by about $\Delta V_f \approx$ 2-3%, possibly because the roll of glass-fibre mat (from which plies were cut) was not of uniform fibre arrangement. The composite with Silane IV treated glass had quite a low average value ($\overline{V}_f$ = 25.4%) compared to other composites.

The composite disks seemed to be fairly homogeneous with respect to V_f measured at different positions. This can be assessed from the data in Table B-2 and the corresponding "standard errors" in Figure 7.2. Differences in measured V_f values at different positions are at least partially due to ordinary random data scatter, not signaling real inhomogeneity. But such variations must also be examined for consistent trends within the entire set of disk specimen data. Such trends, if present, would represent real nonuniformity and could be regarded as indicators of deficiencies in the disk-preparation procedures or the mold design. Such deficiencies would thus build into the disks an inevitable degree of patterned inhomogeneity.

One such case seems to be evident at position "1" (near one edge), where the data show a tendency to have lower V_f than other parts. Among the 12 disks, position

1 had the lowest V_f 11 times. The largest deviation was in ^{1}Silane III (10%), at -5.78% lower than the average for that disk, and among all disks this discrepancy averaged -2.37% (including the one positive deviation in ^{2}Silane III (10%)). A rather consistent exception to disk uniformity in the positive direction was noted at position "3" (close to the disk center), where V_f exceeded the disk average in 9 of the 12 disks. The largest of these was + 3.01%, in ^{2}Silane III (5%) and the average among all disks was + 0.86% (including the 3 negative-deviation cases in this average).

Since the fibre content affects the properties (i.e., tensile strength, impact strength) of the composite, it is necessary to look at the average V_f of each composite disk before comparing the average mechanical properties of them (the comparison of mechanical properties is shown in Chapter 8). It would be even better to evaluate the average fibre fraction of each mechanical-property specimen prior to its testing.

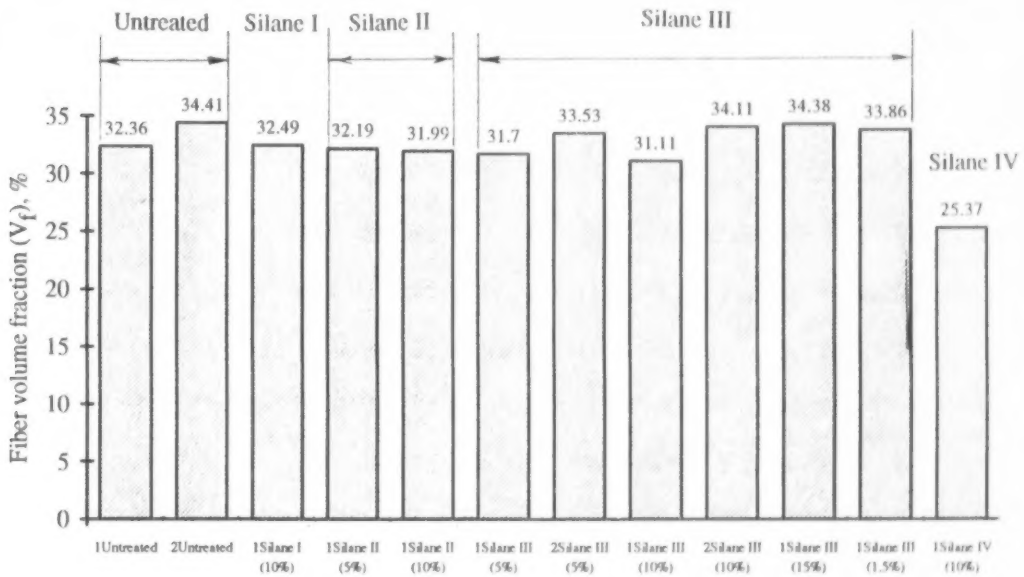

Figure 7.2. Fibre volume fraction of composite disks having different glass fibre treatment and molded on different days. The abscissa "scale" groups together (by parentheses) the disks whose fibres were treated with the same chemical (e.g., Silane II). Within each group, members whose treatments were nominally identical (e.g., Silane III in 5% solution) are clustered together, but always in the chronological order in which the disks were molded (e.g., ^{1}Silane III precedes ^{2}Silane III).

7.2.2. Masking fibre pretreatment effects with variations in V_f

Table B-2 and Figure 7.2 present the average volume fraction of fibre $\overline{V}_f$ for six specimens representing each disk prepared from untreated and silane-treated fibres. Because there is some variation, the question could arise whether subsequent mechanical property variations might be due to V_f-effects or to the effects of surface chemistry and coupling agent. Inspection of the whole set of V_f values shows, fortunately, that there are several cases where disks have virtually the same $\overline{V}_f$ but differing chemicals used in fibre pretreatments, or the same $\overline{V}_f$ but different concentrations of the same coupling agent during pretreatment. In these cases, then, it is possible in principle to separate the various effects.

As one example, we take those cases where it happens that $\overline{V}_f \cong 32.4\%$. From Table B-2, we see these include*: [1]Silane I (10%), $\overline{V}_f = 32.5 \pm 0.5\%$, [1]Silane II (5%), $\overline{V}_f = 32.2 \pm 0.7\%$, and for [1]Untreated, $\overline{V}_f = 32.4 \pm 0.6\%$. Another $\overline{V}_f$-cluster is the 31-32% range: [1]Silane II (10%) with $32.0 \pm 1.1\%$, [1]Silane III (5%) with $31.7 \pm 0.4\%$, and [1]Silane III (10%) with $31.1 \pm 1.2\%$. Finally, we have one more grouping near $\overline{V}_f \cong 34.0\%$: [2]Untreated at $34.4 \pm 1.1\%$, [2]Silane III (5%) at $33.5 \pm 0.8\%$, [2]Silane III (10%) at $34.1 \pm 0.5\%$, [1]Silane III (15%) at $34.4 \pm 1.1\%$, and [1]Silane III (1.5%) at $33.9 \pm 0.4\%$. Given these three close groupings, it should not be difficult to isolate and evaluate the effect of the coupling agents within each group without being concerned about variations in V_f. Also, because the groupings are actually quite close to each other ($\overline{V}_f \cong 34.0\%$, 32.4%, 31-32%), minor corrections for the V_f-factor variation should be possible to facilitate intergroup comparisons as well. The $\overline{V}_f = 25.4\%$ for Silane IV must be addressed separately. These matters will be explored further in Chapter 8, using mechanical property data tabulated in Appendix C.

* Each value of $\overline{V}_f$ is accompanied by ± (standard error of mean); see sample calculation in Appendix A.

7.3. Void volume fraction (V_V)

7.3.1. Correlation with glass fibre treatment

The measurement of V_v followed ASTM: D2734-70 (described in Appendix C). Table B-3 shows that each composite disk had a slightly different $\overline{V}_v$, in the range of 0.7-4.9% for silane-treated composites (ignoring for now the anomalous values for Silane IV) and 3.6-8.9% for untreated composites. A graphical display of all the $\overline{V}_v$ results, analogous to that given in Figure 7.2 for $\overline{V}_f$, is presented in Figure 7.3 (though [1]Silane IV (10%) is omitted). It is clear that $\overline{V}_v$ correlates with the fibre surface treatment, as all values associated with Silane III are very low ($0.65\% < \overline{V}_v^{III} < 2.02\%$), and those associated with Silane II are comparable or somewhat higher ($\overline{V}_v^{II}$= 1.51, 3.41%). The value with Silane I is the highest ($\overline{V}_v^{I}$ = 4.94%) of the silane group, comparable to the untreated cases which were both high ($\overline{V}_v^{0}$ = 3.61 and 8.89%), thus demonstrating that

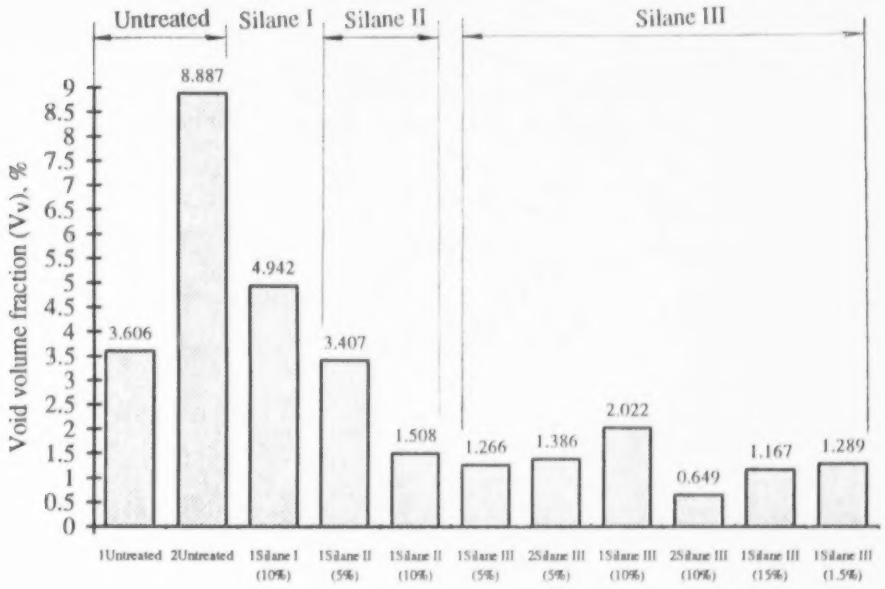

Figure 7.3. Comparing void volume fraction of composites treated with different kinds and concentrations of silane

Silane I is ineffective but that any use of Silane III or Silane II represented a major change (hopefully an improvement) from the baseline case. Indeed, the ultimate goal of zero voids was almost achieved with $\overline{V}_v = 0.65\%$ for [2]Silane III (10%).

7.3.2. Anomalous voidage and ρ_n uncertainty

The case of [1]Silane IV (10%) is perplexing because of the physical impossibility of negative voidage. Computationally, such a result could emerge if the ρ_n value being used here were too low--i.e., if the true ρ_n in this composite was actually higher than 1.125 g/cm^3. If so, the measured mass of these composite samples could be accommodated in the calculations only if the too-low ρ_n (giving a too-low nylon mass) could be compensated by allowing additional nylon mass to be present in the only way computationally possible--i.e., "giving" more volume to the nylon by creation of negative voidage. More specifically, the variables can be related by

$$V_v = 100 - \rho_c \left(\frac{W_m}{\rho_m} + \frac{W_f}{\rho_f} \right) \times 100 \qquad (7.1)$$

where W_f and W_m are the weight fraction of fibre and matrix respectively. This shows that V_v can be driven negative if (ρ_c/ρ_n) is too large--i.e., if $\rho_n = \rho_m$ is erroneously too small. The possibility that ρ_n = 1.125 g/cm^3 could be too small is supported by the fact that the published range of nylon 6 densities (**13**) goes as high as 1.15 g/cm^3, and the value used here is barely on the lower fringe of the published range.

Further contemplation of the possible variation of ρ_n leads to a wide range of speculations.

(a) Why might $\rho_n > 1.125$ g/cm^3, which was measured for pure nylon 6 prepared as disks in the same apparatus ? The twofold answer begins with nylon crystallinity, since crystals are denser than amorphous nylon. One must also contend that the presence of glass fibres in the nylon could promote higher fractional crystallization in

the composites (more surface area for nucleation and growth) than in the pure nylon disks prepared in fibre-free molds with less solid surface area for contacting the caprolactam.

(b) Could the silane fibre treatment play a role in altering ρ_n? It now seems plausible. By making the glass more compatible with crystallizing hydrocarbon chains, the silanes are encouraging nylon adsorption and subsequent further crystallization on the fibre surfaces. Thus, $\rho_n = 1.125$ g/cm^3 might be too low for use with any of the composites here that incorporated surface-bonded-silane glass fibres.

(c) Could the apparent variations of $\overline{V}_v$ with the use of different silanes be explained by these considerations? Maybe, at least in part. Such an explanation would begin with the proposal that Silane IV was the most effective in promoting nylon crystallization, since only here was the computed $\overline{V}_v$ driven to negative values (i.e., the true ρ_n was much higher than 1.125 g/cm^3). Additional evidence is provided by the fact that the Silane IV-produced composite specimens had ρ_c values comparable to those of the other composites (see Table B-1, with $\overline{\rho}_c^{IV} = 1.54$ g/cm^3) despite the fact that far less glass fibre had been used (Table B-2 and Figure 7.2 with $\overline{V}_f^{IV} = 25.4\%$, compared to the others with $\overline{V}_f \geq 31\%$).

The next step in this argument would be to identify Silane III as the next most effective in promoting nylon 6 crystallization on fibre surfaces, with $\overline{\rho}_n^{III} > 1.125$ g/cm^3 but $\overline{\rho}_n^{III} < \overline{\rho}_n^{IV}$. This would give low values of $\overline{V}_v^{III}$ by computation, as was indeed seen in Table B-3 and Figure 7.3. And Silane II would be viewed as fairly effective but less so than Silane III (as also found here). Silane I, with no chemical capacity for bonding to glass at all should be totally ineffective at altering ρ_n and should have high values of calculated $\overline{V}_v$, comparable to the untreated cases (as was indeed found).

All these arguments would point to the expectation that $\overline{\rho}_c$ should be measured as higher for composites involving Silane IV, III, and II (which involve more highly crystalline nylon 6 and thus higher $\overline{\rho}_n$) than for composites involving Silane I or no

treatment. This prediction is consistent with Table B-1, since the latter group had $\overline{\rho}_c \leq$ 1.54 g/cm^3 and former group (Silanes II, III, IV) had $\overline{\rho}_c \geq 1.54$ g/cm^3.

One consequence of this line of reasoning is that the V_v results presented here (all obtained by calculation) could be entirely spurious. For example, one could argue that $V_v = 0$ and this would be found if the "proper" value of ρ_n were used in each type of composite. However, we find this not to be so (see following section, on SEM observations); substantial voidage did exist in these composite samples, though we cannot discern in this section precisely what it was <u>if</u> we cannot trust the value of $\rho_n = 1.125$ g/cm^3 used in analyzing the data of all disks and all specimens.

7.3.3. Distribution of local voidage within disks

Finally, the position-dependence of V_v in the various composite disks can be examined, analogous to what was done for V_f in Section 7.3, above. The discussion will refer in detail to Table B-3. We first note that V_v-variations differ <u>fractionally</u> from V_f-variations, both within a single disk (the non-homogeneity problem) and from disk-to-disk (discussed above, in terms of fibre surface treatment). For example, within single disks we find such extreme V_v-variations as 2.6-13.7% [^{1}Silane I (10%)], 2.3-6.2% [^{1}Silane II (5%)], 0.2-4.9% [^{1}Silane II (10%)], 0.8-3.4% [^{2}Silane III (5%)], 0.009-2.5% [^{2}Silane III (10%)], 0.005-3.6% [^{1}Silane III (1.5%)], and a ΔV_v of 13.2% for ^{1}Silane IV (10%). These are enormous factors of variation and often large absolute-value variations. Part of this is caused by the fact that V_v is being found indirectly, by the differences between larger numbers and normal random experimental errors are magnified by this procedure. Also, the reference base is $V_v = 0$ (since voids are not being built in, unlike the fibre reference base $V_f \approx 32\%$), so that all deviations from this and variations between them <u>seem</u> abnormally large. However, the absolute variations--except in the more extreme cases--are not any worse than with V_f.

The distribution of voidage can also be examined. As stated earlier, for V_f position 1 represented a generally minimum value for all disks, very likely because it is at the disk edge where the packing of solids (i.e., fibre mats) is sterically hindered by the mold wall and we could expect a lower V_f. However, positions 2, 5, and 6 were also quite close to the disk edge (mold wall) as displayed in Figure 7.1, and they were not notably fibre-deficient. Now, for V_v, we note again a tendency for position 1 to have low values within its our disk, but not dramatically so (only in 4 of the 12 disks does position 1 have the absolute minimum value). Position 2 is also the lowest-V_v region on its own disk, in several cases (4 of the 12, again), and the other two outer sampling spots (5 and 6) are often low-valued for voids too. The overall picture is condensed in Figure 7.4a, where absolute values of V_v are given for 11 disks (the negative values of the Silane IV case being omitted).

Table B-3 and Figure 7.4a also reveal a tendency for high V_v values to be registered near the disk centers (position 3) and midrange distances from the center (position 4). In particular, position 3 has the highest V_v value in 8 of the 12 disks. This is reminiscent of the high-fibre spot at position 3, as discussed above. Thus, for V_v and V_f, the distributions across the disks have some degree of similarity and could be correlated in terms of physical principles. For example, a locally higher fibre concentration would be more effective in trapping free bubbles in the caprolactam, thus capturing extra voidage (so, higher local V_f and V_v would go together). An effort was made to establish such a relationship more quantitatively, by plots of local V_v vs. local V_f (Figure 7.5a) and corresponding averages $\overline{V}_v$ vs. $\overline{V}_f$ (Figure 7.5b). No correlations are apparent among the averages, but for each disk there appears to be a monotonic correlation band within the data scatter (as seen in Figure 7.5 c, d, e).

Because Figure 7.4a tends to mask the V_v distributions with the wide discrepancies between V_v values on different disks, another graphical technique will also be used to highlight the distributions themselves. We assign numerical values (points) to

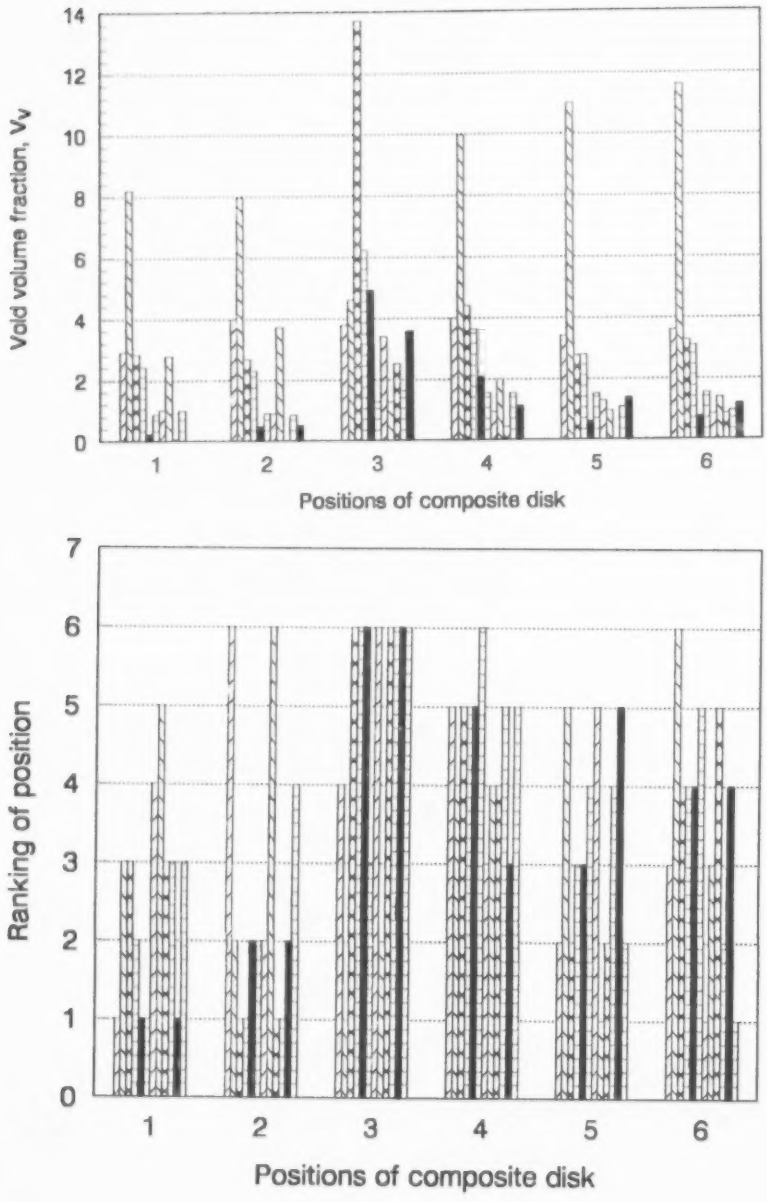

Figure 7.4. Void volume fraction at different positions in composite disks (see Figure 7.1). (a) V_V values expressed as volume percents. (b) V_V ranking, as a scale of 6-1, with 6 highest.

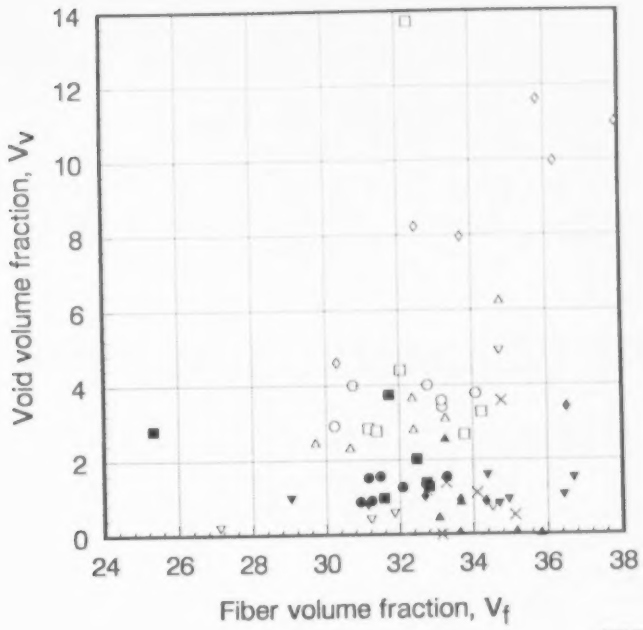

(a)

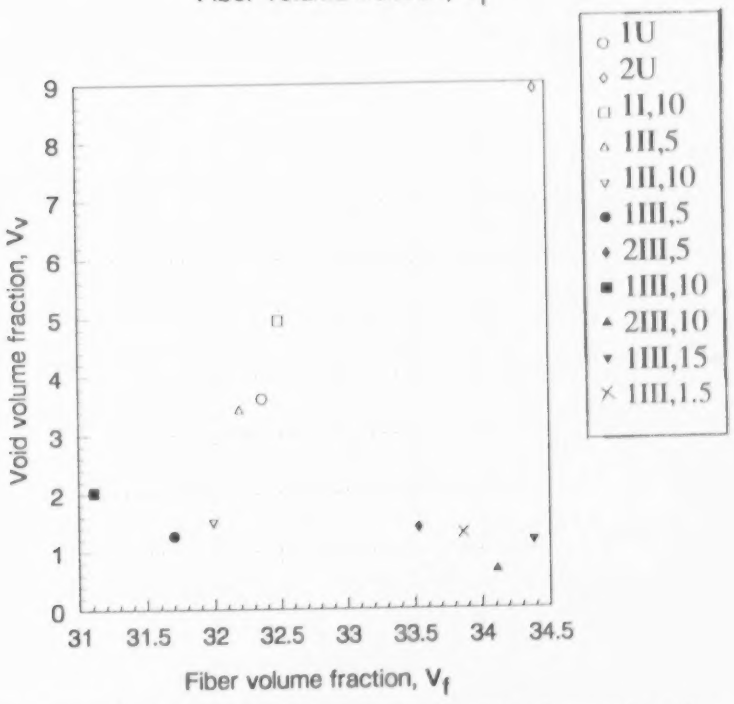

(b)

Figure 7.5. Fibre volume fraction (V_f) vs. void volume fraction (V_v) of composite disks. (a) Local V_v vs. local V_f for all specimens of all disks. (b) $\overline{V}_v$ vs. $\overline{V}_f$ for all disks.

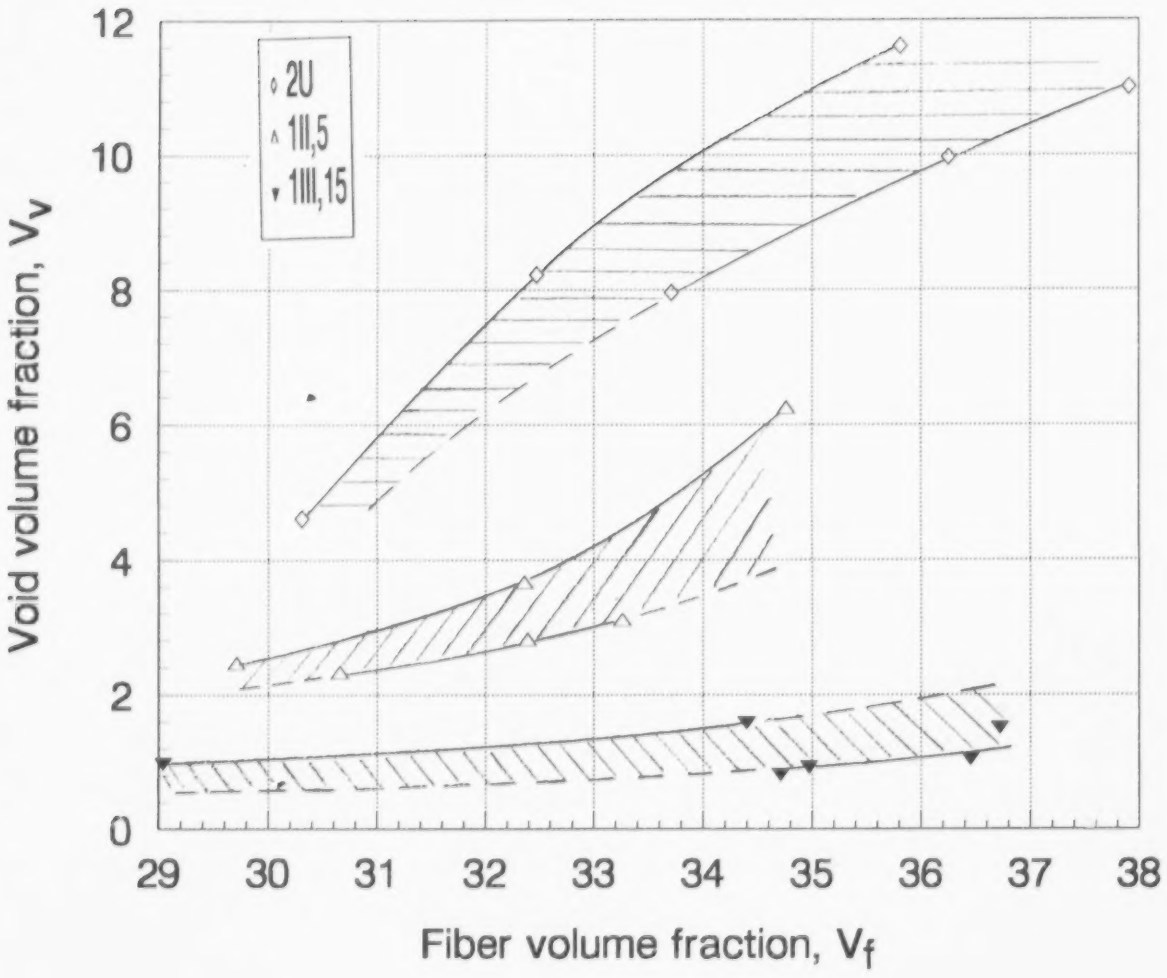

Figure 7.5 (continued). Fibre volume fraction (V_f) vs. void volume fraction (V_v) of composite disks
(c) Local V_v vs. local V_f for all specimens taken from disks ^{2}U, $^{1}II_{5}$, and $^{1}III_{15}$

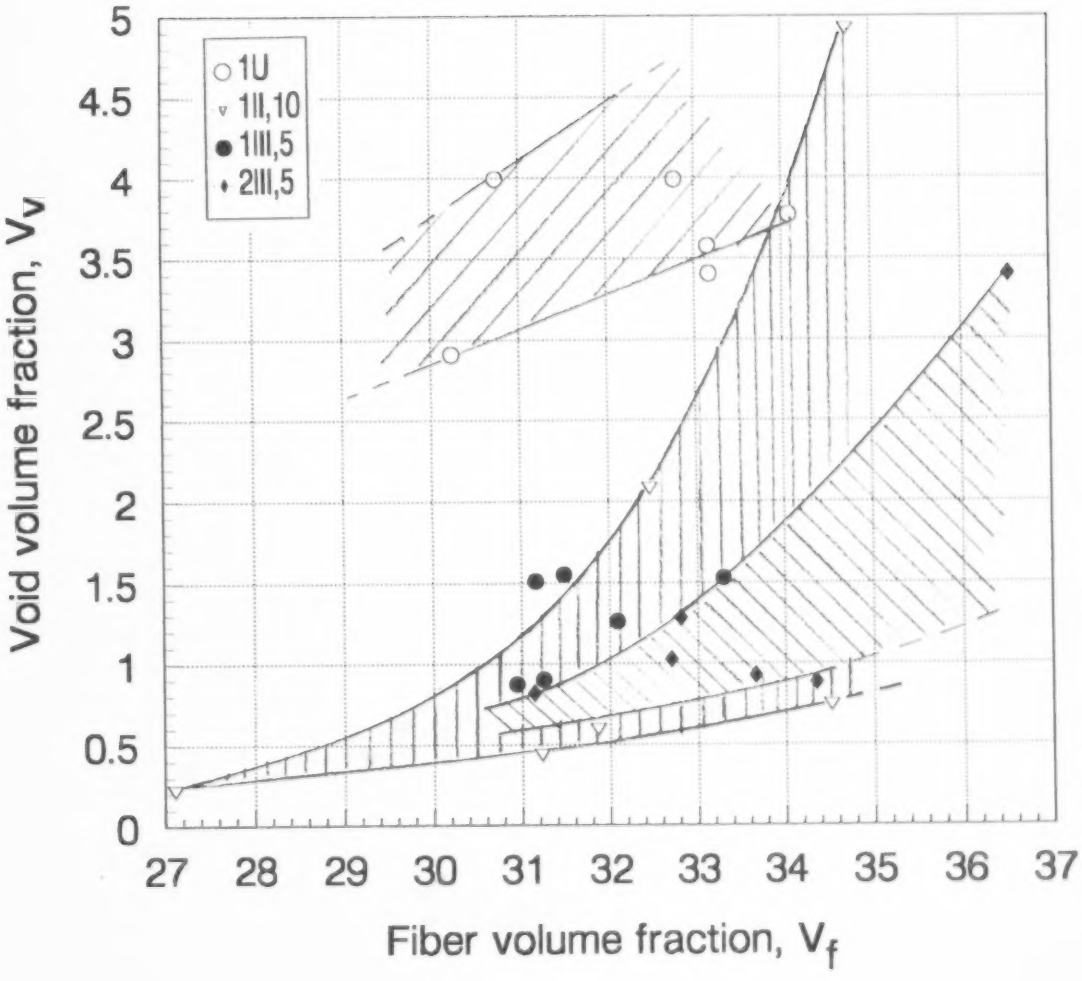

Figure 7.5 (continued). Fibre volume fraction (V_f) vs. void volume fraction (V_v) of composite disks (d) Local V_v vs. local V_f for all specimens taken from disks ${}^{1}U$, ${}^{1}II_{10}$, ${}^{1}III_{5}$, and ${}^{2}III_{5}$

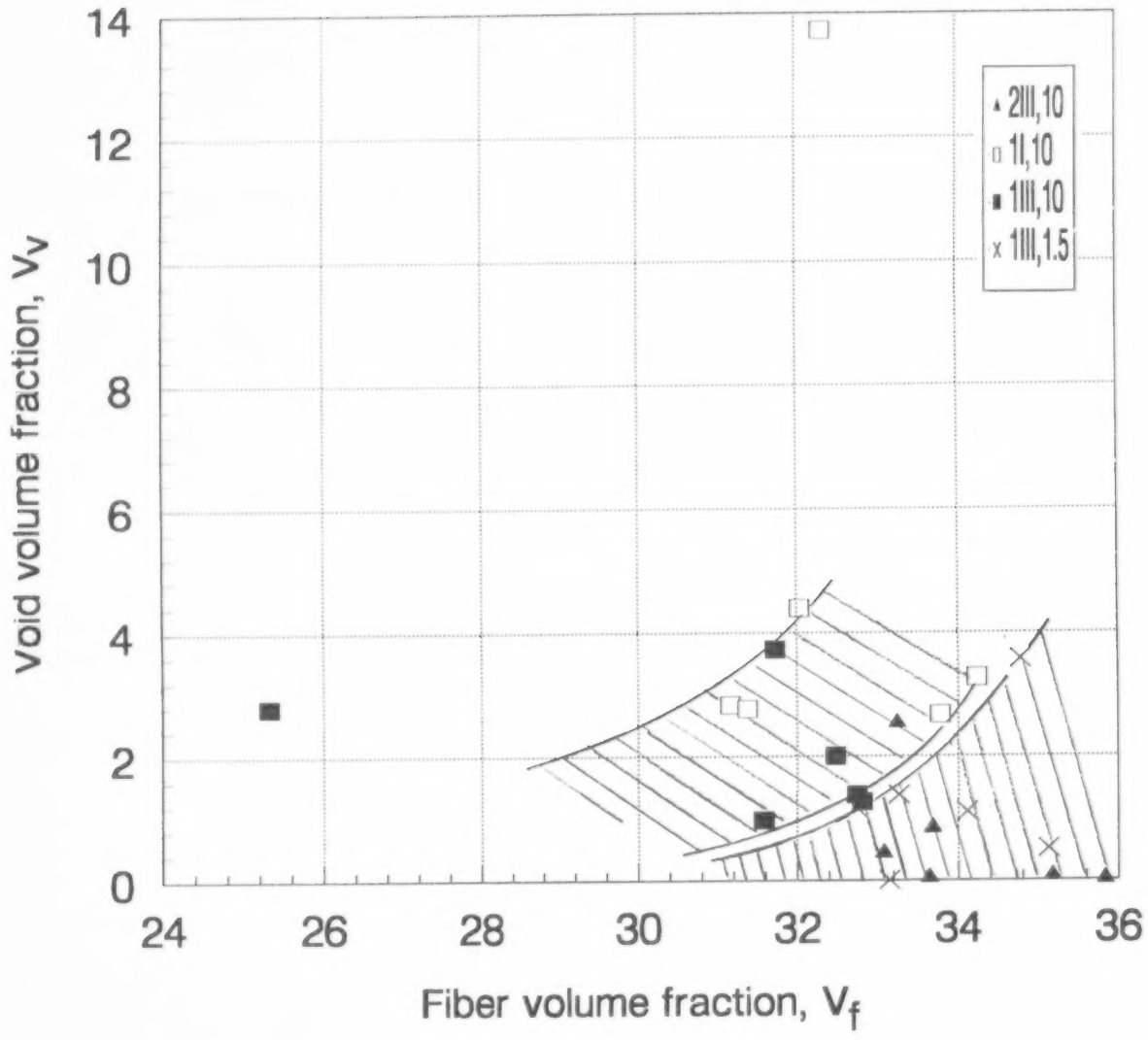

Figure 7.5 (continued). Fibre volume fraction (V_f) vs. void volume fraction (V_v) of composite disks (e) Local V_v vs. local V_f for all specimens taken from disks ${}^{1}I_{10}$, ${}^{1}III_{10}$, ${}^{2}III_{10}$, and ${}^{1}III_{1.5}$

the relative ranks of V_v at the six sampling positions: 6 for highest V_v value, 5 for next-highest, etc., with 1 for the position of lowest value. In these terms, the rank-distributions are displayed in Figure 7.4b, and now the 12th disk (with negative V_v values) is incorporated too. While this presentation also indicates that voidage is not homogeneous, it does a better job than Figure 7.4a in highlighting the relative distributions. Positions 1 and 2 are clearly the low-void leaders, with many entries in the 1, 2, 3 range. Positions 5 and 6 have fewer low-rankers and more in the midrange, while positions 3 and 4 dominate the highest ranks (5, 6).

It is evident that, whether $\overline{V}_v$ is high or low, position 3 (disk center) is likely to be the location of highest voidage for any given disk. Position 4 (about 30% inward from the disk rim toward the center) will generally have high voidage too, suggesting that the large central region of the disk (radial positions r = 0 to r = 0.7R) usually contains most of the voids (with 50% of disk volume and considerably higher void concentration than the outlying regions between r = 0.7 and r = R). These tentative conclusions, of course, are based on analysis of the numbers emerging in Table B-3, which may be unreliable if ρ_n is not the constant value it was originally believed to be.

Other data, such as direct microstructure observation (by optical microscope and SEM) and mechanical property measurement on specimens taken from different regions of the disk, can provide additional evidence on the microstructure question. These possibilities are discussed in Section 7.4, below, and in Chapter 8, respectively.

7.4. Scanning Electron Microscope (SEM) micrographs of composites

The SEM micrographs, taken from composites with untreated fibre and composites with fibre treated with [1]Silane I (10%), [1]Silane II (5%), and [1]Silane III (10%), are shown in Figure 7.6. The pictures were taken at the top faces of original untested composite disks and at fracture surfaces of tensile specimens after breaking. The faces of

(a)

(b)

Figure 7.6. SEM micrographs of glass fiber/nylon 6 composite specimen surfaces corresponding to different pretreatment of fiber. (a) Untreated: fracture in tensile test. (b) Silane I: fracture in tensile test.

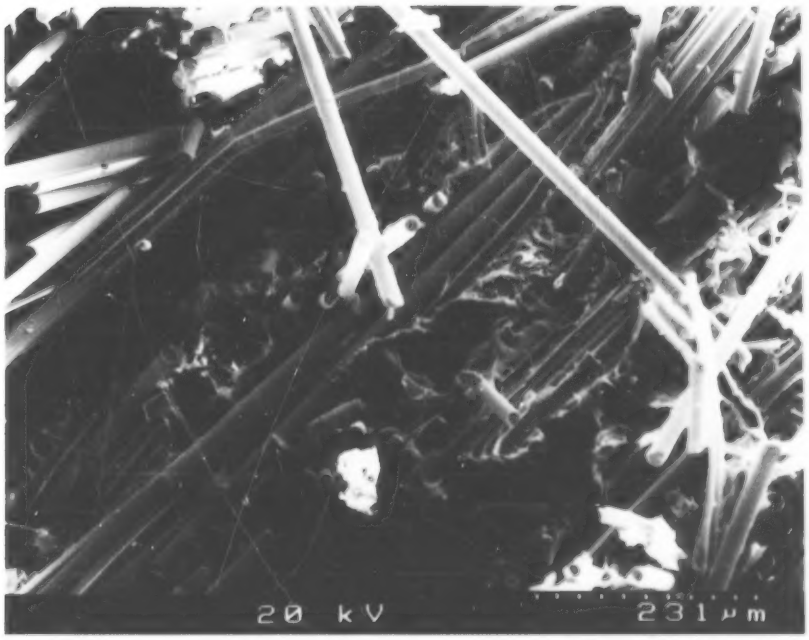

(c)

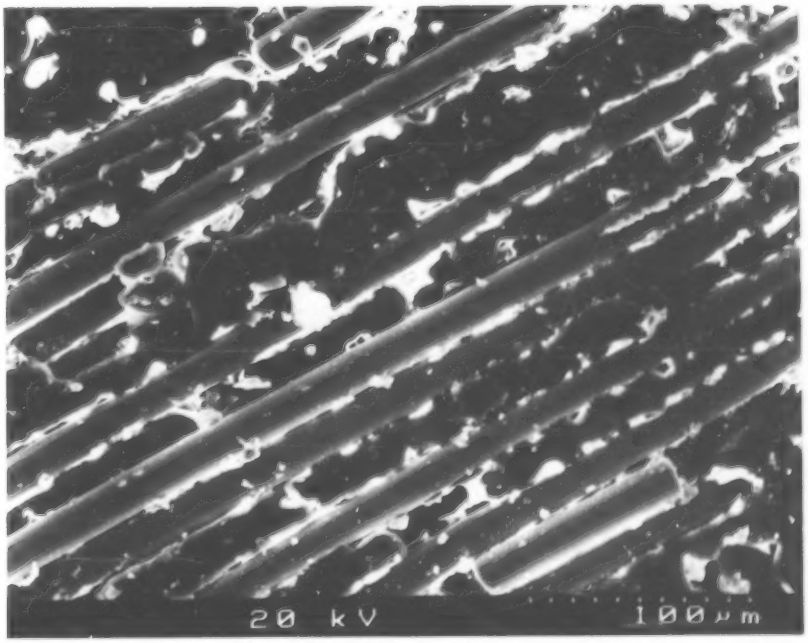

(d)

Figure 7.6 (continued). SEM micrographs of glass fiber/nylon 6 composite specimen surfaces corresponding to different pretreatment of fiber. (c) Silane III: fracture in tensile test. (d) Untreated: top surface.

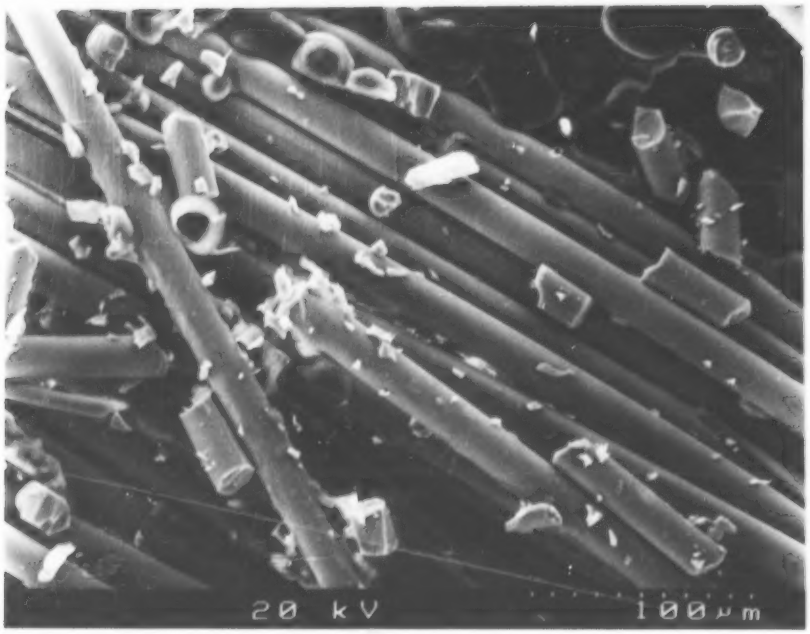

(e)

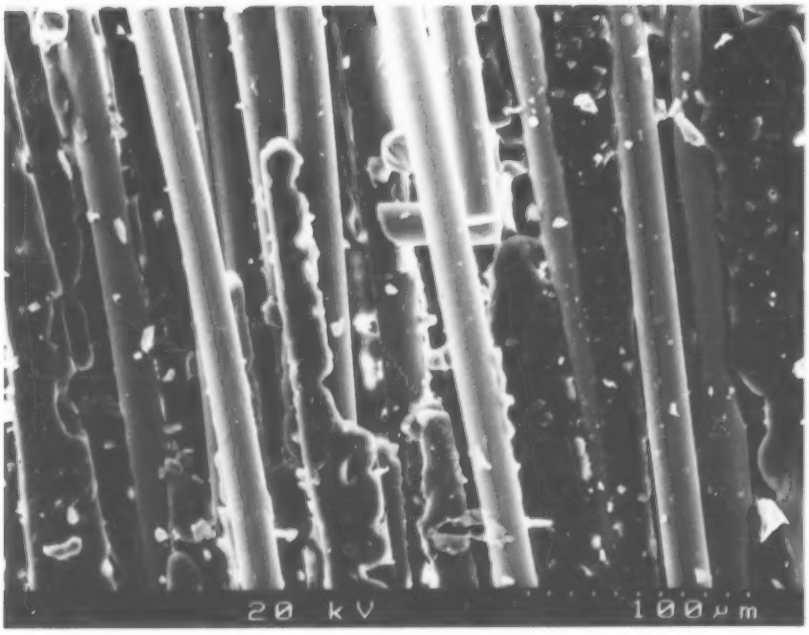

(f)

Figure 7.6 (continued). SEM micrographs of glass fiber/nylon 6 composite specimen surfaces corresponding to different pretreatment of fiber. (e) Silane II: top surface. (f) Silane III: top surface.

all unbroken composite samples appear to be similar, with identical glass-fibre surfaces, fibre morphology, and void size and distribution. The pictures of fracture surfaces also look similar for all samples. No fracture-surface pictures show visual evidence of improvement of adhesion between glass fibre and matrix as might be due to use of the silane coupling agents (no torn-out matrix material adhered at the surface of broken glass fibre). There is no differentiation between specimens that had different surface treatment and for which calculations had indicated void differences. However, this does not justify a conclusion that the voids calculations (or density measurements) were in error, as void differences of this magnitude (only a few percent) would be difficult to see in the SEM. Until a more precise image analyzer than the human eye is used to evaluate the SEM micrographs, or some independent technique is used for direct void measurements (acoustics?), the values of V_v inferred here from density data will be accepted (except for the negative ones with Silane IV). It remains to be seen whether the mechanical property data (Chap. 8) reveal a sensitivity to V_v that can be differentiated from other distinctions between specimens.

CHAPTER 8

MECHANICAL PROPERTIES OF COMPOSITE SPECIMENS

The mechanical testing in this work included both tensile and impact tests. From a single tensile test four properties were received: tensile strength (σ_b), tensile modulus (E), strain at break (ε_b), and toughness (τ) (breaking energy/volume at low tensile strain rates); the impact test gave only a breaking energy (E_s) (under standardized but complex strain condition, and extremely high strain rates). The procedures for both tensile and impact tests and samples of calculation of these properties are shown in Appendix C.

The properties of nylon 6 (N6) and therefore also its glass fibre composites are sensitive to environmental conditions (e.g., atmospheric humidity). The tensile tests were made on three different days, whereas for impact testing all samples were tested on a single day. For the tensile tests, Day I, Day II, and Day III were defined for each day of testing. Five types of composites were made: those with untreated (U) (i.e. clean glass) fibre surfaces, and those treated with Silane I (S^I), or Silane II (S^{II}), or Silane III (S^{III}), or Silane IV (S^{IV}). The aim of testing these materials was to see whether there was an improvement of mechanical properties when the glass fibres were treated with silanes and which silanes gave the best improvement of properties.

8.1. Impact properties

All composite disks and one nylon disk were evaluated for their impact properties on the same day, at NAIT, where the laboratory temperature was 24-24.5°C and the relative humidity (RH) dropped gradually from 46% to 42.5% during the 3 hours of testing. From each disk, impact specimens were cut from the same positions (Figure 7.1).

Over a period of several weeks, all disks were processed in this way and the specimens preserved in a desiccator at about 50% RH until tested together with a Tinius Olsen Izod Testing Machine (25-lb pendulum). The average E_s value of all 6 specimens represented the impact strength of a composite disk. These values, for 14 disk preparations, are shown in Table B-4, and results for all the 78 individual test specimens are contained in Tables B-5.0-5.12, Appendix B.

8.1.1. Improvement of E_s by glass-fibre reinforcement

Table B-4 shows that E_s was enormously enhanced by the presence of untreated glass-fibre. Comparison of pure nylon 6-E_s value with those of the two untreated dry-composites, gives improvement factors $E_s^U/E_s^N = 8$ for the first untreated composite ($\overline{V}_f = 32.4$, $\overline{V}_v = 3.6$) and 11.4 for the second ($\overline{V}_f = 34.4$, $\overline{V}_v = 8.9$). The greater improvement in the latter case could be due to its greater glass content (by $\Delta\overline{V}_f = 2.0\%$), or the higher void content, or to both factors. It is likely the latter, as the $\overline{V}_f$ advantage is only a factor of 6.2% and E_s^{U2}/E_s^N exceeds E_s^{U1}/E_s^N by 42.5%. It should also be understood that these improvement factors are vastly greater than is usually associated with glass reinforcement of the short fibre commercial type. For example, Modern Plastics Encyclopedia (**12**) reports an improvement ratio of only about 2 in E_s when chopped glass fibres are present in nylon 6 at the 30-35% level. Use of the long fibres associated with the mats ("continuous") may be the key to such large improvement found in the present work.

However, it should be pointed out that "improvement" in impact strength is often not a good predictor of improvement in other mechanical properties. In fact, the reverse is often true (**3**); good impact strength is commonly associated with poor tensile performance, and good impact behavior is often a sign of easy fibre/matrix delamination that is the objective of so much research to rectify. Such delamination in an impact test

allows the fibre to "pull out" of its matrix sheath without breaking and dissipate in sliding friction the energy that would otherwise be used to form matrix cracks. In a tensile experiment, easy delamination leads to easy (low σ_b) failure at low strain (ε_b)

8.1.2. Effect of silanes on E_s

In focusing on chemical influences, we should examine E_s values for composites containing fibres treated in identical fashion except for the coupling agent chemical identity. Using Table B-4, we isolate the cases of pretreating fibres from 10% solution and with $\overline{V}_f$ = 32%, and display these results in Figure 8.1. It is clear that all silanes used in this study yielded composites with impact properties superior to those N6 without reinforcement. However, Silane I was markedly inferior to the other additives because it led to an impact performance poorer than that of ^{1}U (itself poorer than ^{2}U)

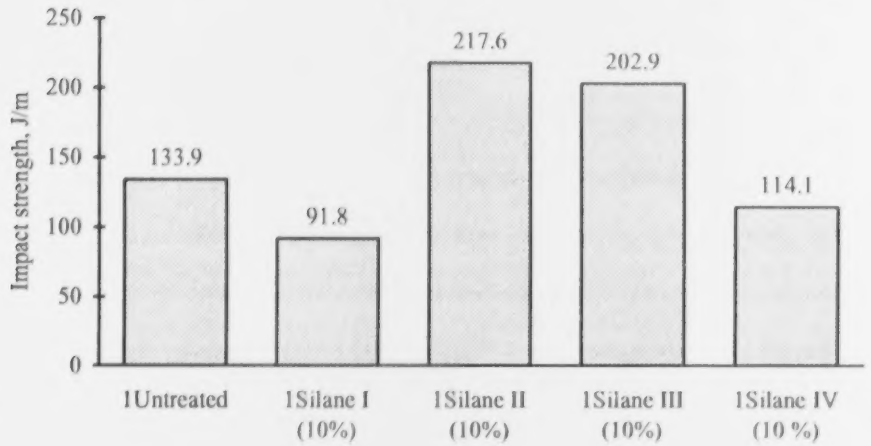

Figure 8.1. Impact strength (E_s) of composites using fibres treated with different silanes, and untreated fibres.

Also appearing in Figure 8.1 are the data for Silane IV, used at the level of 10% solution like the others. However, here $\overline{V}_f$ was much lower than in the other cases, only 25.4% compared to about 32% so a true comparison is not possible. However, its impact performance is already seen to be quite good, almost up to the ^{1}U case despite the deficit of fibres. An approximate prediction of how the Silane IV case would behave, if it had 32% fibre, would use a multiplying factor based on the ratio 32/25.4. When this is done, then Silane IV emerges as better than ^{1}U although not as good as S^{III} or S^{II}. The $\overline{V}_f$-correction gives $E_s^{IV} = 114.1 \times (32.4\%/25.4\%) = 146$ J/m, compared to 134 J/m for ^{1}U and, for the two other successful silanes, $E_s^{III} = 203$ (average) and $E_s^{II} = 218$ J/m.

Thus, the order of silane effectiveness for E_s enhancement is

Silane II ≥ Silane III > Silane IV > Silane I

when performances are compared at $V_f \approx 32\%$, and Silane I actually causes a deterioration in property quality when compared to the untreated glass case. This is more severe than just being ineffective or neutral, and will be seen again for Silane I in connection with other composite properties. To rationalize such behavior, we speculate that Silane I, being unable to react with hydroxyl or other groups on the glass surface, is simply trapped there indefinitely by physical mechanisms and can act only as a lubricant for the surrounding N6 matrix. Even if it dissolves in the matrix nearest to the fibre surface, that would serve only to plasticize the polymer and soften it, creating a thin but important zone of mechanical weakness which fails easily under stress. This serves to highlight the significance of achieving true covalent bonding between the fibre and the proposed coupling agent. Simply having silicon atoms in that molecular structure is not sufficient.

8.1.3. Dependence of E_s on the concentration of silane solutions used for treatment of fibres in composites.

Coating fibres from solutions with 5%, 10%, and 15% of Silane III at various times led to fabrication of composite disks on Day I, Day II and Day III. We compare E_s for Silane III 0%, 5%, 10%, and 15%. A plot of the E_s data, using values normalized to $V_f = 34.4\%$ and averaged when tests on replicated disks were made (5%, 10%) are shown in Figure 8.2. The curve seems to suggest that (a) E_s increases monotonically with concentration, and (b) Further improvements beyond concentrations above 15% are unlikely, because a plateau value seems to be approached.

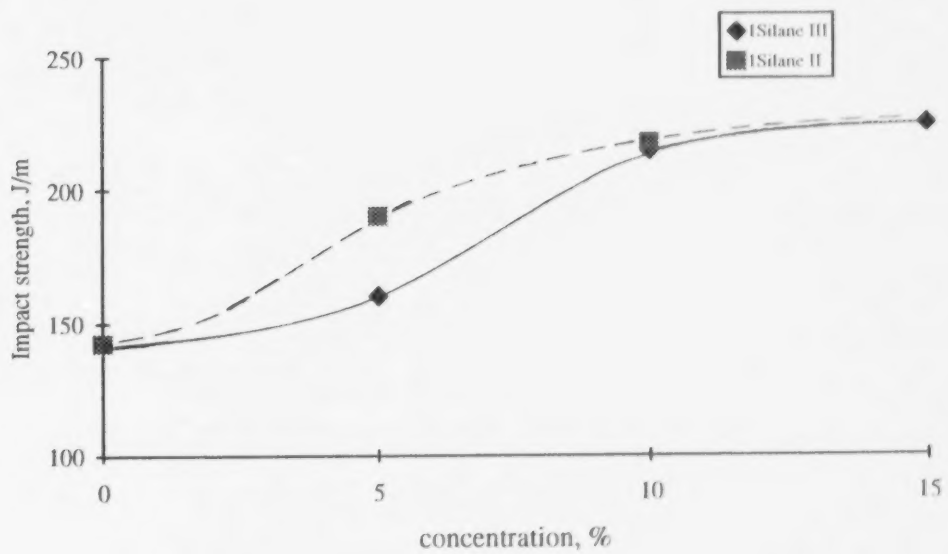

Figure 8.2. Impact strength (E_s) of composite treated with Silane III and Silane II at different concentrations.

Use of data for Silane II gives a similar result, as far as only two data points (5% and 10%) can be used for this judgement. The absolute values of E_s are about the same as with Silane III, although the lower-c performance of Silane II seems the better of the two. Again it appears that the increase of E_s with concentration occurs primarily for $c < 10\%$.

8.1.4. The role of moisture

Moisture can enter the picture in at least two ways: through direct imbibition of water when the composite makes physical contact with the liquid phase, and through variations of humidity that lead to continual exchange of water vapor with the environment. The effects of both are reflected in the data here.

The most obvious effect comes from contact with liquid water and this was deliberately investigated. A disk containing untreated fibres was cut into the usual variety of specimens. With the six impact specimens divided into two groups ("wet" = I1, I3, I5; "dry" = I2, I4, I6). The "dry" group was handled normally, equilibrating with atmospheric water vapor at 24.5°C and RH = 42-46%. The "wet" samples were immersed in cold liquid water for 48 hours, removed, resoaked, removed, etc. achieving a weight gain of about 3%. Table B-4 shows that liquid-soaked specimens averaged E_s = 235 J/m, while the normal "dry" ones gave 191 J/m. The higher value for the wet specimens reflects accurately their performance in an impact test, but this is not to be taken as an indicator of structural integrity (since fibre pull-out from the polymer matrix can dissipate energy and thus resist the energy build-up that leads to fracture). In these tests, we must interpret the high $\overline{E}_s$ value for the "wet" group as an indication that liquid water had reached the glass fibre surface, loosening whatever adhesive or compressive physical adsorption bonding

that might have prevailed until then. The high water concentration would also have plasticized (softened) the nylon throughout the specimen.

The other way that test specimens are sensitive to moisture is through their response to humidity in the air around them. Absorption here, too, leads to a diffusion process as H_2O migrates slowly toward the glass/nylon interface. A reduction of external humidity can reverse the driving force and the moisture can be expelled. Thus, a steady state condition is difficult to achieve and is easily misinterpreted. It is difficult to identify these effects, but one seems to stand out in Table B-5.0 for pure nylon 6. Sample I6 there has an anomalously low value of E_s (= 12.7 J/m) while the other five samples average 17.5 J/m. Testing proceeded in the order I1→I6, and during the first 5 tests the RH was at 46%. Then, a meteorological fluctuation brought in some dryer air (RH = 42.5%) which led to loss of moisture from all specimens--but only I6 had yet to be tested. Its lower level of moisture content then led to the lower impact performance, E_s = 12.7 J/m, which brought down the final reported average disk value to 16.7 J/m (Table B-5.0).

A survey of the data in Tables B-5.0-5.12 reveals no other situations as dramatic as that one; nowhere else was any RH change recorded during the I1→I6 testing sequence.

8.1.5. Reproducibility of composite disks

In Chapter 7, the study of microstructures of specimens taken from different disks prepared in nominally the same way permitted scrutiny of factors related to reproducibility of microstructures during the disk fabrication process. Another assessment of our control of variables in the molding process can be made by determining whether the mechanical properties in nominally identical disks can be reproduced.

Composites containing fibres treated with Silane III 5% and 10% were prepared twice. Reproducibility could not be evaluated from tensile data because they

were tested on different days, in different environments, and different testing machines. However, for impact tests all samples were tested on the same day, in the same location, and with the same piece of equipment. Therefore, the results of impact testing can show whether there was reproducibility of these composites. From Table B-4 we see that [1]Silane III 5% and [2]Silane III (5%) had average impact energies of 142.7 J/m and 161.3 J/m, while [1]Silane III (10%) and [2]Silane III (10%) had $\overline{E}_s$ = 202.9 J/m and 203.8 J/m, respectively. These results seem to confirm that these composites are reproducible in a mechanical property sense, giving $(\overline{E}_s)_{av}$ = 152.0 ± 9.3 and 203.4 ± 0.5 J/m for Silanes III (5%) and (10%), respectively. This is well within the typical range of experimental uncertainty for failure tests such as these.

The [1]Untreated and [2]Untreated should not be compared for reproducibility, because the [2]Untreated disk was made without degassing the monomer solution before the mold filling step, which is believed responsible for the [2]Untreated composite disk showing a higher void content (8.89%) than that of [1]Untreated (3.61%). The impact strength of these two are much different (190.6 vs. 133.9 J/m, respectively), which may occur from the anomalously high void contents of the [2]Untreated disk. The high voidage could be responsible for easier slippage of fibre through the matrix and corresponding energy dissipation as heat, thus increasing the apparent impact strength of the [2]Untreated.

8.1.6. Comparison of two different methods of fibre treatment

There are two methods of glass fibre treatment in this work. In the first method, silane in toluene solution was used to react with the surface of immersed fibreglass; excess solution then was washed off, to assure that no other chemicals would interact with caprolactam and possibly create some undesirable side effects to the polymerization of caprolactam. In the second method, silane was added directly into the

monomer solution, which then was supposed to deliver the silane to the glass fibres as the mold was being filled at 100°C. The latter technique led to a disk which had higher impact strength than any of the other silane-treated composites (see Table B-4). This might be explained by the excess silane itself, or by the presence of byproducts of reaction of the silane with glass (HCl byproduct) or caprolactam (byproduct uncertain), or possibly reaction between HCl and caprolactam, plasticizing the polymer--perhaps preferentially near the fibre surfaces--and thus producing easier fibre slippage and pull-out during impact failures, resulting in high E_S test readings.

Alternatively, the glass/nylon bonding might really have been improved because of (a) kinetic effects that favored more complete surface coverage, (b) thermodynamic effects that did the same, or (c) other chemical reactions that served to bond the adsorbed silane molecule more effectively to the nylon matrix. For example, among the (a)-type factors is the elevated temperature (100°C vs. 22°C), enhancing diffusional mass transfer rates from liquid to glass and then surface diffusion on the glass itself. The (b)-type factors would include the solvent being different, since deposition could be more favored from an unfavorable solvent. The (c)-type explanation could involve the chloride (on Silanes III and II) in a two-step reaction, first with hot caprolactam (and the catalyst there) to initiate a ring-opening to produce a linear reactive chain with a silane (chloride) on one end. Such a chain would bond to glass through the silane end and become part of the nylon matrix by polymerization on the other end. Further research along these lines is recommended.

8.2. Tensile properties

For each disk, five tensile specimens (cut from the disk positions indicated in Figure 7.1) were subjected to tensile stress-strain tests at an elongational rate of 5 mm/min. Since the gauge length of the specimen was initially 60.0 mm, the strain rate was

$\dot{\varepsilon} = \frac{d\varepsilon}{dt} = \frac{d}{dt}\left(\frac{L - L_0}{L_0}\right) = \frac{dL}{dt} \cdot \frac{1}{L_0}$ = (5 mm/min)/60 mm = 0.083 min^{-1}. Forty of the $\sigma(\varepsilon)$ curves from among the 65 runs are contained in Appendix D. Values of σ_b, ε_b, toughness, and E were taken from each curve* and are displayed for each specimen (T1→T5) of each given disk in Appendix B, in Table B-7 (tested on Day I, with RH = 53%), Table B-8 (tested on Day II, with RH = 75%), and Table B-9 (Day III, RH = 40%). Also displayed there are the average $\bar{\sigma}_b$, $\bar{\varepsilon}_b$, $\bar{\tau}$, and $\bar{E}$ for each disk, which will be taken as representative for that disk.

Table B-6 in Appendix B summarizes the average property values in a sequence that segregates each data set according to the coupling agent used and, within that scheme, arranges results in the order of silane concentration in the treatment solution. The layout parallels Table B-4 for impact test results.

However, for convenience of reference and to facilitate discussion, we shall employ here a data display (Table 8.1) that is organized chronologically--Day I, Day II, Day III--and thus groups the tests also according to the relative humidity on those days. This factor proves to be surprisingly important for data interpretation.

Before beginning with assessment of these results, it is worthwhile to recall that the writer personally performed all the Day I and Day II measurements on an Instron machine at U of A, without computerized data analysis but with desirable internal consistency. The tensile specimens, cut from disks in the Department of Chemical Engineering machine shop, were pre-conditioned for moisture equilibration by storage in a closed desiccator with open dishes containing a water/glycerol solution whose composition (water : glycerol = 1 : 7 by volume) was selected to provide an atmosphere of 50.0% relative humidity at 22°C (laboratory temperature). Thus, the only uncontrolled

---

* Data obtained at U of A were extracted from each curve by the writer, using judgement. Values of τ were obtained by weighing the paper cut-out of each tracing, yielding the desired integral $\tau = \int \sigma\left(\frac{dL}{L_0}\right)$. Data from NAIT came from computer analysis and direct property readout.

variable was the RH in the open laboratory (704 CME) where tensile tests were made. As it happened, major RH differences prevailed on those two days, and it is therefore necessary to evaluate those data in terms of the known ability of nylon 6 to absorb moisture.

When access to the Instron was lost, the measurements were continued and concluded at NAIT. Access to a laboratory of controlled temperature (22.5°C) and humidity (RH = 40%, different from the other two test days) was granted by Mr. Jack Foster, Head, Plastics Engineering. Specimens were preconditioned at NAIT so that no changes could occur between the storage and testing phases. A new tensile testing machine (Lloyds L6000R Universal Testing Machine) was employed, with on-line data analysis which provided the four numerical parameters characterizing each $\sigma(\varepsilon)$ curve; hard copy of the curve was also produced. All tests at NAIT were completed in one afternoon (Day III). However, another unlikely complication arose, not apparent at that time: the ε scales on the Lloyds machine and the Instron machine did not agree. (The reasons for this presumption are discussed below.) Therefore, parameters involving ε cannot be compared confidently between the U of A and NAIT measurements. Nonetheless, a wealth of useful data were obtained.

Because of the different circumstances surrounding the three test days, the following discussion is organized to address the three data sets separately to a first approximation. As discussion continues, interconnections between the data sets will be made, and references to the impact testing results will be supplied.

Table 8.1. Average mechanical properties from tensile tests

Table 8.1.I. Day I, RH = 53%, T = 25°C

Properties*	Nylon 6	Untreated glassfibre (average)	Treated glassfibre# (average)		
			^{1}Silane I	^{1}Silane II	^{1}Silane III
			10%	5%	10%
σ_b (MPa)	56.90 ± 1.08	39.31 ± 1.55	31.25 ± 0.75	45.35 ± 0.45	45.71 ± 1.09
ε_b (%)	7.08 ± 0.45	0.614 ± 0.04	0.813 ± 0.08	0.884 ± 0.11	0.900 ± 0.12
Toughness (MPa)	2.99 ± 0.17	0.15 ± 0.03	0.17 ± 0.02	0.24 ± 0.04	0.24 ± 0.05
E (GPa)	2.81 ± 0.09	8.76 ± 0.50	7.71 ± 0.26	8.36 ± 0.39	7.71 ± 0.42

* Using Instron machine

Notation: ^{i}Silane J (i = 1,2; J = I, II, III, IV) = composite disk with silane type J made at i^{th} time

Table 8.1.II. Day II, RH = 75%, T = 25°C

Properties*	Treated glassfibre# (average)	
	^{1}Silane II	^{1}Silane III
	10%	5%
σ_b (MPa)	41.77 ± 0.44	42.46 ± 0.69
ε_b (%)	0.78 ± 0.05	0.73 ± 0.05
Toughness (MPa)	0.19 ± 0.02	0.17 ± 0.02
E (GPa)	7.80 ± 0.62	7.72 ± 0.57

* Using Instron machine

#Notation: ^{i}Silane J (i = 1,2; J = I, II, III, IV) = composite disk with silane type J made at i^{th} time

Table 8.1.III. Day III, RH = 40%, T = 22.5°C

Properties*	Untreated glassfibre (average) (wet)	Untreated glassfibre (average) (dry)	Treated glassfibre# (average)				
			Silane III			Silane III	Silane IV
			$^{2}5\%$	$^{2}10\%$	$^{1}15\%$	$^{1}1.5\%$ (dissolved)	$^{1}10\%$
σ_b (MPa)	6.30 ± 0.19	40.41 ± 2.18	58.26 ± 1.52	42.30 ± 0.93	45.25 ± 1.20	35.70 ± 1.77	95.21 ± 3.56
ε_b (%)	3.11 ± 0.43	1.88 ± 0.07	2.67 ± 0.11	2.07 ± 0.13	2.35 ± 0.12	2.04 ± 0.16	3.50 ± 0.19
Toughness (MPa)	0.59 ± 0.09	0.45 ± 0.04	0.82 ± 0.04	0.49 ± 0.04	0.61 ± 0.05	0.41 ± 0.04	1.67 ± 0.11
E (GPa)	2.70 ± 0.11	2.38 ± 0.48	3.93 ± 0.76	2.49 ± 0.21	2.41 ± 0.43	2.95 ± 0.52	2.90 ± 0.10

* Using Lloyds L6000R Universal Testing Machine (at NAIT)
#Notation: $^{1}X\%$ (i = 1,2; X=5, 10, 15, 1.5) = composite disk at silane concentration of X% made at i^{th} time

Day I (Table 8.1.I)

8.2.1. Nylon, and the role of glass fibre reinforcement

The enormous enhancement of E_s caused by the incorporation of ~ 32% glass fibres, as described in section 8.1.1 for the impact strength studies, has no parallel in the tensile properties studied here. If we take σ_b as the mechanical property of major interest (e.g., to use for comparison with E_s in impact test), we note that the composite made from untreated glass fibres is weaker than the pure nylon (σ_b = 56.9 and 39.3 MPa for nylon and composite, respectively). This is clear evidence that there is an almost total

lack of adhesion between the fibre and matrix. For example, a simple parallel-element model for additive load sharing between the two phases would interpret this result as being equivalent to no fibre contribution: using $V_f = 32.4\%$ (Table B-6), and requiring that the nylon phase ($V_m = 67.6\%$) take 100% of the load, gives a prediction that the unbonded composite tensile strength would be $\sigma_b^{1U} = 0.676 \times 56.9$ MPa = 38.4 MPa, almost exactly what is measured (39.3 MPa).

Thus, when the tensile load becomes large enough to fracture the nylon phase, there is no load transfer from the nylon matrix to the glass fibre to help. Because there is no mechanical or chemical link between matrix and fibre, the failure is characterized by separation of fractured nylon fragments with glass fibres cleanly pulled out of their "sockets" from one side or the other. This is illustrated by an SEM micrograph in Figure 7.6, where the fracture surface reveals the intact nature of the fibres and the total absence of "contaminating" matrix material on the fibre surfaces.

Such behavior is not always seen in composites that lack special coupling agents between fibre and matrix, but the case of nylon and glass fibre causes special problems. The nylon absorbs moisture from the air and transmits it to the hydrophillic glass interface, where it serves to disrupt whatever weak adhesive forces would have existed between nylon and glass in a dry environment. It also serves as a lubricant to reduce interphase load transfer and assist the separation of the two solid phases upon matrix rupture and fibre pull-out. Thus, the nylon/glass fibre combination can be used in a practical composite material only with the use of coupling agents.

The nylon 6 itself, as produced by the *in-situ* process employed here, seems to be of good quality and comparable or superior to established commercial products. For example, 6 parameters cited in Table 2.3 for commercial nylon compare with ours as shown in Table 8.2.

Our value of σ_b (57 MPa) is higher than the commercial values are expected to be, at the same density (crystallinity) and humidity. This is consistent with

having an E_s (16.7 J/m) that is somewhat lower than the published one (≈ 32 J/m). These differences could arise from a unique crystal morphology or orientation produced by our particular *in-situ* mold polymerization. To see if this might be reflected in a shift of the melting point (T_m), we employed a differential scanning calorimeter (TA Instruments DSC 2910) to examine the thermal behavior of our nylon 6 and the composites.

Results of DSC testing, shown for the pure nylon 6 in Figure 8.3, are in good agreement with reports in the literature. The overall performance of the material on a full heating/cooling cycle (temperature scan rates at 10°C/min), displayed in Figure 8.3(a), indicates a strong endothermic peak in the range 220-225°C which we assign to crystalline melting, identifying the peak position as T_m. There is also a small inflection visible in the 40-50°C range, which we interpret as the glass transition and label the

Table 8.2. Comparison of commercial nylon 6 and our nylon 6

	This study	Table 2.3 (column b)
ρ, g/cm^3	1.12-1.13 * ($\overline{\rho}$ = 1.125)	1.12-1.14
σ_b, MPa	56.9** (@RH = 53%)	41-165
ε_b,%	7.1**	30-300
E, GPa	2.81 ** (@RH = 53%)	0.7 (@RH = 50%)
Izod, E_s, J/m	16.7*** (RH = 46%)	32-160

* Table B-1.....** Table 8.1.....***Table B-4

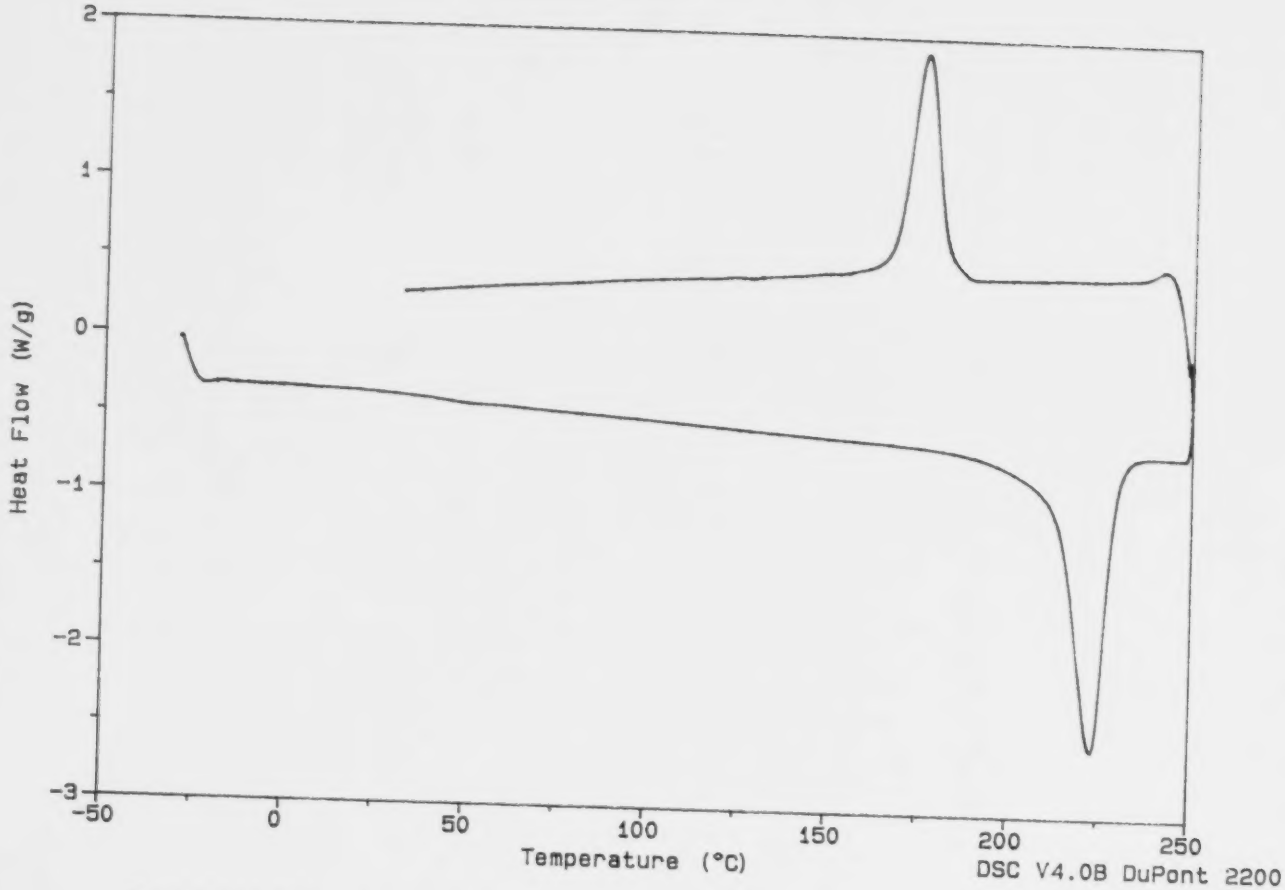

Figure 8.3 (a). Differential scanning calorimeter (DSC) scan for nylon 6 sample taken from pure-nylon 6 disk. A full cycle is shown, heating from -30°C to 250°C, holding for 5 minutes at 250°C, and then cooling back to room temperature. Scan speed 10°C/min.

midpoint as T_g. Magnifications of these two regions, with software analysis superimposed, are given in Figures 8.3b (T_m) and 8.3c (T_g). From the former, we find that $T_m \cong 223°C$, in perfect agreement with the commercial product reports in Table 2.3 (see reference **13** column). From Figure 8.3c we see that $T_g \cong 42°C$, somewhat below the 49°C from Table 2.3 (**13**), but with an effective range that reaches to 49°C. The cooling peak in Figure 8.3a is displaced to a temperature (≈175°C) well below the heating peak, but this is normal with polymer crystallizations.

Two examples are also presented of DSC analysis of the nylon composites. First, with no silane involved, we see results for a specimen from the [1]Untreated disk in Figure 8.4. The overall thermal cycle, in Figure 8.4.(a), shows several differences from that for pure nylon 6 (Figure 8.3.(a)): the heating peak is shifted downward about 5°C, the glass transition is more visible and broader, and the cooling peak much smaller (but <u>not</u> shifted). The detailed analyses, in Figure 8.4.(b) and 8.4.(c), give $T_m = 218°C$ and $T_g \cong 40$ °C. Thus, the presence of the glass fibres <u>did</u> alter the crystallization process in the mold enough to drop the average T_m by 5°C; perhaps "transcrystalline" crystallites were formed on the glass fibres as reported by Verdeau and Bunsell (**29**) in connection with PEEK crystallization on carbon fibres. However, the non-shifted cooling peak (relative to pure nylon) differs from the observations made in PEEK/carbon fibre systems by Lee and Porter (**24**), who reported higher crystallization temperature when fibres are present; possibly their experience cannot be generalized to apply to markedly different systems, such as nylon/glass. Concerning Figure 8.4.(c), the apparent drop in T_g of 2°C is consistent with the T_m drop. But more importantly, the greater prominence of the glass transition itself indicates that the nylon matrix in the composite was formed with a higher fraction of amorphous material than existed in the pure-nylon disk (as is also consistent with the small cooling peak in Figure 8.4.(a)). Nylon melt appears to be rejected by the

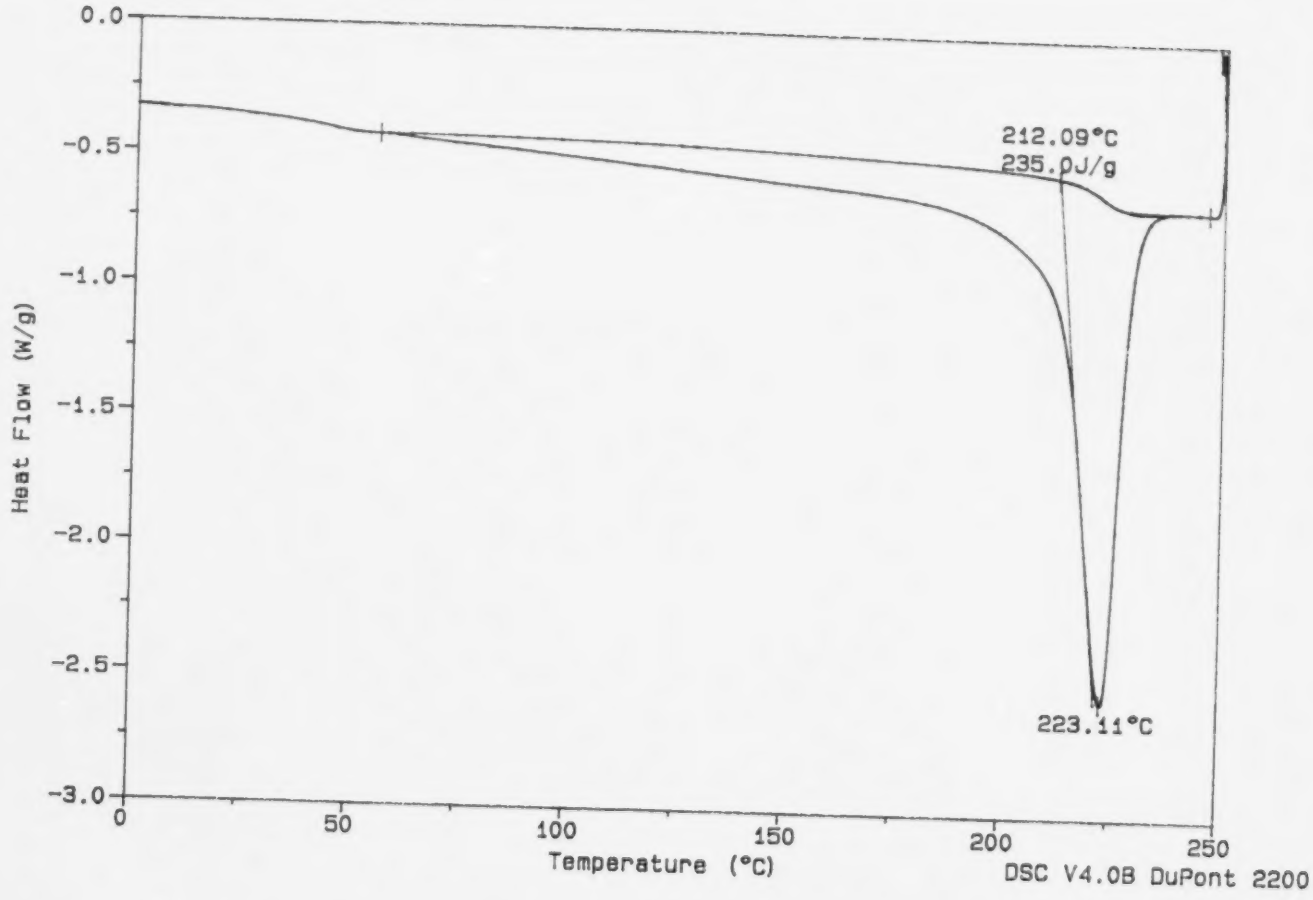

Figure 8.3 (b). Expanded region of DSC heating trace, for pure nylon 6, near crystalline melting regime.

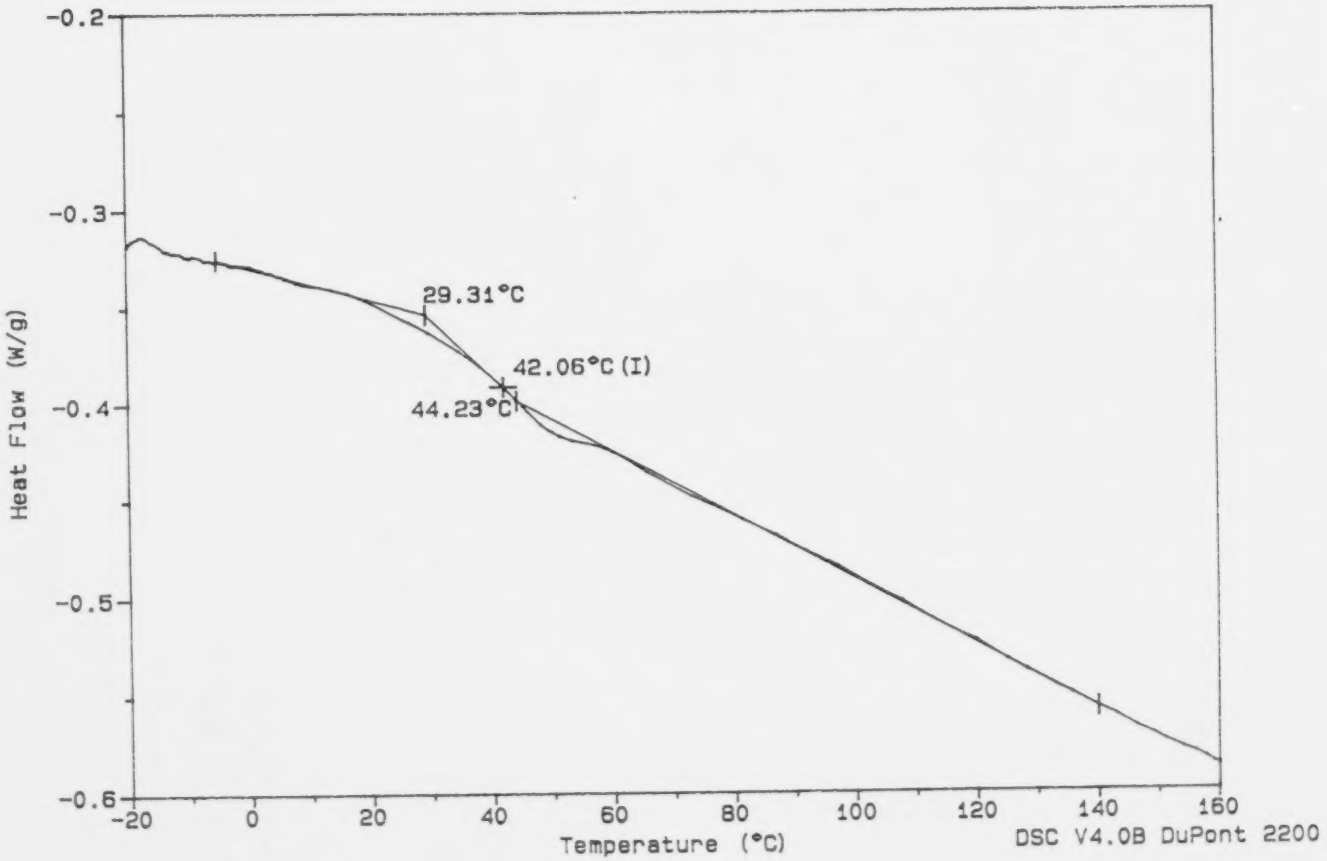

Figure 8.3 (c). Expanded region of DSC heating trace, for pure nylon 6, near glass transition regime.

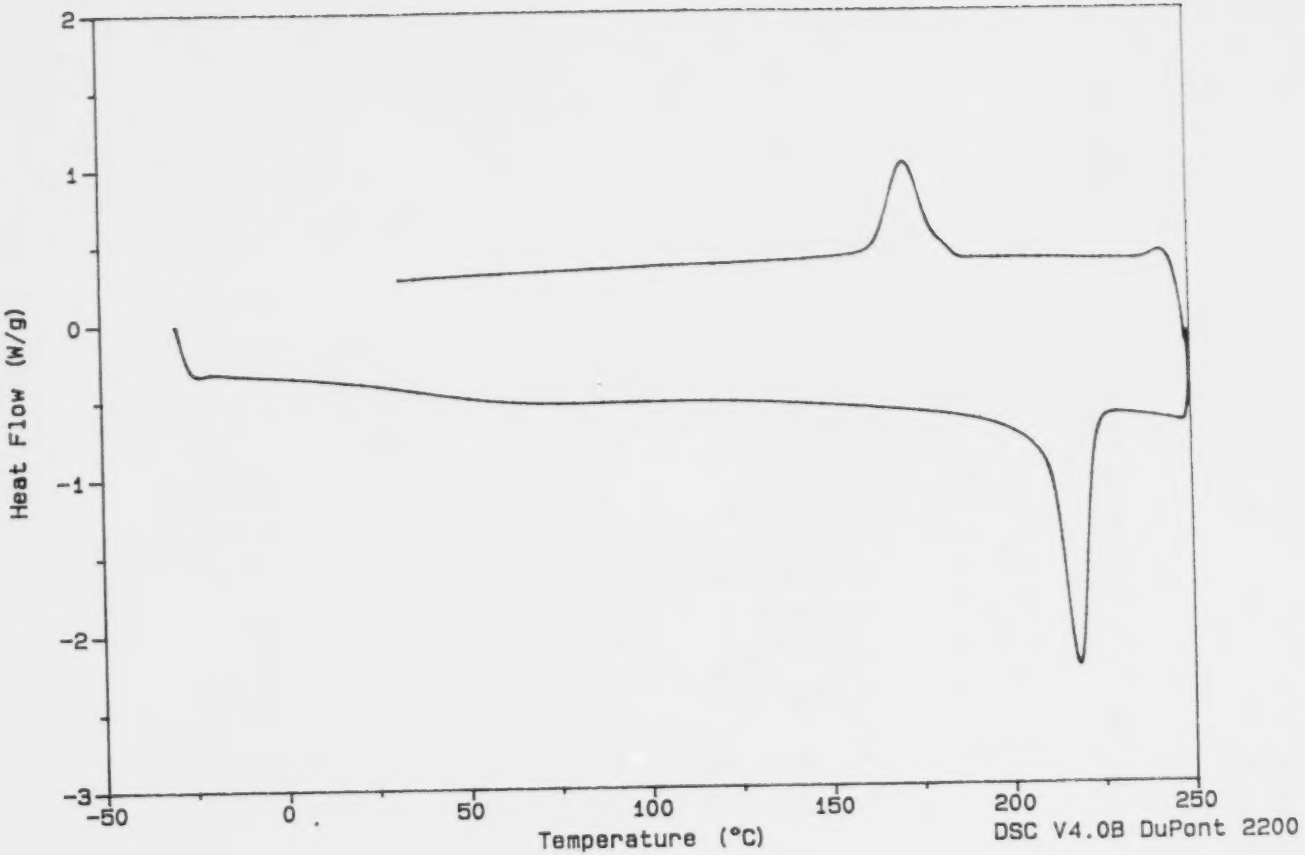

Figure 8.4 (a). DSC scan for composite sample taken from specimen of [1]Untreated disk ($\overline{V}_f$ = 32.4%). A full heating-cooling cycle is shown, with scan speed 10°C/min.

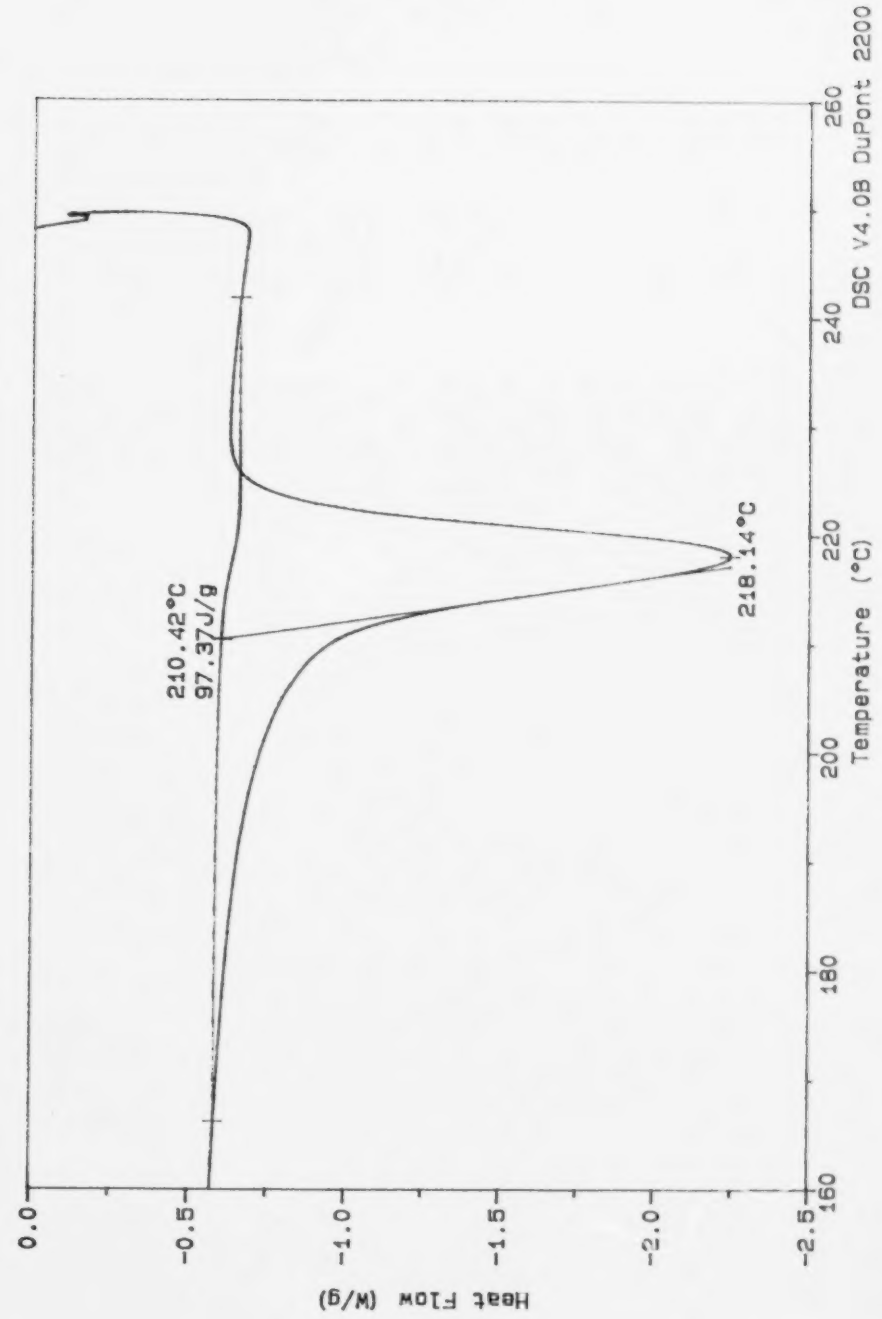

Figure 8.4 (b). Expanded region of DSC heating trace, near the nylon 6 melting regime, for [1]Untreated composite of nylon 6 and glass fibres with $\overline{V}_f = 32.4\%$.

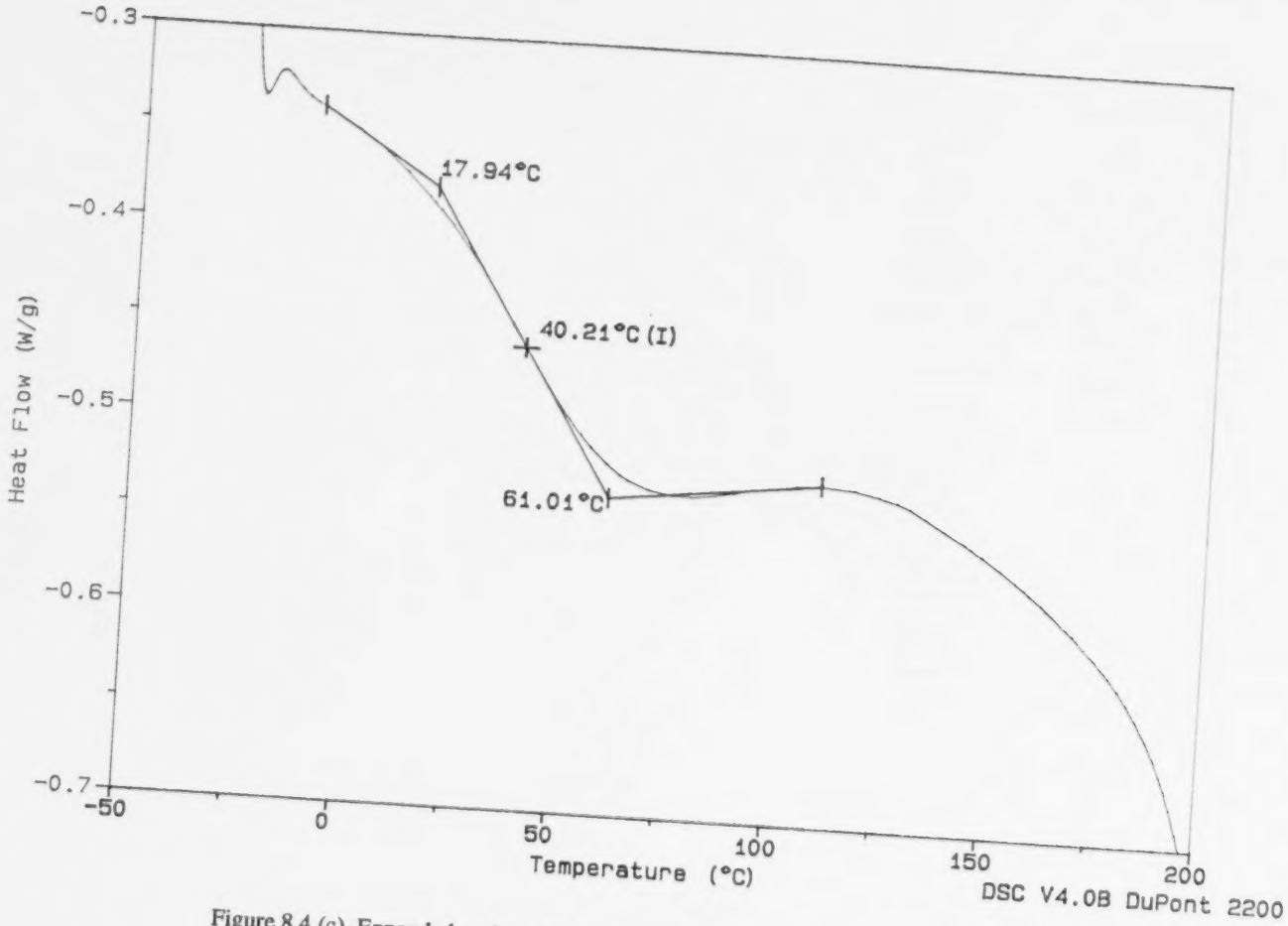

Figure 8.4 (c). Expanded region of DSC heating trace, near T_g for nylon 6, for [1]Untreated composite with $\overline{V}_f = 32.4\%$.

incompatible glass surface, to the point where the total volume fraction of crystalline nylon is diminished in untreated fibre-mat composites.

The final thermal analysis described here involves a silane-containing composite, Silane II (10%). Its overall thermal cycle, in Figure 8.5.(a), is far more like that of the untreated composite (Figure 8.4.(a)) than the pure nylon (Figure 8.3.(a)), suggesting that the silane had little improvement to offer in terms of enhancing the crystalline volume fraction of nylon in the composite. Figure 8.5.(b) shows that T_m was reduced still further (by 1°, to 217°C), which is not favorable either. However, the glass transition (Figure 8.5.(c))--which resembles the one in Figure 8.4.(c)--has a T_g which manages to jump up by 4° (to 44°C), above that of pure nylon 6. The consequences of these seemingly small shifts of T_g and T_m can be evaluated only by mechanical-property testing, which follows.

One feature of the pure-nylon data in Table 8.1.I is a source of concern, however--ε_b = 7.1% is smaller than published values for nylon 6 of comparable crystallinity ($\varepsilon_b \cong$ 25-30%) by a factor of 1/3-1/4. Whereas this could be a manifestation of a unique and strong crystal structure, the measured ε_b seems too small to interpret in this way. Thus, the reported small value for ε_b suggests that the U of A Instron (or the extensometer that was used) was providing ε measures in error by a factor of 3 or so (too small). This would also force the corresponding values of $E = \left.\frac{d\sigma}{d\varepsilon}\right|_{\varepsilon \to 0}$ and $\tau = \int \sigma d\varepsilon$ to be in error by being reported, respectively, too large by 3 and too small by 1/3, and comparison of our E = 2.81 GPa with the published (Table 2.3) value E = 0.7 GPa seems to support this suspicion.

8.2.2. Silanes as coupling agents

Inspection of σ_b values in Table 8.1.I for composites prepared from silanes demonstrates that (a) Silane I was not only ineffective but actually harmful, dropping σ_b(I)

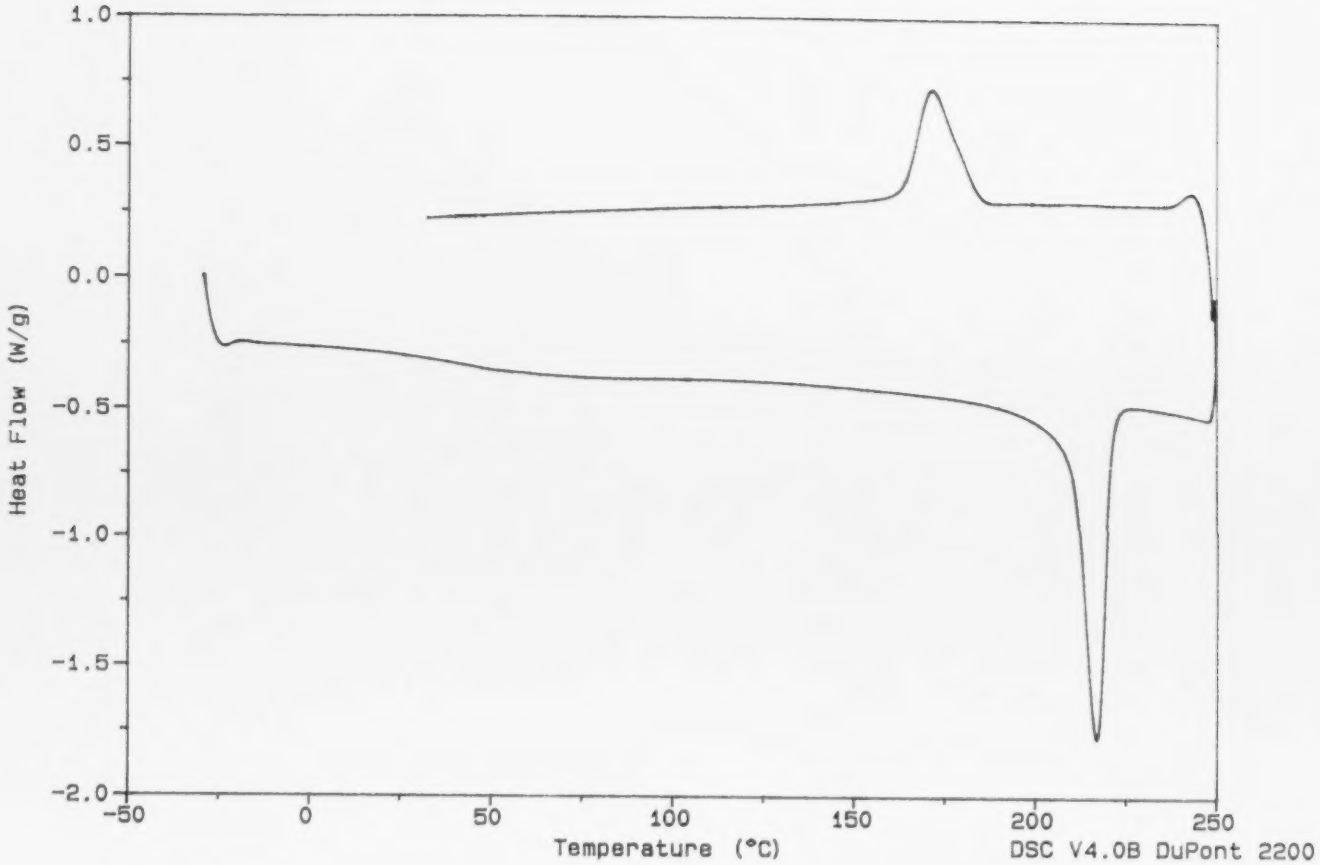

Figure 8.5 (a). DSC scan for composite sample taken from specimen of Silane II (10%) disk ($\overline{V}_f$ = 32%). A full heating-cooling cycle is shown, with scan speed 10°C/min.

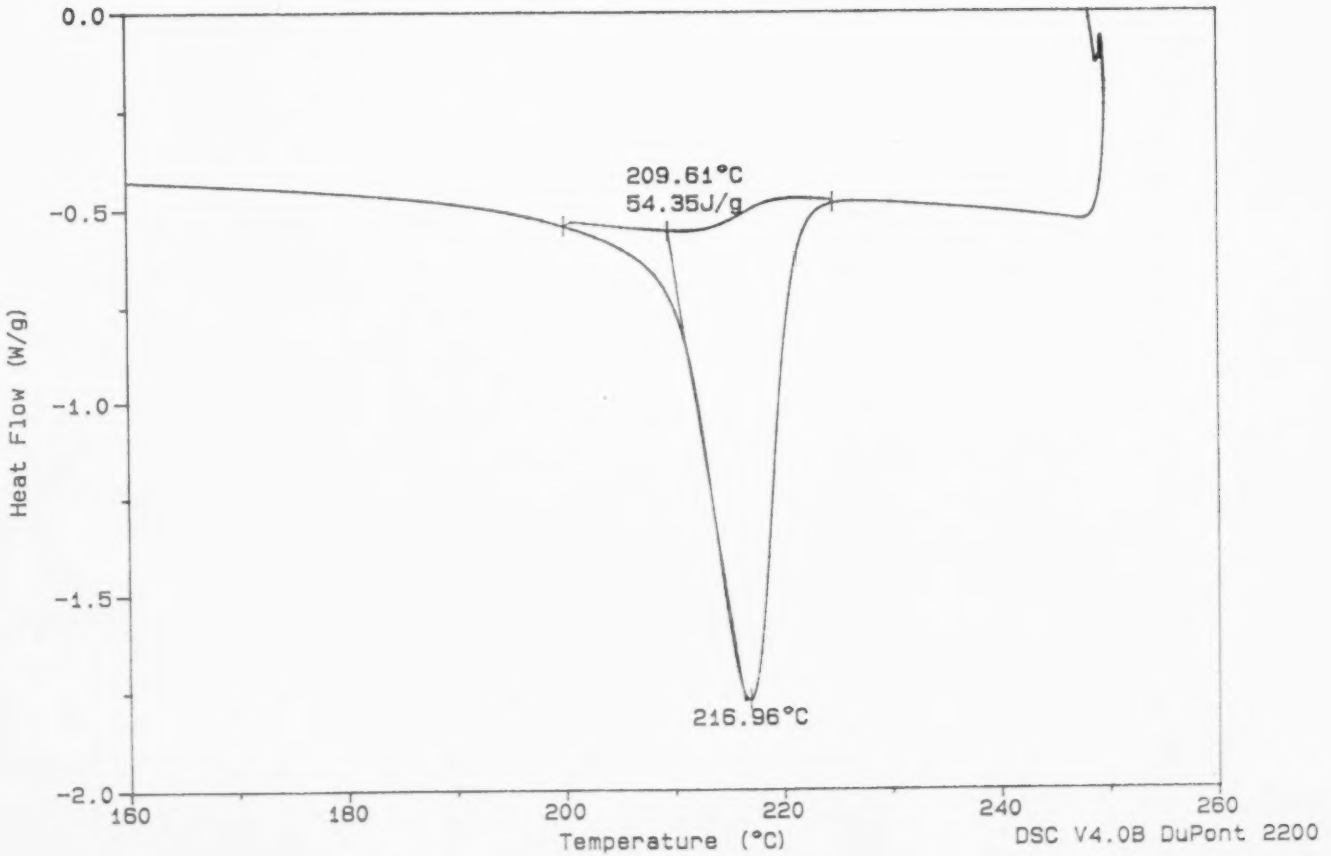

Figure 8.5 (b). Expanded region of DSC heating trace near the nylon 6 melting regime, for Silane II (10%) composite disk ($\overline{V}_f$ = 32%) of nylon 6 and glass fibres.

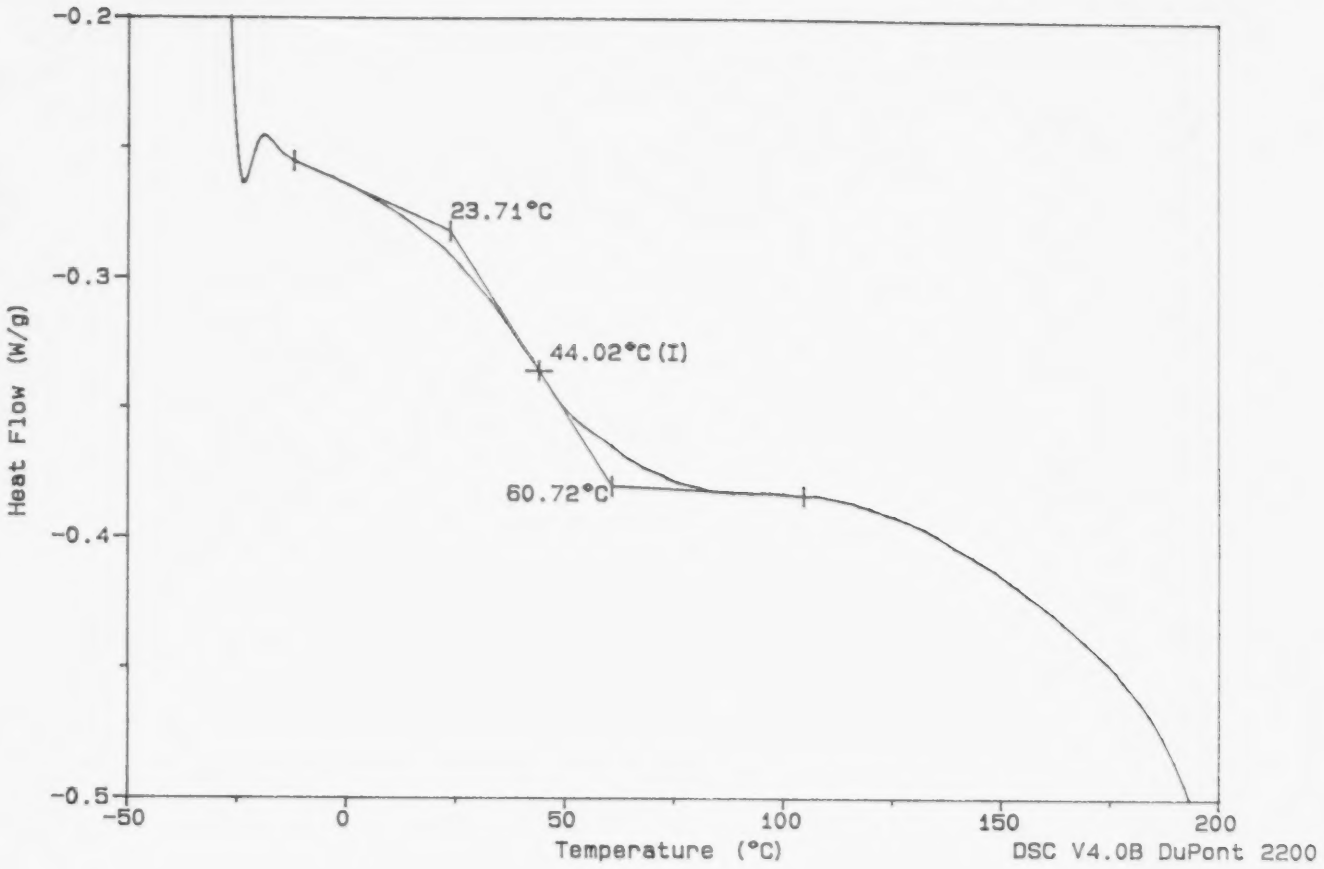

Figure 8.5 (c). Expanded region of DSC heating trace, near the nylon 6 T_g, for Silane II (10%) composite disk ($\overline{V}_f$ = 32%) of nylon 6 and glass fibres.

even below that of the untreated-glass composite by about 20%; and (b) Silanes II and III were successful, to an equal extent, in securing enough coupling to increase σ_b about 15% above the untreated-fibre case. Furthermore, Silanes II and III had an increase in τ of 60%. Thus, all three "failure properties" responded favorably to Silanes II and III.

Silanes I was not expected to do well since its molecular structure (Chapter 6) did not give it the capability to bond with a glass surface. However, its net effect could not be predicted, and there seemed to be some opportunity for a physical adsorption of Silane I because of possible affinities between the silicon atoms in silane and glass. However, its deleterious performance with σ_b suggests that it not only offered no coupling by physical adsorption, but functioned as a better lubricant than water and probably as a nylon 6 plasticizer (diluent/solvent) as well. In the latter capacity, it could have dissolved and/or disrupted crystal structures as well as softened the amorphous regions of the nylon matrix too. Such behavior would, indeed, tend to produce the observed effects of reduced σ_b but mild increase of ε_b and τ.

The low-strain (non-failure) parameter E is presumably measured without disruption of microstructure; hence, slippage between fibre and matrix is excluded as an explanation for poor performance. Thus, the drop in E seen for the use of all silanes, relative to the untreated-fibre case, must be explained in some other way. We speculate that an excess of non-bonded silane--perhaps physically adsorbed on the glass fibres--was carried into the mold despite the effort made to wash it off. Thus, the same dilution/plasticization of the nylon might have occurred, making it easier to deform (lower E, but also larger ε_b, as is also seen here). Rather unexpectedly, the effect is identical in magnitude for the non-bonding Silane I and the good-bonding Silane III, but this could simply mean that their solubilities in the nylon matrix were comparable. Possibly because of having both been deposited from 10% toluene solutions, they carried equal (non-bonded) excess into the mold. Since Silane II caused far less of a drop in E than the other

two, we must again speculate that either its solubility in nylon is less (unlikely) or that those fibres had less adsorbed excess--coming from a 5% treating solution--than did the others.

8.2.3. Concentration effects with silanes

For complete silane coverage of all glass surfaces in one mold-filling fibre mat, very little silane is needed. A rough calculation in Appendix E shows that about 10^{20} molecules will suffice, whereas our fibre-treating procedures normally involved toluene solutions containing about 100 ml of silane (about one mole, or 6×10^{23} molecules). The excess was enormous, intended to saturate the glass surface as quickly as possible. However, if only a monolayer of silane was involved here, then there should be no direct-coupling differences between any of the solution treatments used here. This was clearly not true for impact studies, lending additional support to our speculation above, about excess adsorbed silane layers on the glass surfaces contributing the results.

However, the role of the concentration variable (c) in the fibre-treating process (or other influences the silane may have, as concentration is varied) is highly ambiguous in the tensile data. In fact, the easiest interpretation of data in Table 8.1.I--for Silanes II and III only, since we will have no further use for Silane I--is that there is no c-effect at all. That is, the properties of the composites produced from fibres treated with 5% Silane II and 10% Silane III are virtually identical, within the normal data scatter. The one exception is E, the only parameter which drops for all silanes (relative to the untreated composite) and simply drops least for c = 5% (and this could be independent of silane type).

Thus, it appears from Table 8.1.I that the three ultimate properties reported are independent of treatment-solution silane concentration and silane type, having in both (bonding) cases the values σ_b = 45 MPa, ε_b = 0.89%, and τ = 0.24 MPa. We should also point out that these tests (Day I) were carried out in air having RH = 53% and the

numerical results--since we are dealing with nylon--could change on other days having different RH (see below).

Day II (Table 8.1II): RH = 75%, T = 25°C

8.2.4. Further study of silane type and concentration

In section 8.2.3, it was argued that the production of identical results in the failure properties of composites using glass treated by two different silanes, at two very different concentrations, could be due to both treatments merely completing the fibre saturation coating and those coatings being functionally equivalent (in bonding to glass, and compatibility with the surrounding nylon matrix). However, the clear c-dependence of impact test results and their sensitivity to silane type encourages the further search for such influences in tensile data.

For example, one might also explain the Day I results by proposing that Silane II was the more effective agent, since it did as well when deposited from 5% solution as Silane III (hypothetically, now, less effective) did from 10% solution. Such an argument, though seemingly unlikely, could not be ruled out from the Table 8.1.I data. Therefore, on Day II the c-roles were reversed: Silane II at 10% and Silane III at 5% were used.

Results, displayed in Table 8.1.II, demonstrate that the premise seems to fail. The Silane II and III systems again produced virtually identical values of the failure parameters (and E), within the data scatter. While this would seem to lay to rest the contention that c-effects reside within the tensile data, there remain a few unanswered questions about it. For example, in the Day I results, the lower-c silane treatment produced a substantially high value of E, which has bearing on the silane influence on matrix quality rather than on bonding. And, in the Day II data, there is a hint that the

lower-c silane treatment produced a marginally higher value of σ_b. More about this will emerge on Day III, below.

8.2.5. The role of humidity

The composite failure parameters measured on Day II are different from those measured on Day I, being "poorer" in each case: weaker (σ_b drops from 45 to 42 MPa), more brittle (ε_b drops from 0.89% to about 0.75%), and correspondingly less tough (τ drops from 0.24 to 0.18 MPa). Only the value of E, unrelated to microstructural change upon specimen deformation, seems to be about the same ($\approx$ 7.7 GPa) on both days.

The fact that these parameter differences are individually distinct and statistically significant is worth noting; that they occur together and collectively move in the same direction (toward poorer performance) is worth investing some thought; and that two independently-produced disks, utilizing two different silanes for treating their fibres from solutions of two different concentrations, showed agreement with each other so closely on these points means that some independent physical variable is at work and needs to be identified, controlled, and studied.

We believe this variable is the humidity. We are seeing here how a complex physico/chemical assembly (our nylon-glass composites, with and without coupling agents) can respond to environmental factors that would normally be ignored in most human activity. The changes in humidity between Day I (RH = 53%) and Day II (RH = 75%) are definitely large enough to have an influence on the nylon 6 matrix of these composites, and that means also an influence on the nylon 6 matrix of these composites, and that means also an influence on the nylon/glass fibre interface. The direction of change observed during the higher humidity on Day II was in the direction of what one would expect from these composites, as nylon would absorb more moisture from the air

(becoming plasticized, and weaker) and transmit more moisture to the glass fibre interface (weakening the bonding already there, to permit interface failure at low strain).

Day III (Table 8.1III): RH = 40%, T = 22.5°C

All these tests were made at NAIT, using a different tensile testing machine (Lloyds L6000R Universal Testing Machine) which was highly automated and produced the data analysis quickly. The major problem which emerged later was that the strain scale of the Lloyd did not agree with that of the Instron in Room 704 CME at U of A. We now believe the Lloyd instrument is correct and the Instron system (with extensometer) incorrect; arguments were advanced earlier in this direction, after comparing the ε-related material properties of nylon 6 as measured with the Instron with those published in reputable encyclopedias and trade literature. Since the Lloyd agreed with the literature, and disagreed with the Instron in a consistent fashion, we feel the material parameters emerging from those measurements are accurate. Although a correction to the Instron ε-data (ε, τ, E) is possible, there seems to be little need for doing it now; no conclusions based on Day I or Day II data would be altered in any way.

The other unique feature of the tests at NAIT was the use of their temperature/humidity-controlled testing laboratory. All Day III tensile specimens were kept there for about 10 days for equilibration at 22.5°C and RH = 40%. This low value of RH was in a range where nylon is especially sensitive and composite properties behaved differently than at higher RH, both qualitatively and quantitatively. While this initially caused some confusion, it ultimately proved to be vital factor in defining the nature and scope of the humidity variable.

It was decided to do most of our final work with Silane III. Its behavior seemed to be about the same as Silane II, and its cost was much less. (Silane II: $39/100ml; Silane III: $9.55/100ml)

8.2.6. Standardization and assessment of the Lloyds data

An untreated disk and its five tensile specimens were used, in a sense, to calibrate and evaluate the laboratory facility at NAIT. It also served to give us a second look at the untreated composite case under different humidity conditions.

Equivalence of stress data between the Lloyd and the Instron is established by the extremely close agreement of the two on the untreated samples. For example, the Day I test by Instron gave $\bar{\sigma}_b = 39.3 \pm 1.6$ MPa and the Day III test by Lloyds gave $\bar{\sigma}_b = 40.4 \pm 2.2$ MPa. Even though these values are so close as to be statistically equivalent, one could point out that the difference in their $\bar{\sigma}_b$ is in the direction expected from humidity considerations: the dryer air on Day III would lead to a lower moisture level in the nylon and thus enhanced nylon properties, as well as less moisture at the nylon/glass interface.

Disagreement on strain data between the two machines is established by the consistent difference in all the material properties related to the strain variable. Table 8.1.III gives $\varepsilon_b = 1.88.\%$ on Day III, while Table 8.1.I gave $\varepsilon_b = 0.61\%$ on Day I. While a skeptic could point out that this discrepancy might be explained on terms of sample non-reproducibility, we doubt this very much, in view of the agreement on σ_b and the consistent reproducibility shown throughout this study. One might also argue that the RH difference played a role--except that the direction of change would then be opposite to what is observed (ε_b on Day III would then be smaller than ε_b on Day I, as dryness reduces ductility and straining capacity). Finally, we note that if the ratio of the two strain measurements is used as an Instron strain calibrator,

$$k = \left.\frac{(\varepsilon_b)_{III}}{(\varepsilon_b)_I}\right|_{2_U} = \frac{1.88\%}{0.61\%} \cong 3.0, \qquad (8.1)$$

then k can be applied also to the ε-related properties of pure nylon 6 (Day I data) and determined whether they would then agree better with published values:

Nylon 6 property	This study (ρ = 1.125)		Published
	Day I	Corrected Day I	Table 2.3
ε_b,%	7.1	$k(\varepsilon_b)_I = 21.3$	25 (for ρ = 1.12)
$\tau = \int_0^{\varepsilon_b} \sigma d\varepsilon$	2.99	$k\tau_I = 8.97$	n/a
$E = \left(\frac{\sigma}{\varepsilon}\right)_0$, GPa	2.81 (RH = 53%)	$E_I/k = 0.94$	0.7 (RH = 50%)

Clearly, use of the objective k-correction comes very close to bringing the Day I nylon property data into agreement with accepted values. One could also work backward, noting that k = 4 does an even better job with the pure nylon 6 data, but would require $(\varepsilon_b)_I = (\varepsilon_b)_{III}/k = 1.88/4 = 0.47\%$ rather than the directly "measured" 0.61% with the faulty strain scale. Use of the k-factor to compare the twice-measured ε-related properties of the untreated composite gives:

Property	Instron Measured Day I	Corrected Day I	Lloyd Measured Day III
ε_b,%	0.61	$k\,\varepsilon_b = 1.83$	1.88
τ, MPa	0.15	$k\tau_I = 0.45$	0.45
E, GPa	8.76 ± 0.50	$E_I/k = 2.92 \pm 0.17$	2.38

Here, the agreement is perfect (using k = 3.0) for τ but a bit short for E; use of k = 4.0 would give $E_f/4 = 2.19$ and thus be an over-correction.

In any event, it is rather conclusively demonstrated that all the Day I and Day II strain-related data in Tables 8.1.I and 8.1.II are in error by a factor of about 3.0 and possibly as large as 4.0. (This information will be transmitted to other users of the Instron). Also demonstrated by this exercise are (a) reproducibility of composite (untreated) samples, (b) complete consistency of nylon 6 properties with accepted values emanating from commercial production sources, and (c) reliability of the Lloyd/NAIT resource for such measurements.

8.2.7. Concentration effects revisited

A complete set of data was obtained with Silane III composites, over the treatment range c = 5%, 10%, and 15% (for the first time), all on the same day. Since the 5% and 10% cases had been tested before (Days II and I, respectively), they served as useful sources of information about reproducibility and possible humidity effects.

Inspection of Table 8.1.III shows that the functions σ_b (c), ε_b (c), and τ (c) are definitely not constants with some weak secondary dependence on humidity, as the data sets on Day I and Day II have suggested. Instead, the c-dependence appears to be highly complex, with a minimum for all three functions in the vicinity of $c \approx 10\%$. (Recall that $E_s(c)$ was just reaching its high plateau at c = 10%, too ; see Fig. 8.2). This behavior is shown graphically in Figure 8.6, along with E(c) which appears not to have a local minimum at c = 10% or elsewhere.

Figure 8.6 is drawn with the c = 0 point taken to be the untreated sample, which adds to the complexity of these functions because the failure properties must have low-c maxima as well as the minima near c = 10%. One must be careful when assessing such apparent behavior, since both the maxima and minimum rely for their existence upon

the surprisingly high set of points at c = 5%. Inspection also shows that a smooth monotonic curve for the "failure" curves could be drawn downward to c = 0 from the c = 15% and 10% points, if the high c = 5% points could be ignored (lending plausibility to the argument that the 5% points are simply wrong). However, the presence of E(c) supports the validity of those points; E(c) is the one function which would not extrapolate monotonically to the c = 0 point, if the c = 5% point were absent. It is already heading upward from at least c = 15%, and the requirement that it go through a maximum at lower c is already clear.

It remains to explain the physics responsible for the peculiar curve-shapes in Figure 8.6. We suspect that the implied maxima at very low c (say, c_m) will be found to be real, corresponding--at the pinnacle--to 100% saturation of the glass fibre surfaces with the coupling agent and no excess of that agent. For $c < c_m$, complete coupling would deteriorate until reaching the c = 0 limit of virtually no coupling between fibre and matrix. For $c > c_m$, the excess coupling agent can serve no positive purpose, either; it merely rides along as a contaminant on the glass mat and is present as the caprolactam flows into the mold and surrounds the fibres. There, it could serve several negative purposes: (a) shield the fibre-bonded silane from the polymerizing matrix and thus interfere with proper thermodynamic compatibility at the surface; (b) form a layer of increasing thickness around the fibre which could also make proper gripping impossible; (c) interfere with the nylon crystallization next to the fibre surface, so whatever coupling occurs is very weak; (d) ultimately, dispersion or dissolution into the hot caprolactam, interfering with polymerization and the development of good high-polymer properties; (e) plasticization and softening of the polymer matrix, most seriously near the fibre surface but also elsewhere.

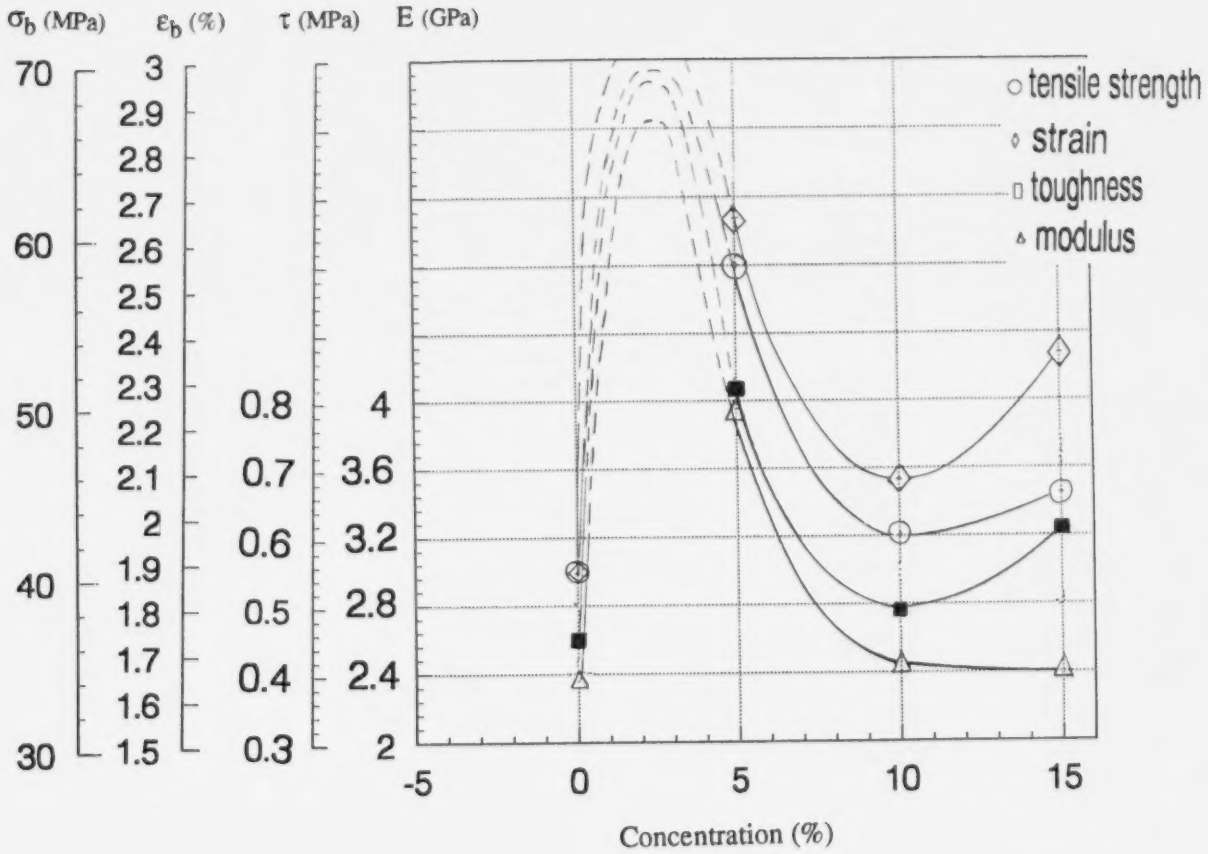

Figure 8.6. Mechanical properties from tensile test (σ_b, ε_b, τ, E) of Silane III at different concentrations (5, 10, and 15%).

The presence of the minimum value (at c_0, say) for the failure curves is not easy to understand. It implies that some strengthening mechanism exists and is ultimately going to become prominent at $c > c_0$. Possibly the transmitted excess silane film is participating chemically in the polymerization or crystallization to make a better nylon, or is itself forming a particulate dispersion of nonsolubilized solids that provides additional reinforcement. This would definitely be a byproduct of the process and, though having a positive nature, would not be part of a commercial process. The major thrust in future work should be to exploit the lowest-c regime, both because it is cheaper and because the potential for property improvement is far greater--if Figure 8.6 proves to be correct. Fiberglass surface analysis should also be studied in order to understand this phenomenon.

8.2.8. Tensile properties of composites made with Silane IV

This silane is believed **(32)** to function at a higher level than the others, with its amino group participating is stronger interactions (perhaps chemical bonding) with the surrounding matrix as well as bonding to the glass surface. While its performance in impact tests was rather poor (partly because the one disk fabricated with Silane IV was unfortunately made with lower fibre content (V_f = 25.4%), the potential for good tensile performance from that sample remains, because of the commonly observed inverse relationship between impact and tensile performances.

This potential is indeed fulfilled in the tensile tests of the Silane IV (10%) ($\overline{V}_f$ = 25.4%) disk specimens. Table 8.1.III shows that this material outperformed all others tested here, for tensile failure behavior, by a very wide margin. For example, in relation to the next-best material ([2]Silane III (5%), $\overline{V}_f$ = 33.9%). Its failure properties can be expressed by these impressive ratios: σ_b/σ_{b0} = 1.63, $\varepsilon_b/\varepsilon_{b0}$ = 1.31, and τ/τ_0 = 2.04, where the "o" subscript means the reference Silane III material. The Silane IV specimens

did not do as well with E, which at 2.90 GPa was good but was exceeded by [2]Silane III (5%) with a value of 3.93 GPa, and also one other on Day III.

8.2.9. Alternate method for delivering coupling agent to fibre surface

In this work, glass fibres were usually treated as described in Chapter 6. This method consumes an undesirable amount of time and solvent and silane agent. If, by adding a small amount of silane directly into the monomer solution the resulting composite had properties comparable to those obtained with the other method, it will be more economical to add silane coupling agent directly into the monomer. Silane III, chosen for evaluation of this method, was added directly to the hot melted monomer before filling into the mold. The amount added, following Otaigbe (**32**), was computed as 1.5% of the mass of glass fibre mat (150g), or 2.25 g. This corresponds to a silane concentration of about 1.1 wt% in the molten caprolactam that entered the mold. Because of the recipe, this composite is designated as Silane III (1.5%). From Table 8.1.III, testing on Day III showed that Silane III (1.5%) had the lowest tensile strength (except for a wet specimen, discussed below). This suggests that relatively little bonding to the glass occurred and that the addition of the silane to the monomer caused a plasticizing effect in the polymer. Other tensile properties of this composite also proved to be inferior to those of other composites. But, again, this material registered the highest E_s of all that were tested for impact response.

Comparing the Silane IV results of Otaigbe (**32**) and this work allows another assessment of this *in-situ* fiber treatment; both works used the same chemistry of polymerization and mold preparation, but different methods of fiber treatment (Otaigbe delivered the silane as 1.1% solution in hot caprolactam, while we employed a 10.0% solution in toluene at room temperature). The results of both works are tabulated below

for easy consideration. However, one should keep in mind that the Silane IV composite in this work contained $\overline{V}_f$ of only 25.4% while in Otaigbe's specimen $\overline{V}_f$ = 33%.

	$\overline{V}_f$ (%)	σ_b (MPa)	E (GPa)	ε_b (%)
Otaigbe's (O)	33	95.4	3.71	3.7
This work (T)	25.4	95.2	2.9	3.5
Ratio O/T	1.3	1.0	1.3	1.1

Although Silane IV specimens in this work had $\overline{V}_f \cong 25.4\%$ (less than 75% of Otaigbe's), the σ_b and ε_b had almost the same value in both works. If the $\overline{V}_f$ of Silane IV disk in this work had been equal to $\overline{V}_f$ of Otaigbe's disk, the Silane IV disk in this work should have given higher σ_b than the Otaigbe value and virtually the same for E (2.9 GPa × 33/25.4 = 3.77) (It is recommended to study the effect of increasing $\overline{V}_f$ for Silane IV in future work). These results showed that for a failure property like σ_b, the treatment method of immersing the glass fibers in a toluene and silane solution is more effective than that of adding silane into the monomer solution and making hot contact with the glass just prior to polymerization. For E, a non-failure property, the silane delivery system is irrelevant; only $\overline{V}_f$ (and $\overline{V}_v$) is significant.

8.2.10. Performance of a wet composite

The tensile curves of wet untreated specimens (Appendix D) showed yielding and usually a maximum stress, followed by a drop in stress and then failure. The average tensile strength of wet samples was 6.3 MPa while that of the dry untreated ones was 40.4 MPa. This showed the effect of water to debond and deteriorate the already-small adhesion at the interface. From the test results in Table 8.1.III, wet samples had

higher ε_b, τ, and E than those of the dry samples. The higher ε_b was expected because water plasticizes the nylon matrix, and the higher $\tau = \int_0^{\varepsilon_b} \sigma d\varepsilon$ was expected because ε_b is so large, even though σ is diminished. The higher E, however, was a mild surprise, even if only by 12%.

8.3. Correlation of impact tests, tensile tests, and humidity

The previously-mentioned generalization about impact test results and tensile test results being related in some inverse fashion can be put to the test here. Ten disks were involved, including pure polymer (nylon 6) and representatives of the three bonding composites (Silane II, III, and IV). An additional variable, often perplexing to those working with nylon systems, is the humidity on the test day, which certainly alters mechanical properties. To our knowledge, there has never been an effort to correlate these three material and environmental variables. As correlational variables, to represent the two mechanical test types, we select E_s and σ_b as the two parameters of greatest interest. For humidity, we use RH (%).

The final correlation is shown as Figure 8.7. The σ_b vs. E_s inverse relationship appears to be valid, but of differing stength and functionality depending on humidity. For example, when the RH parameter (a line, on Figure 8.7) corresponds to 40%, a nearly pure hyperbolic inverse relationship between σ_b and E_s appears to exist. As humidity increases, the line drops and assumes less upward curvature. Our data extend only to RH = 75%, so that line represents the boundary of our evidence for the correlation for materials internally bonded together.

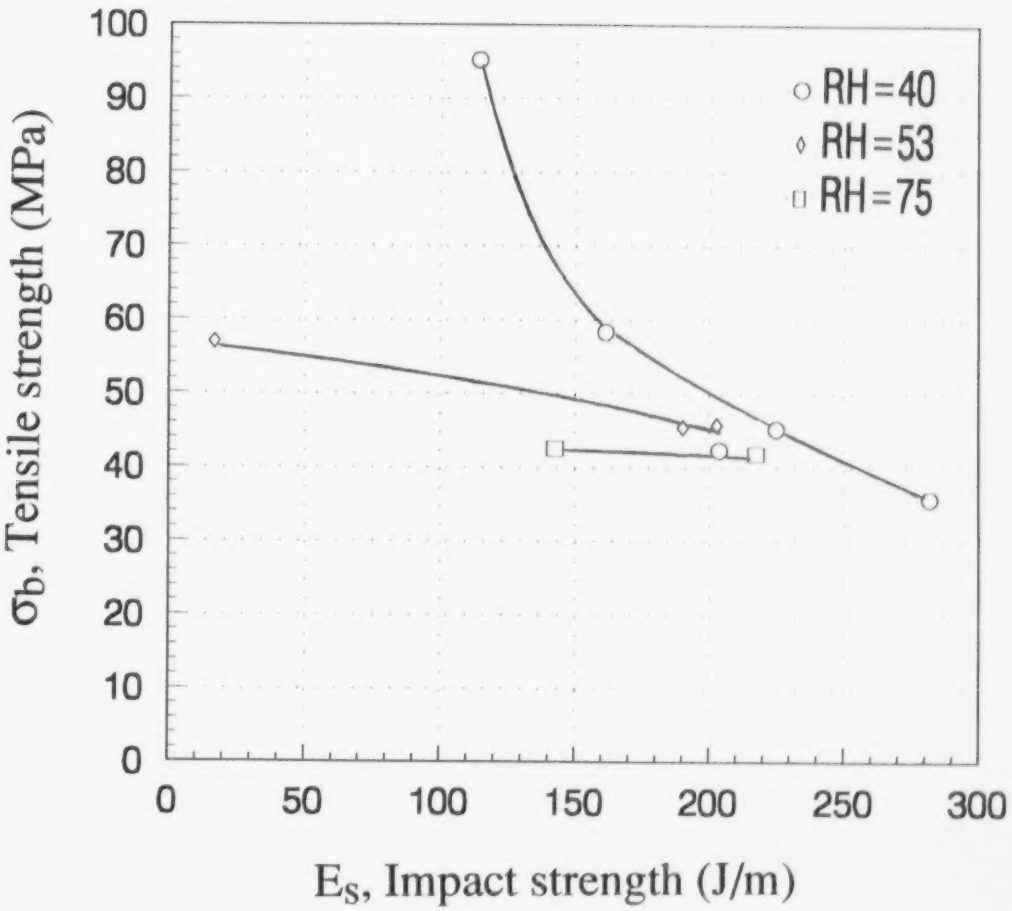

Figure 8.7. σ_b vs. E_s for the bonded composites (Silane II, III, and IV) at different relative humidities.

In general, we can agree that the "inverse" relationship between σ_b and E_s holds true: through RH = 75%, the curves in Figure 8.7 all have negative slopes. The increase in humidity has a striking effect, however, as the functional correlation weakens to the point of being lost altogether. At RH = 75%, for example, the line becomes almost horizontal, and true "correlation" is lost. Instead, Figure 8.7 then becomes more like a map or a phase diagram.

It is noted that the correlation is actually independent of microstructure, since only the phenomenological material parameters (E_s, σ_b) are being correlated. Thus, it is successful in linking the behavior of materials that may be homogeneous (pure polymer, nylon 6), or polymer/fibre composites of different fibre content (mostly 32%, one 24%), or wet and dry forms of complex materials such as composites.

CHAPTER 9

CONCLUSIONS AND RECOMMENDATIONS

9.1. Conclusions

The structural properties of the composites made by *in-situ* polymerization were quite reproducible. Densities were always in a narrow range, $\overline{\rho}$ = 1120-1130 kg/m^3, and the $\overline{V}_f$ were in the range 31.1-34.4%, with differences probably due to non uniformity of the fibreglass mat in the roll, not from the fabrication process. If it is possible to control the uniformity of the mat, uniform fibre composites can be obtained. With fibres treated by Silanes II, III, and IV, $\overline{V}_v$ was consistently at the level of 2% or less.

In each composite disk, there were local variations in V_f, V_v, and ρ. Indications were that higher V_v was found in regions of higher V_f. This may be because there was higher resistance to flow and less penetration, especially around the area that most fibres were highly packed, usually at the center of the mold. Voids can be reduced by improving the wettability of the fibre, as was seen when using silanes which bonded covalently to the glass surface to convert the fibre from hydrophilic to hydrophobic, making it compatible with caprolactam and nylon 6. Thus, silane could improve the wettability of polymer to the glass fibre (reduce γ_c of fibreglass close to the γ_c of polymer). Silanes II, III and IV therefore helped to keep $\overline{V}_v \leq 2\%$, whereas without these $\overline{V}_v$ was in the 3-8% range.

The ρ of nylon 6 was believed to change due to a change of crystal morphology when glass fibre was present. From DSC analysis, pure nylon 6 in disks without reinforcement showed higher crystallized structure than the nylon 6 in composite disks. Its morphological structure (without glass present) was more effective than in commercial nylon 6, since our nylon 6 seemed to have higher σ_b than those in commercial samples at

the same range of density. This high and effective crystallization of our nylon 6 may result from a very slow cooling rate (air-cool), and from the contact of molten nylon 6 with the mold's aluminium surface (some metal surfaces can nucleate the crystal structure of polymer). However, fibreglass surface did not promote crystallization very well, as in this case we found (with DSC) less crystallinity in the composite matrix than in pure nylon 6.

The mechanical properties (both impact and tensile tests) were affected by these structural properties. Higher $\overline{V}_f$ seemed to improve impact strength but, for tensile, it depended on how good the adhesion was at the interface. If no bonding occurs, "reinforced polymer" will give worse properties than unreinforced (pure) polymer; we found lower σ_b on untreated and Silane I composites than σ_b with nylon 6 alone (no stress transfer from matrix to the fibre at the interface, and even worse because there was less matrix to support the load than in pure nylon 6). However, if the bonding is good it will improve σ_b, such as in Silane III (5%) and especially for Silane IV (10%). These displayed a far higher σ_b value than the unbonded filled system and even improved on σ_b for pure nylon (only slightly for Silane III (5%), but significantly for Silane IV (10%)--about a 67% increase). Increases of E_s for all the composites were more than an order of magnitude over the unreinforced nylon. The improvement was due partly to the intrinsic strength of glass and partly to fibre pull-out effects which apparently dissipated considerable energy and made even the poorly bonded fibre systems effective (indeed, this seems to explain much of the inverse relationship found between E_s and σ_b).

The variation of void content also varied the mechanical properties, especially on impact strength. In this study it did not show much effect on tensile properties, since ^{1}U ($\overline{V}_f$ = 32.36%, $\overline{V}_v$ = 3.6%) had almost the same tensile strength (σ_b = 39.3 MPa) as the ^{2}U ($\overline{V}_f$ = 34.41%, $\overline{V}_v$ = 8.9%) with σ_b = 40.4 MPa.

But we have to consider the effect of RH too. Water can penetrate the matrix (nylon is very hydrophilic, for a polymer), and from matrix to the glass interface. Debonding at the surface can cause slippage and consequent higher breaking energy, E_s.

For our tensile tests, the debonding prevented stress transfer to the fibre and the composite broke at very low tensile strength. The extreme case of the moisture effect was observed from the wet untreated composite (σ_b = 6.30 MPa, E_s = 235 J/m) compared to the dry ones (σ_b= 40.41 MPa, E_s = 191 J/m) These also produced the inverse correlation between impact and tensile strength; materials with high tensile strength tended to have lower impact strength and vice versa.

Different kinds of silane had different effects on the fibre/nylon adhesion. Silane I was the least effective among all of them. It did not improve either impact or tensile properties. The physical adsorption between -Si-OR of Silane I and -Si-OH of the glass surface seemed to be very weak, unlike the presence of a Cl group of Silane II and III which can react with the hydroxyl groups at the glass surface. The R-groups of Silane II and III are very similar to each other, but Silane II has a longer R-group than that of Silane III. From the test results, Silane II showed obviously higher impact strength than Silane III and almost the same σ_b in the tensile test (but slightly lower). There are two possible influences that a long R-group can have. One is that long/big R-groups can entangle with the nylon 6 chain and improve by this mechanical effect adhesion to the matrix (in this case the longer Silane II should be better than Silane III). The other mechanism is that the big R-group prevents other silane molecules from reacting with nearby hydroxyl groups (in this case Silane III should be better than Silane II). In our case, the latter effect may be the stronger one, since Silane III had a little higher σ_b than that of Silane II.

By varying the concentration of silane in toluene, for impact strength, it was shown that higher E_s resulted from using higher concentrations, possibly because the non bonding excess silane (believed to be physically adsorbed on the fibres) caused a plasticizing effect in the adjoining polymer. In tensile tests with Silane III (at constant T and RH), we found that all the properties (σ, ε, τ, and E) at 5% were higher than at other concentrations used

here (c>5%). We are therefore led to expect better properties at concentrations less than 5%. From our rough calculation, c = 5% is far greater than what is necessary for the saturation fibre treatment, so the excess silane probably adheres to the silane that reacts to the glass fibre surface. The adhesion of excess silane to the reacted silane at glass surface is probably by physical adsorption, not the covalent bond, so that this excess silane creates some weak bonding between silane itself. This hypothesis should be investigated in further experiments.

Silane IV is undoubtedly the best one in this experiment, as confirmed by the tensile test results. Silane IV has three ethoxy groups which can be hydrolyzed by water to form three silanol groups. One silanol group can form a covalent bond to the glass surface and the other two silanol groups can form bonds to the silanol groups of the neighbor silanes on glass surfaces. This gives a strong network of silane. Moreover, the R-group of Silane IV has NH_2 which can react with the nylon 6 molecule. The covalent bond produced by reaction between the NH_2 group of Silane IV and C=O of nylon 6 was observed by Jenneskens et al. (**33**). In their work glass beads were immersed in the solution mixture of toluene, water, and silane; in our work, no water was added to the toluene solution, but we also got very good results. It is possible that there was some water adsorbed to the glass fibre surface since glass fibre is very hydrophilic. It would be interesting for a future experiment to treat the fibreglass in toluene solution with and without water in the mixture.

9.2. Recommendations

9.2.1. Mold improvements

There are some weak points of this mold design. One is that more voids are permitted around the centre part of the composite. This problem may come from the

remaining small bubbles in the feed tube (silicone rubber), even after degassing, which cannot be eliminated. These voids may also come from the remaining air in the mold, or because access to small crevices in the mat is prevented by the poor wettability of monomer to the fibreglass surface. These problems are possibly solved by applying additional pressure to the monomer solution, forcing the remaining air (if it is there) to the edge of the disk (which will be cut off anyway). This increased pressure will also force the monomer to flow into the microcracks in the fibre surface and into the small crevices between crossed fibres. We recommend that the reaction vessel and connector tube be made with metal in order to stand up to high pressure and to avoid cold spots. High power vacuum pump is also recommended to eliminate the remaining gas in the mold, together with an ejection space at the upper corners of the mold, for the residual gas to move into, as the caprolactam rises.

Opening and closing this mold seems unnecessarily difficult. For opening, each lifting screw must be turned in small increments in sequence with the other three screws. If these are not turned properly, the male part of the mold will become tilted and bind, so the mold cannot open. If so, the whole procedure must be reversed and tried once more: loosen all screws, use C-clamps to close the mold, tighten screws, release C-clamps, and then repeat the opening sequence. This process is wasteful of time and is potentially damaging to some parts of the mold, since aluminum is soft and could be harmed by the metal-to-metal binding and use of force. The mold closing procedure is also awkward, requiring struggle with the large ungainly C-clamps. For many reasons, then, a redesign of the mold opening and closing processes is desirable. Hydraulic mechanisms would be preferred. If mold-opening by hand is preferred, using the four-screw system is still an appropriate method. However, to make this an easily managed step (i.e. to reduce the physical resistance), the o-ring seal should be relocated to the exterior lip of the mold where the male part and female part make a flush contact with each other. In this work,

the o-ring could not be relocated because the exterior lip was too narrow; greater width at this point would be needed in an upgraded design.

The connection between the glass reaction vessel and mold is another weak point of this design. This connector (silicone tube) gets cold easily, allowing the molten caprolactam to freeze and block the flows. In our operation we used a heat gun to melt the caprolactam in the tube and also some upper part of the flask above the isomantle that is not as hot as the bottom part. Better heating and insulation of this region is needed.

The valve between mold and vacuum pump was redesigned as part of this project, as shown in Appendix F, and this improvement should be incorporated in any new overall design of the mold. The silicone o-ring seal inside this valve should be checked each time before making a composite.

Because the chemical reaction is accelerated and completed over a small temperature range (somewhere, not exactly known, between 100°C and 150°C), it is possible that the relatively small temperature variations across the upper and lower mold surfaces--and between upper and lower surfaces--could be creating some problems of matrix inhomogeneity, internal stress and separation of matrix from fibre. An effort should be made to reduce these internal temperature variations $\Delta T(r,z)$ still further, to less than 1° C. Better external insulation should be used, and with an entirely new mold insulating layers should be built in as well. With a new mold, too, the number of heaters and their placement could be altered--i.e., use more of them, spaced more uniformly (especially around the rim)--in order to reduce the temperature gradients that now exist.

9.2.2. New experiments

We have found that Silane IV is the best silane in this work, but it needs to be tested much more. It should be used in experiments that vary $\overline{V}_f$, vary the concentration of silane in toluene solution, and vary the method of treating the glass fibre surface.

Several different methods should be used: treating in solution of toluene and silane, in mixture of toluene, silane, and water, and adding Silane IV directly in the monomer solution (to repeat Otaigbe's experiment but with different higher concentrations).

Next, find new silanes that are similar to Silane IV ($H_2N(CH_2)_3Si(OCH_3)_3$) but potentially better because of having a C=O and perhaps more NH_2 groups, and also with a longer chain and branches to enhance entanglements. One candidate to try is (3-Chloropropyl)trimethoxysilane, $Cl(CH_2)_3Si(OCH_3)_3$, which has three methoxy groups to bond with the glass surfaces (as does Silane IV) and also one Cl group which can react with the NH group in nylon 6 chain or with the glass.

Use the pull-out method to test the interfacial adhesion between glass and matrix. By this method, the other variations in the full composite structure will be eliminated, leaving only the interfacial adhesion to be measured without complication. Use other methods to measure voids, such as optical image analysis or acoustical analysis, and compare the results with the value obtained from calculation with measured densities.

There is no evidence that the thermal program used here for polymerization and post-reaction treatment is anywhere close to optimal. While good reasons exist for keeping $T < 150^{\circ}C$ (or some ceiling below $T_m = 223^{\circ}C$) until polymerization is completed, there is a wide range of heating and cooling and annealing programs that remain to be explored and should be. Improvements in product performance might then emerge from better nylon crystal development, relief of internal stresses caused by too-rapid polymerization and crystallization, and more effective fibre/matrix adhesion (perhaps from post-reaction annealing). Coupled to such a study would be also a better fundamental understanding of the chemical reaction and crystallization processes both of which are functions of time and temperature and are occurring simultaneously. In view of such complexity, it seems likely that a study that explores variation of time and temperature (and perhaps also catalyst concentration) would be certain to produce composite specimens with superior properties.

REFERENCES

1. A.A. Berlin, S.A. Volfson, N.S. Enikolopian, S.S. Negmatov, *Principles of Polymer Composites*, Springer-Verlag, New York, 1986.

2. R. Yosomiya, K. Morimoto, A. Nakajima, Y. Ikada, and T. Suzuki, *Adhesion and Bonding in Composites*, Marcel Dekker, New York, 1990.

3. D. Hull, *An Introduction to Composite Materials*, Cambridge University Press, Cambridge, U.K., 1981.

4. K.K. Chawla, *Composite Materials*, Springer-Verlag, New York, 1987.

5. S. Be'land, *High Performance Thermoplastic Resins and Their Composites*, Noyes Press, New Jersey, 1990.

6. E.P. Plueddemann, *Silane Coupling Agents*, Plenum Press, New York, 1982.

7. K. Szijarto and P. Kiss, Filling of Polymers with the Aid of Coupling Agents, *Polymer Composites*, Proceedings 28th Microsymposium on Macromolecules Prague, Czechoslovakia, (July 8-11, 1985).

8. S.J. Bonfield, M.H. Berger, A.R. Bunsell, J.F. Watts, S.J. Greaves, F. Grosjean, E. Rosenberg, and J.M. Bain, Influence of the Fibre/Matrix Interface on the Behaviour of Thermoplastic Composites: The Fibre/Size Interphase, *J. Comp. Polym.*, 5, 3, 161-172 (1992).

9. L. Holliday, *Composite Materials*, Glass Systems, K.L. Loe Wentein, Elsevier, New York, 1966.

10. G. Odian, *Principles of Polymerization*, 3rd ed., John Wiley & Sons, New York, 1981.

11. M.P. Stevens, *Polymer Chemistry*, Oxford University Press, New York, 1990.

12. Encyclopedia' 92, *Modern Plastics*, Mc Graw Hill, mid-October, 1991.

13. H.K. Reimschuessel, Nylon 6 Chemistry and Mechanisms, *J. Polym. Sci. Macromol. Rev.*, 12, 68 (1977).

14. A. Kelly, *Strong Solids*. Clarendon Press, Oxford, 1973.

15. E.P. Plueddeman, Mechanism of Adhesion Through Silane Coupling Agents, *Composite Materials*, Academic Press, New York, 6, 174-216 (1974).

16. H. Ishida, and J.L. Koenig, Hydrolytic Stability of Silane Coupling Agents on E-Glass Fibers Studied by Fourier Transform Infrared Spectroscopy, *Proceedings of the 35th SPI/RP Annual Technology Conference, paper 23 - A. Society of the plastics Industry*, New York (1980).

17. D.J. Blundell, J.M. Chalmers, M.W. MacKenzie, and W.F. Gaskin, Crystalline Morphology of the Matrix of PEEK-Carbon Fiber Aromatic Polymer Composites. I. Assessement of Crystallinity, *SAMPE Quarterly*, 16, 4, 22-30 (July 1985).

18. M.F. Talbott, G.S. Springer, and L.A. Berglund, The Effects of Crystallinity on the Mechanical Properties of PEEK Polymer and Graphite Fiber Reinforced PEEK, *J. Comp. Mat.*, 21, 1056-1081 (Nov. 1987).

19. C.N. Velisaris and J.C. Sereris, Crystallization Kinetics of Polyetheretherketone (PEEK) Matrices, *J. Polym. Eng. Sci.*, 26, 1574-1581 (1986).

20. National Materials Advisory Board, The Place for Thermoplastic Composites in Structural Components, *National Research Council*, U.S.A. (1987).

21. W.H. Beever, C.L. Ryan, F.E. O'Connor, and A.Y. Lou, Ryton-PPS Carbon Fiber Reinforced Composites: The How, When and Why of Molding, *Toughened Composites*, ASTM STP 937, 319-327 (March 1985).

22. C.C.M. Ma, H.C. Hsia, W.L. Liu and J.T. Hu, Studies on Thermogravimetric Properties of Polyphenylene Sulfide and Polyetheretherketone Resins and Composites, *J. Thermoplastic Comp. Mat.*, 1, 39-49 (Jan. 1988).

23. H.X. Nguyen and H. Ishida, Poly(Aryl-Ether-Ether-Ketone) and Its Advanced Composites: A Review, *J. Polym. Comp.*, 8, 2, 57-73 (April 1987).

24. Y. Lee and R.S. Porter, Crystallization of Poly(etheretherketone) (PEEK) in Carbon Fiber Composites, *J. Polym. Eng. Sci.*, 26, 4, 633-639 (May 1986).

25. D.J. Blundell, R.A. Crick, B. Fife, J. Peacock, A. Keller and A. Waddon, Spherulitic Morphology of the Matrix of Thermoplastic PEEK/Carbon Fiber Aromatic Polymer Composites, *J. Mat. Sci.*, 24, 2057-2064 (1989).

26. W.I. Lee, M.F. Talbott, G.S. Springer and L.A. Berglund, Effects of Cooling Rate on the Crystallinity and Mechanical Properties of Thermoplastic Composites, *J. Reinforced Plastics and Composites*, 6, 2-12 (Jan. 1987).

27. P. Cebe, H. S. Don, S. Chung and A. Gupta, Mechanical Properties and Morphology of Poly(etheretherketone), *ASTM Symposium on Toughened Composites*, ASTM STP 937, 342-357 (1987).

28. M. Adams, C. Mosier, and G.A. Campbell, Pressure and Cooling Rate Effects on Carbon Fiber Adhesion to Thermoplastics, ANTEC 9-13th May 1993, New Orleans, *SPE*, 318 (1993).

29. C. Verdeau and A.R. Bunsell, Effect of Processing Conditions of the Interfacial Zone of High Performance Thermoplastic Composites, *J. Comp. Polym.*, 5, 3, 215-226 (1992).

30. S.V. Nair, M.L. Shiao, P.D. Garret, and R.E. Pollard, Mechanics and Mechanisms of Fracture in Glass Fiber Reinforced Semicrystalline Thermoplastics, ANTEC 9-13th May 1993, New Orleans, *SPE*, 2552 (1993).

31. J.U. Otaigbe and W.G. Harland, Studies in the Properties of Nylon 6-Glass Fiber Composites, *J. Appl. Polym. Sci.*, 36, 165-175 (1988).

32. J.U. Otaigbe, Effect of Coupling Agent and Absorbed Moisture on the Tensile Properties of a Thermoplastic RRIM Composite, *J. Appl. Polym. Sci.*, 45, 1213-1221 (1992).

33. L.W. Jenneskens, A. Venema, N.V. Veenendaal, and W.G.B. Huysmans, Evidence for Interphasial Amide Formation between Surface-Bound Poly (3-Aminopropyltrisiloxane) and Polyamide-6 in Glass Bead Reinforced Polyamide-6 Model Composites, *J. Polym. Sci : Part A: Polymer Chemistry*, 30, 133-136 (1992).

34. H. Hamada, J.C. Coppola, and D. Hull, Effect of Surface Treatment on Crushing Behaviour of Glass Cloth/Epoxy Composite Tubes, *Composites*, 23, 2 (March 1992).

35. H.G. Karian and H.R. Wagner, Assessment of Interfacial Adhesion in Chemically Coupled Glass Fiber Reinforced Polypropylene, ANTEC 9-13th May 1993, New Orleans, *SPE*, 3449-3455 (1993).

36. K.A. Borden, R.C. Well and C.R. Manganaro, The Effect of Polymeric Coupling Agent on Mica-Filled Polypropylene: Optimization of Properties Through Statistical Experimental Design, ANTEC 9-13th May 1993, New Orleans, *SPE*, 2167-2170 (1993).

37. H.R. Allcock and F.W. Lampe, *Contemporary Polymer Chemistry*, 2nd ed., New Jersey, 1990, p.115.

38. T.C. Chang and B.Z. Jang, The Effects of Fiber Surface Treatments by a Cold Plasma in Carbon Fiber/Bismaleimide Composites, *Mat. Res. Soc. Symp. Proc.*, 170, 321 (1990).

39. J.A. Hinkley, W.D. Bascom, and R.E. Allred, Interlaminar Fracture in Carbon Fiber/Thermoplastic Composites, *Mat. Res. Soc. Symp. Proc.*, 170, 351-356 (1990).

40. V.G. Gaur and T. Davidson, Interfacial Effects of Plasma Treatment on Fiber Pull-Out, *Mat. Res. Soc. Symp. Proc.*, 170, 309 (1990).

41. L.Y. Yuan, S.S. Shyu, and J.Y. Lai, Plasma Surface Treatments of Carbon Fibers. Part 2: Interfacial Adhesion with Poly(Phenylene Sulfide), *J. Comp. Sci. and Tech.*, 45, 9-16 (1992).

42. P.W. Yip and S.S. Lin, Effect of Surface Oxygen on Adhesion of Carbon Fiber Reinforced Composites, *Mat. Res. Soc. Symp. Proc.*, 170, 339 (1990).

43. S.M. Lee, Influence of Fiber/Matrix Interfacial Adhesion on Composite Fracture Behavior, *J. Comp. Sci. and Tech.*, 43, 317-327 (1992).

44. T.C. Fan, Design Consideration of Composites With Voids, *J. SAMPE* , 29(4), 15 (1993).

45. S.R. Ghirose, Effect of Void Content on The Mechanical Properties of Carbon/Epoxy Laminates, *SAMPE Q.*, 24(2), 54-59 (1993).

46. U.K. Pat. Appl. GB 2,001,282A (1978).

47. C.S. Temple, et al. (to PPG Industries, Inc.) U.S. Pat. 3, 684, 645 (1972).

48. H. Ishida and G. Rotter, RIM-Pultrusion of Thermoplastic Matrix Composites, *J. Comp. Polym.*, 4, 1, 1-11 (1991).

49. F. Rodriguez, *Principles of Polymer Systems*, 3rd ed., Hemisphere Publishing Corp., New York, 1989; p. 509.

APPENDIX A

Table A-1. Temperature Upper Part of Mold (°C)

Table A-2. Temperature Lower Part of Mold (°C)

Table A-1. Temperature upper part of mold (°C)

T_{set}	$^{1}U_{36}$	$^{1H}U_{76}$	$^{1}U_{116}$	$^{2}U_{36}$	$^{2}U_{116}$
100.00	103.24	102.71	102.17	102.66	102.01
	102.99	102.71	102.17	102.41	102.01
	103.24	102.96	102.42	102.66	102.26
	103.24	102.71	102.17	102.66	102.01
	103.24	102.96	102.42	102.66	102.26
Average	103.19	102.81	102.27	102.61	102.11
150.00	153.64	152.94	152.40	152.74	152.24
	152.39	151.69	150.90	151.49	152.49
	152.89	152.44	151.65	152.24	151.49
	152.89	152.69	151.90	152.24	151.49
	153.64	152.94	152.40	152.74	151.99
Average	153.09	152.54	151.85	152.29	151.54

Table A-2. Temperature lower part of mold (°C)

T_{set}	L_0	$^{1}L_{30}$	$^{1}L_{60}$	$^{1}L_{90}$	$^{1}L_{120}$	$^{2H}L_{60}$	$^{2H}L_{90}$	T_{ref}
100.00	101.73	100.99	101.21	100.42	98.61	101.41	100.68	101.01
	102.73	101.24	101.46	100.42	99.86	101.41	100.68	101.01
	102.48	101.74	101.71	100.67	99.36	101.91	101.18	101.51
	102.73	100.99	101.21	100.17	99.61	101.16	100.68	101.01
	102.23	101.74	101.96	100.92	99.11	101.91	101.18	101.51
Average	102.38	101.34	101.51	100.52	99.31	101.56	100.88	101.21
150.00	*	150.64	150.94	149.15	147.28	150.74	149.71	150.24
	*	150.89	151.19	149.40	*	150.99	150.21	150.49
	*	150.89	151.19	149.65	*	151.24	150.21	150.74
	*	150.89	151.19	149.90	*	151.24	150.21	150.74
	*	150.89	151.19	149.65	*	150.99	150.21	150.74
Average	*	150.84	151.14	149.55	147.28	151.04	150.11	150.59

* Thermocouple was broken

APPENDIX B

Table B-1. ρ

Table B-2. V_f

Table B-3. V_v

Figure B-1. Dimensions of test specimens

Table B-4. Average Breaking Energies from Izod Type Impact Tests, RH = 44 %, T = 24.5 °C

Table B-5. Izod Impact Tests on All Specimens

Table B-6. Average Mechanical Properties

Table B-7. Mechanical Properties from All Tensile Tests on Day I, RH = 53 %, T = 25°C

Table B-8. Mechanical Properties from All Tensile Tests on Day II, RH = 75 %, T = 25°C

Table B-9. Mechanical Properties from All Tensile Tests on Day III, RH = 40-42 %, T = 22.5°C

Table B-1. Density measurement

Types of sample	Sample no.	W_1 Wt. of sample in air (g)	W_2 Wt. of sample in liquid (g)	ρ Density (g/cm^3)	$\bar{\rho}$ Avg.density (g/cm^3)
[1]Nylon 6	1	1.079	0.321	1.118	
	2	0.997	0.303	1.129	
	3	0.890	0.269	1.126	
	4	0.812	0.244	1.123	
	5	0.576	0.175	1.129	1.125
[1]Untreated	1	0.592	0.286	1.520	
	2	0.588	0.283	1.515	
	3	0.685	0.341	1.565	
	4	0.623	0.306	1.544	
	5	0.689	0.341	1.556	
	6	0.631	0.312	1.554	1.542
[2]Untreated	1	0.673	0.319	1.492	
	2	0.749	0.360	1.513	
	3	0.759	0.362	1.502	
	4	0.759	0.368	1.526	
	5	0.757	0.370	1.538	
	6	0.741	0.353	1.501	1.512
[1]Silane I (10%)	1	0.816	0.398	1.534	
	2	0.847	0.424	1.573	
	3	0.767	0.345	1.428	
	4	0.821	0.399	1.529	
	5	0.818	0.400	1.538	
	6	0.837	0.419	1.573	1.529
[1]Silane II (5%)	1	0.875	0.422	1.518	
	2	0.876	0.427	1.533	
	3	0.904	0.445	1.547	
	4	0.895	0.439	1.542	
	5	0.881	0.435	1.552	
	6	0.898	0.446	1.561	1.542
[1]Silane II (10%)	1	0.713	0.341	1.506	
	2	0.739	0.371	1.578	
	3	0.729	0.362	1.561	
	4	0.723	0.359	1.561	
	5	0.733	0.366	1.569	
	6	0.756	0.386	1.605	1.563
[1]Silane III (5%)	1	0.751	0.371	1.553	
	2	0.775	0.384	1.557	
	3	0.791	0.394	1.565	
	4	0.777	0.384	1.553	
	5	0.773	0.381	1.549	
	6	0.786	0.395	1.579	1.559

Table B-1. Density measurement (continued)

Types of sample	Sample no.	W_1 Wt. of sample in air (g)	W_2 Wt. of sample in liquid (g)	ρ Density (g/cm^3)	$\bar{\rho}$ Avg.density (g/cm^3)
[2]Silane III (5%)	1	0.799	0.401	1.576	
	2	0.813	0.414	1.601	
	3	0.826	0.421	1.604	
	4	0.815	0.413	1.591	
	5	0.805	0.404	1.575	
	6	0.793	0.393	1.556	1.584
[1]Silane III (10%)	1	0.878	0.403	1.452	
	2	0.887	0.432	1.532	
	3	0.892	0.447	1.575	
	4	0.873	0.434	1.562	
	5	0.864	0.429	1.561	
	6	0.883	0.442	1.573	1.543
[2]Silane III (10%)	1	0.768	0.396	1.622	
	2	0.771	0.400	1.632	
	3	0.759	0.378	1.567	
	4	0.758	0.383	1.588	
	5	0.740	0.377	1.601	
	6	0.778	0.394	1.592	1.600
[1]Silane III (15%)	1	0.773	0.375	1.525	
	2	0.811	0.414	1.607	
	3	0.819	0.415	1.594	
	4	0.834	0.432	1.627	
	5	0.855	0.443	1.629	
	6	0.828	0.424	1.609	1.598
[1]Silane III (1.5%)	1	0.833	0.422	1.594	
	2	0.866	0.445	1.616	
	3	0.848	0.425	1.577	
	4	0.847	0.430	1.595	
	5	0.834	0.419	1.580	
	6	0.841	0.422	1.575	1.590
[1]Silane IV (10%)	1	0.787	0.379	1.515	
	2	0.843	0.410	1.529	
	3	0.810	0.381	1.485	
	4	0.858	0.424	1.553	
	5	0.876	0.446	1.599	
	6	0.851	0.430	1.589	1.545

Table B-2. Volume fraction of fibre

Types of samples	Sample no.	Wt. of composite (g)	Wt. of fibre (g)	ω_m Wt.fraction of matrix (%)	Wt. fraction of fibre		Volume fraction of fibre	
					ω_f (%)	$\overline{\omega}_f$ (%)	V_f (%)	$\overline{V}_f$ (%)
[1]Untreated	1	0.592	0.299	49.49	50.51		30.23	
	2	0.588	0.303	48.47	51.53		30.74	
	3	0.685	0.379	44.67	55.33		34.09	
	4	0.623	0.336	46.07	53.93		32.78	
	5	0.689	0.373	45.86	54.14		33.17	
	6	0.631	0.342	45.80	54.20	53.27	33.16	32.36
[2]Untreated	1	0.673	0.372	44.73	55.27		32.47	
	2	0.749	0.424	43.39	56.61		33.71	
	3	0.759	0.389	48.75	51.25		30.31	
	4	0.759	0.458	39.66	60.34		36.25	
	5	0.757	0.474	37.38	62.62		37.91	
	6	0.741	0.449	39.41	60.59	57.78	35.81	34.41
[1]Silane I (10%)	1	0.816	0.421	48.41	51.59		31.16	
	2	0.847	0.462	45.45	54.55		33.78	
	3	0.767	0.441	42.50	57.50		32.33	
	4	0.821	0.437	46.77	53.23		32.04	
	5	0.818	0.424	48.17	51.83		31.38	
	6	0.837	0.463	44.68	55.32	54.00	34.24	32.49
[1]Silane II (5%)	1	0.875	0.435	50.29	49.71		29.71	
	2	0.876	0.445	49.20	50.80		30.66	
	3	0.904	0.516	42.92	57.08		34.76	
	4	0.895	0.477	46.70	53.30		32.36	
	5	0.881	0.467	46.99	53.01		32.39	
	6	0.898	0.486	45.88	54.12	53.00	33.26	32.19
[1]Silane II (10%)	1	0.713	0.326	54.28	45.72		27.11	
	2	0.739	0.385	47.90	52.10		31.22	
	3	0.729	0.412	43.48	56.52		34.74	
	4	0.723	0.382	47.16	52.84		32.47	
	5	0.733	0.378	48.43	51.57		31.86	
	6	0.756	0.413	45.37	54.63	52.23	34.52	31.99
[1]Silane III (5%)	1	0.751	0.380	49.40	50.60		30.94	
	2	0.775	0.395	49.03	50.97		31.24	
	3	0.791	0.412	47.91	52.09		32.09	
	4	0.777	0.400	48.52	51.48		31.48	
	5	0.773	0.395	48.90	51.10		31.16	
	6	0.786	0.421	46.44	53.56	51.63	33.30	31.70
[2]Silane III (5%)	1	0.799	0.421	47.31	52.69		32.70	
	2	0.813	0.443	45.51	54.49		34.35	
	3	0.826	0.478	42.13	57.87		36.54	
	4	0.815	0.438	46.26	53.74		33.66	
	5	0.805	0.426	47.08	52.92		32.81	
	6	0.793	0.403	49.18	50.82	53.76	31.14	33.53

Table B-2. Volume fraction of fibre (continued)

Types of samples	Sample no.	Wt. of composite (g)	Wt. of fibre (g)	ω_m Wt.fraction of matrix (%)	Wt. fraction of fibre		Volume fraction of fibre	
					ω_f (%)	$\bar{\omega}_f$ (%)	V_f (%)	$\bar{V}_f$ (%)
[1]Silane III (10%)	1	0.878	0.389	55.69	44.31		25.33	
	2	0.867	0.456	47.40	52.60		31.73	
	3	0.892	0.472	47.09	52.91		32.81	
	4	0.873	0.461	47.19	52.81		32.48	
	5	0.864	0.444	48.61	51.39		31.58	
	6	0.883	0.467	47.11	52.89	51.15	32.75	31.11
[2]Silane III (10%)	1	0.768	0.423	44.92	55.08		35.17	
	2	0.771	0.430	44.23	55.77		35.83	
	3	0.759	0.409	46.11	53.89		33.25	
	4	0.758	0.401	47.10	52.90		33.08	
	5	0.740	0.395	46.62	53.38		33.64	
	6	0.778	0.418	46.27	53.73	54.12	33.68	34.11
[1]Silane III (15%)	1	0.773	0.374	51.62	48.38		29.04	
	2	0.811	0.445	45.13	54.87		34.71	
	3	0.819	0.449	45.18	54.82		34.40	
	4	0.834	0.478	42.69	57.31		36.72	
	5	0.855	0.486	43.16	56.84		36.45	
	6	0.828	0.457	44.81	55.19	54.57	34.97	34.38
[1]Silane III (1.5%)	1	0.833	0.440	47.18	52.82		33.15	
	2	0.866	0.478	44.80	55.20		35.12	
	3	0.848	0.475	43.99	56.01		34.78	
	4	0.847	0.460	45.69	54.31		34.11	
	5	0.834	0.446	46.52	53.48		33.27	
	6	0.841	0.444	47.21	52.79	54.10	32.74	33.86
[1]Silane IV (10%)	1	0.787	0.291	63.02	36.98		22.06	
	2	0.843	0.352	58.24	41.76		25.14	
	3	0.810	0.384	52.59	47.41		27.71	
	4	0.858	0.377	56.06	43.94		26.87	
	5	0.876	0.360	58.90	41.10		25.87	
	6	0.851	0.334	60.75	39.25	41.74	24.55	25.37

Table B-3. Void volume fraction

Types of samples	Sample no.	ω_m Wt.percent of matrix (%)	ω_f Wt.percent of fibre (%)	ρ_c Density (g/cm^3)	V_v Void volume fraction (%)	$\overline{V}_v$ Avg.void volume fraction (%)
[1]Untreated	1	49.49	50.51	1.520	2.907	
	2	48.47	51.53	1.515	3.992	
	3	44.67	55.33	1.565	3.768	
	4	46.07	53.93	1.544	3.989	
	5	45.86	54.14	1.556	3.404	
	6	45.80	54.20	1.554	3.575	3.606
[2]Untreated	1	44.73	55.27	1.492	8.214	
	2	43.39	56.61	1.513	7.945	
	3	48.75	51.25	1.502	4.599	
	4	39.66	60.34	1.526	9.957	
	5	37.38	62.62	1.538	10.996	
	6	39.41	60.59	1.501	11.610	8.887
[1]Silane I (10%)	1	48.41	51.59	1.534	2.833	
	2	45.45	54.55	1.573	2.668	
	3	42.50	57.50	1.428	13.727	
	4	46.77	53.23	1.529	4.392	
	5	48.17	51.83	1.538	2.763	
	6	44.68	55.32	1.573	3.268	4.942
[1]Silane II (5%)	1	50.29	49.71	1.518	2.433	
	2	49.20	50.80	1.533	2.297	
	3	42.92	57.08	1.547	6.215	
	4	46.70	53.30	1.542	3.632	
	5	46.99	53.01	1.552	2.784	
	6	45.88	54.12	1.561	3.079	3.407
[1]Silane II (10%)	1	54.28	45.72	1.506	0.229	
	2	47.90	52.10	1.578	0.445	
	3	43.48	56.52	1.561	4.934	
	4	47.16	52.84	1.561	2.089	
	5	48.43	51.57	1.569	0.601	
	6	45.37	54.63	1.605	0.752	1.508
[1]Silane III (5%)	1	49.40	50.60	1.553	0.868	
	2	49.03	50.97	1.557	0.898	
	3	47.91	52.09	1.565	1.257	
	4	48.52	51.48	1.553	1.545	
	5	48.90	51.10	1.549	1.507	
	6	46.44	53.56	1.579	1.523	1.266
[2]Silane III (5%)	1	47.31	52.69	1.576	1.023	
	2	45.51	54.49	1.601	0.880	
	3	42.13	57.87	1.604	3.396	
	4	46.26	53.74	1.591	0.924	
	5	47.08	52.92	1.575	1.278	
	6	49.18	50.82	1.556	0.815	1.386

Table B-3. Void volume fraction (continued)

Types of samples	Sample no.	ω_m Wt.fraction of matrix (%)	ω_f Wt.fraction of fibre (%)	ρ_c Density (g/cm^3)	V_v Void volume fraction (%)	$\overline{V}_v$ Avg. void volume fraction (%)
[1]Silane III (10%)	1	55.69	44.31	1.452	2.793	
	2	47.40	52.60	1.532	3.726	
	3	47.09	52.91	1.575	1.266	
	4	47.19	52.81	1.562	2.003	
	5	48.61	51.39	1.561	0.968	
	6	47.11	52.89	1.573	1.375	2.022
[2]Silane III (10%)	1	44.92	55.08	1.622	0.056	
	2	44.23	55.77	1.632	0.009	
	3	46.11	53.89	1.567	2.521	
	4	47.10	52.90	1.588	0.434	
	5	46.62	53.38	1.601	0.031	
	6	46.27	53.73	1.592	0.840	0.648
[1]Silane III (15%)	1	51.62	48.38	1.525	1.004	
	2	45.130	54.87	1.607	0.840	
	3	45.18	54.82	1.594	1.610	
	4	42.69	57.31	1.627	1.531	
	5	43.16	56.84	1.629	1.068	
	6	44.81	55.19	1.609	0.947	1.167
[1]SilaneIII (1.5%)	1	47.18	52.82	1.594	0.005	
	2	44.80	55.20	1.616	0.512	
	3	43.99	56.01	1.577	3.566	
	4	45.69	54.31	1.595	1.109	
	5	46.52	53.48	1.580	1.377	
	6	47.21	52.79	1.575	1.166	1.289
[1]SilaneIV (10%)	1	63.02	36.98	1.515	-6.941	
	2	58.24	41.76	1.529	-4.318	
	3	52.59	47.41	1.485	2.869	
	4	56.06	43.94	1.553	-4.262	
	5	58.90	41.10	1.599	-9.591	
	6	60.75	39.25	1.589	-10.346	-5.431

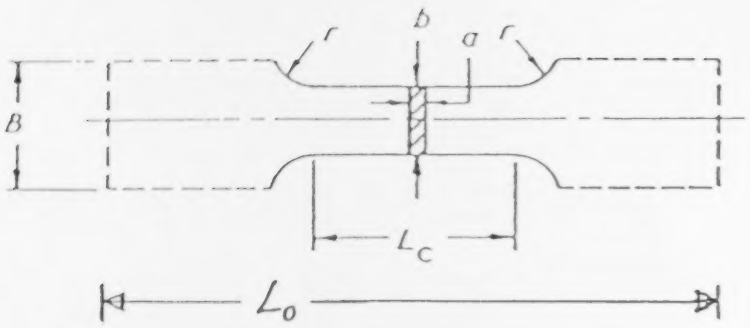

B = 20 mm, L_o = 150 mm, L_c = 60 mm, r = 60 mm, a = 4 mm, a × b ≥ 40 mm^2

(a) Tensile

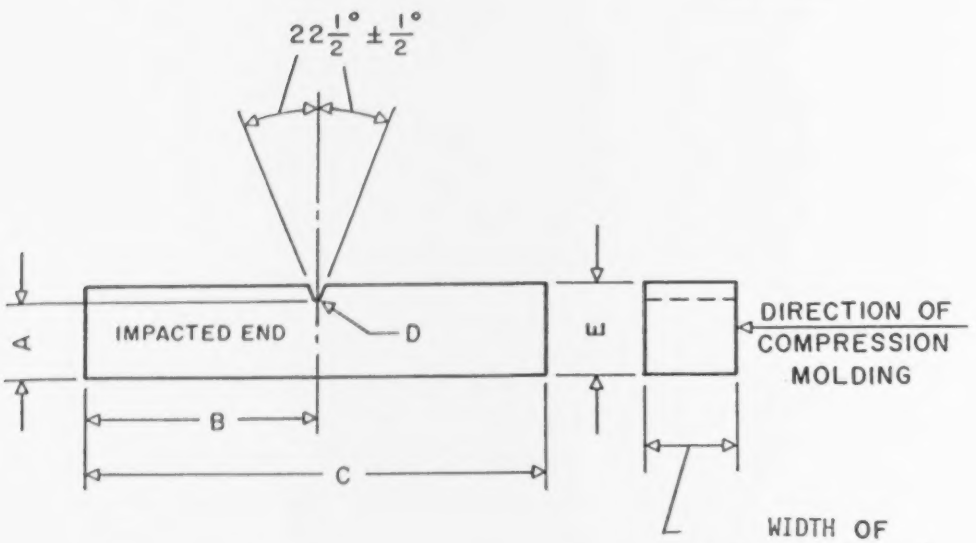

	mm	in.
A	10.16 ± 0.05	0.400 ± 0.002
B	32.00 max	1.260 max
	31.50 min	1.240 min
C	63.50 max	2.500 max
	60.30 min	2.375 min
D	0.25R ± 0.05	0.010R ± 0.002
E	12.70 ± 0.15	0.500 ± 0.006

(b) Izod type impact test

Figure B-1. Dimensions of test specimens. (a) Tensile; (b) Izod type impact test

Table B-4. Average breaking energies from Izod type impact tests ($V_f \cong 32\%$, RH = 42-46%, T = 24.5°C)

Silane type	Sample	RH (%)	Breaking energy (average), E_S, per notch width (J/m)
-	Nylon 6	~ 46	16.7
-	1Untreated	46	133.9
	2Untreated (dry)	42.5	190.6
	2Untreated (wet)	42.5	235.4
I	1Silane I (10%)	45	91.8
II	1Silane II (5%)	45	190.2
	1Silane II (10%)	44	217.6
III	1Silane III (5%)	44	142.7
	2Silane III (5%)	43	161.3
	1Silane III (10%)	44	202.9
	2Silane III (10%)	43	203.8
	1Silane III (15%)	43	225.0
	1Silane III (1.5%)	43	282.0
IV	1Silane IV (10%)	43	114.1*

* $V_f \cong 24\%$

Table B-5. Izod impact tests on all specimens

Table B-5.0. Pure nylon 6

Sample	A (mm)	E (mm)	Width (mm)	C (mm)	* Failure code	Breaking energy, E_S (J/m)	T (°C)	RH (%)
I1	10.00	12.66	4.00	63.50	C	14.1	24	46
I2	10.20	12.70	4.00	63.60	C	16.9	24	46
I3	10.00	12.60	4.00	63.60	C	19.8	24	46
I4	10.00	12.66	4.00	63.50	C	19.8	24	46
I5	10.10	12.66	4.00	63.64	C	16.9	24	46
I6	10.00	12.56	4.00	63.78	C	12.7	24	42.5

Table B-5.1. 1Untreated

Sample	A (mm)	E (mm)	Width (mm)	C (mm)	* Failure code	Breaking energy, E_S (J/m)	T (°C)	RH (%)
I1	9.82	12.40	4.10	63.40	P	126.8	24	46
I2	10.10	12.56	4.10	63.40	P	137.8	24	46
I3	10.0	12.64	4.10	63.40	P	137.8	24	46
I4	10.0	12.36	4.02	63.30	P	112.4	24	46
I5	9.9	12.20	4.10	63.40	P	148.8	24	46
I6	9.8	12.30	4.04	63.30	P	139.8	24	46

Table B-5.2. [1]Silane I (10%)

Sample	A (mm)	E (mm)	Width (mm)	C (mm)	* Failure code	Breaking energy, E_S (J/m)	T (°C)	RH (%)
I1	10.10	12.80	4.00	63.30	P	101.7	24.5	45
I2	10.20	12.80	4.00	63.40	P	104.5	24.5	45
I3	10.10	12.80	4.00	63.44	P	93.2	24.5	45
I4	10.20	12.80	4.00	63.50	C	90.4	24.5	45
I5	10.10	12.70	4.00	63.44	C	79.1	24.5	45
I6	10.20	12.70	4.00	63.44	C	81.9	24.5	45

Table B-5.3. [1]Silane II (5%)

Sample	A (mm)	E (mm)	Width (mm)	C (mm)	* Failure code	Breaking energy, E_S (J/m)	T (°C)	RH (%)
I1	10.20	12.80	4.00	63.80	P	161.0	24.5	45
I2	10.20	12.80	4.00	63.60	P	192.1	24.5	45
I3	10.30	12.70	4.00	63.60	P	175.1	24.5	45
I4	10.20	12.70	4.00	63.50	P	180.8	24.5	45
I5	10.20	12.70	4.00	63.70	P	220.3	24.5	45
I6	10.20	12.80	4.00	63.60	P	211.8	24	45

Table B-5.4. [1]Silane III (10%)

Sample	A (mm)	E (mm)	Width (mm)	C (mm)	* Failure code	Breaking energy, E_S (J/m)	T (°C)	RH (%)
I1	10.20	12.70	4.00	63.40	P	226.0	24	44
I2	10.20	12.70	4.00	63.40	P	189.2	24	44
I3	10.20	12.80	4.00	63.50	P	178.0	24	44
I4	10.20	12.70	4.00	63.40	P	198.0	24	44
I5	10.20	12.74	4.00	63.30	P	223.1	24	44
I6	10.20	12.70	4.00	63.70	P	203.4	24	44

Table B-5.5. [1]Silane II (10%)

Sample	A (mm)	E (mm)	Width (mm)	C (mm)	* Failure code	Breaking energy, E_S (J/m)	T (°C)	RH (%)
I1	9.90	12.90	4.02	63.58	P	230.5	24	44
I2	10.10	12.82	4.10	63.50	P	220.5	24	44
I3	9.88	12.70	4.02	63.46	P	230.5	24	44
I4	9.86	12.86	4.08	63.48	P	235.4	24	44
I5	10.00	12.80	4.06	63.70	P	172.5	24	44
I6	9.92	12.88	4.02	63.60	P	216.4	24	44

Table B-5.6. [1]Silane III (5%)

Sample	A (mm)	E (mm)	Width (mm)	C (mm)	* Failure code	Breaking energy, E_S (J/m)	T (°C)	RH (%)
I1	9.70	12.46	4.10	63.50	P	124.0	24.5	44
I2	9.92	12.50	4.02	63.66	P	154.6	24.5	44
I3	10.00	12.56	4.16	63.50	P	124.9	24.5	44
I4	9.96	12.40	4.10	63.54	P	143.3	24.5	44
I5	10.00	12.40	4.10	63.60	P	129.5	24.5	44
I6	10.08	12.54	4.08	63.66	P	180.0	24.5	44

Table B-5.7. [2]Silane III (5%)

Sample	A (mm)	E (mm)	Width (mm)	C (mm)	* Failure code	Breaking energy, E_S (J/m)	T (°C)	RH (%)
I1	10.10	12.70	4.10	63.40	P	135.0	24	43
I2	10.10	12.58	4.10	63.44	P	162.6	24	43
I3	10.06	12.70	4.06	63.50	P	183.7	24	43
I4	10.10	12.70	4.08	63.40	P	152.3	24	43
I5	10.06	12.80	4.08	63.44	P	177.2	24	43
I6	10.10	12.96	4.10	63.60	P	157.1	24	43

Table B-5.8. [2]Silane III (10%)

Sample	A (mm)	E (mm)	Width (mm)	C (mm)	* Failure code	Breaking energy, E_S (J/m)	T (°C)	RH (%)
I1	10.20	13.04	4.00	63.34	P	209.0	24.5	43
I2	10.10	13.00	4.00	63.44	P	200.5	24.5	43
I3	10.00	12.80	4.00	63.40	P	203.4	24.5	43
I4	10.00	12.86	4.00	63.44	P	146.9	24.5	43
I5	10.10	12.90	4.00	63.40	P	189.2	24.5	43
I6	10.00	13.00	4.00	63.40	P	274.0	24.5	43

Table B-5.9. [1]Silane III (15%)

Sample	A (mm)	E (mm)	Width (mm)	C (mm)	* Failure code	Breaking energy, E_S (J/m)	T (°C)	RH (%)
I1	10.00	12.60	3.94	63.40	P	272.4	24.5	43
I2	10.00	12.56	4.10	63.34	P	259.0	24.5	43
I3	10.00	12.56	4.00	63.30	P	203.4	24.5	43
I4	9.82	12.56	4.00	63.44	P	223.1	24.5	43
I5	10.00	12.64	4.00	63.36	P	200.5	24.5	43
I6	10.10	12.76	4.10	63.30	P	191.5	24.5	43

Table B-5.10. [1]Silane III (1.5%)

Sample	A (mm)	E (mm)	Width (mm)	C (mm)	* Failure code	Breaking energy, E_S (J/m)	T (°C)	RH (%)
I1	10.10	13.00	4.10	63.64	P	292.1	24.5	43
I2	10.00	12.80	4.00	63.40	P	268.3	24.5	43
I3	9.90	12.70	4.00	63.40	P	251.4	24.5	43
I4	9.90	12.70	4.10	63.40	P	281.1	24.5	43
I5	9.90	12.80	4.00	63.50	P	324.8	24.5	43
I6	9.92	12.80	4.10	63.40	P	274.2	24.5	43

Table B-5.11. [1]Silane IV (10%)

Sample	A (mm)	E (mm)	Width (mm)	C (mm)	* Failure code	Breaking energy, E_S (J/m)	T (°C)	RH (%)
I1	10.02	12.70	4.10	63.60	C	143.3	24.5	43
I2	10.00	12.60	4.10	63.74	C	104.7	24.5	43
I3	10.00	12.60	4.10	63.50	C	110.2	24.5	43
I4	10.00	12.64	4.10	63.54	C	115.7	24.5	43
I5	10.00	12.64	4.10	63.54	C	115.7	24.5	43
I6	10.00	12.80	4.10	63.64	C	95.1	24.5	43

Table B-5.12. [2]Untreated

Sample	A (mm)	E (mm)	Width (mm)	C (mm)	* Failure code	Breaking energy, E_S (J/m)	T (°C)	RH (%)
I1(wet)	10.20	12.70	4.00	63.60	P	223.1	24	42.5
I2(dry)	10.30	12.60	4.00	63.54	P	206.2	24	42.5
I3(wet)	10.20	12.60	4.00	63.60	P	240.1	24	42.5
I4(dry)	10.20	12.60	4.10	63.60	P	179.1	24	42.5
I5(wet)	10.20	12.76	4.00	63.60	P	242.9	24	42.5
I6(dry)	10.20	12.70	4.00	63.64	P	186.4	24	42.5

Note: Testing Machine used: TINIUS OLSEN Testing Machine Co., Willow Grove, PA
Capacity: 200 lbs.

Pendulum weight = 25 lbs

*Code P : Partial break

C : Complete break

Table B-6. Summary of tensile testing results

Silane type	Sample	RH** %	$\overline{V}_f$ %	$\overline{V}_v$ %	σ_b (MPa)	ε_b %	Toughness (MPa)	E (GPa)
none	Pure nylon 6	53	0	0	56.9	7.1	2.99	2.81
"	1Untreated	53	32.4	3.6	39.3	0.61	0.15	8.76
"	2Untreated (d)*	40	34.4	8.9	40.4#	1.88#	0.45#	2.38#
"	2Untreated (w)*	40	-	-	6.3#	3.11#	0.59#	2.70#
I	1Silane I (10%)	53	32.5	4.9	31.2	0.81	0.17	7.71
II	1Silane II (5%)	53	32.2	3.4	45.4	0.88	0.24	8.36
	1Silane II (10%)	75	32.0	1.5	41.8	0.78	0.19	7.80
	1Silane III (5%)	75	31.7	1.3	42.5	0.73	0.17	7.72
III	2Silane III (5%)*	40	33.5	1.4	58.3#	2.67#	0.82#	3.93#
	1Silane III (10%)	53	31.1	2.0	45.7	0.90	0.24	7.71
	2Silane III (10%)*	40	34.1	0.6	42.3#	2.07#	0.49#	2.49#
	1Silane III (15%)*	40	34.4	1.2	45.2#	2.35#	0.61#	2.41#
	1Silane III (1.5%)*	40	33.9	1.3	35.7#	2.04#	0.41#	2.95#
IV	1Silane IV (10%)*	40	25.4	-	95.2#	3.50#	1.67#	2.90#

* Measured at NAIT, with Lloyds L6000R (Universal Testing Machine).
All other measurements made with Instron, U of A, CME

** RH = relative humidity. This also differentiates the days of testing: Day I (RH = 53%) at U of A, Day II (75%) at U of A, Day III (40%) at NAIT.

\# These values, recorded by computer operation of the Lloyds instrument at NAIT, incorporate a strain measure which appears larger than the ε scale at U of A by a factor of 3. The scales for loading (hence, σ_b) appear to agree.

Table B-7. Mechanical properties from tensile tests of all specimens on Day I

(RH = 53%, T = 25°C)

**** Using Instron machine**

Table B-7.0. Nylon 6

Nylon 6	σ_b (MPa)	ε_b (%)	E (GPa)	Toughness (MPa)
T1	59.60	6.10	2.79	2.71
T2	57.58	7.3	2.95	3.28
T3	55.60	*	*	2.73
T4	58.20	8.20	2.55	3.51
T5	53.40	6.70	2.94	2.71
average	56.90	7.08	2.81	2.99
S.E	1.08	0.45	0.09	0.17

Table B-7.1. Untreated

Untreated	σ_b (MPa)	ε_b (%)	E (GPa)	Toughness (MPa)
T1	40.59	0.75	6.78	0.20
T2	36.37	0.57	8.98	0.11
T3	35.36	0.50	9.34	0.11
T4	40.31	0.57	9.34	0.10
T5	43.93	0.68	9.34	0.24
average	39.31	0.61	8.76	0.15
S.E	1.55	0.04	0.50	0.03

Table B-7.2. Silane I (10%)

Silane I (10%)	σ_b (MPa)	ε_b (%)	E (GPa)	Toughness (MPa)
T1	33.36	1.00	7.12	0.22
T2	32.47	0.60	7.90	0.12
T3	29.48	0.85	7.48	0.18
T4	31.14	0.80	8.34	0.15
T5	29.80	*	*	*
average	31.25	0.81	7.71	0.17
S.E	0.75	0.08	0.26	0.02

* Recording paper moved backward.

Table B-7.3. Silane II (5%)

Silane II (5%)	σ_b (MPa)	ε_b (%)	E (GPa)	Toughness (MPa)
T1	45.04	0.75	8.23	0.20
T2	43.93	1.30	6.89	0.37
T3	45.59	0.82	8.90	0.22
T4	45.48	0.65	8.90	0.15
T5	46.71	0.90	8.90	0.27
average	45.35	0.88	8.36	0.24
S.E	0.45	0.11	0.39	0.04

Table B-7.4. Silane III (10%)

Silane III (10%)	σ_b (MPa)	ε_b (%)	E (GPa)	Toughness (MPa)
T1	48.93	0.70	8.01	0.16
T2	46.71	0.67	8.85	0.16
T3	45.26	0.90	7.67	0.25
T4	45.37	1.35	7.78	0.43
T5	42.26	0.88	6.23	0.20
average	45.71	0.90	7.71	0.24
S.E	1.09	0.12	0.42	0.05

Table B-8. Mechanical properties from tensile tests on all specimens on Day II

(RH = 75%, T = 25°C)

**** Using Instron machine**

Table B-8.1. Silane II (10%)

Silane II (10%)	σ_b (MPa)	ε_b (%)	E (GPa)	Toughness (MPa)
T1	40.92	0.94	6.00	0.24
T2	43.15	0.87	9.79	0.23
T3	41.70	0.75	7.74	0.20
T4	40.81	0.64	8.23	0.14
T5	42.26	0.72	7.23	0.16
average	41.77	0.78	7.80	0.19
S.E	0.44	0.05	0.62	0.02

Table B-8.2. Silane III (5%)

Silane III (5%)	σ_b (MPa)	ε_b (%)	E (GPa)	Toughness (MPa)
T1	41.70	0.75	8.90	0.19
T2	44.26	0.78	8.00	0.22
T3	42.70	0.59	8.23	0.13
T4	40.26	0.65	5.56	0.09
T5	43.37	0.90	7.90	0.21
average	42.46	0.73	7.72	0.17
S.E	0.69	0.05	0.57	0.02

Table B-9. Mechanical properties from tensile tests on all specimens on Day III

(RH = 40%, T = 22.5°C)

**** Using Lloyds L6000R Universal Testing Machine**

Table B-9.1. Untreated

Untreated	σ_b (MPa)	ε_b (%)	E (GPa)	Toughness (MPa)
T1 (wet)	6.44	2.54	2.81	0.47
T3(wet)	5.93	2.83	2.47	0.54
T5(wet)	6.54	3.96	2.81	0.77
average	6.30	3.11	2.70	0.59
S.E.	0.19	0.43	0.11	0.09
T2(dry)	38.23	1.81	2.86	0.41
T4(dry)	42.58	1.94	1.90	0.49
average	40.41	1.88	2.38	0.45
S.E.	2.18	0.07	0.48	0.04

Table B-9.2. Silane III (5%)

Silane III (5%)	σ_b (MPa)	ε_b (%)	E (GPa)	Toughness (MPa)
T1	61.13	2.99	2.53	0.94
T2	55.87	2.67	4.57	0.76
T3	54.76	2.71	2.86	0.74
T4	56.99	2.29	*	0.77
T5	62.55	2.67	5.76	0.90
average	58.26	2.67	3.93	0.82
S.E	1.52	0.11	0.76	0.04

* Error

Table B-9.3. Silane III (10%)

Silane III (10%)	σ_b (MPa)	ε_b (%)	E (GPa)	Toughness (MPa)
T1	44.94	2.23	2.09	0.56
T2	42.20	1.75	2.92	0.46
T3	39.13	1.81	2.65	0.37
T4	42.49	2.11	2.90	0.49
T5	42.74	2.44	1.91	0.57
average	42.30	2.07	2.49	0.49
S.E	0.93	0.13	0.21	0.04

Table B-9.4. Silane III (15%)

Silane III (15%)	σ_b (MPa)	ε_b (%)	E (GPa)	Toughness (MPa)
T1	46.36	2.36	1.95	0.60
T2	46.07	2.49	1.93	0.70
T3	48.39	2.73	1.90	0.75
T4	44.12	2.12	2.17	0.50
T5	41.30	2.05	4.11	0.50
average	45.25	2.35	2.41	0.61
S.E	1.20	0.12	0.43	0.05

Table B-9.5. Silane III (1.5%)

Silane III (1.5%)	σ_b (MPa)	ε_b (%)	E (GPa)	Toughness (MPa)
T1	35.32	1.68	2.85	0.35
T2	36.80	2.19	4.91	0.45
T3	34.53	2.36	2.23	0.41
T4	41.41	2.32	2.84	0.56
T5	30.46	1.64	1.91	0.30
average	35.70	2.04	2.95	0.41
S.E	1.77	0.16	0.52	0.04

Table B-9.6. Silane IV (10%)

Silane IV (10%)	σ_b (MPa)	ε_b (%)	E (GPa)	Toughness (MPa)
T1	106.10	4.01	*	2.00
T2	94.17	3.93	2.82	1.76
T3	98.37	3.44	3.10	1.74
T4	84.30	3.03	2.84	1.33
T5	93.09	3.24	*	1.54
average	95.21	3.53	2.92	1.67
S.E	3.56	0.19	0.09	0.11

* Error

APPENDIX C

C-1. Mechanical Properties of Composite Samples Determination

C-2. Density Determination

C-3. Fiber and Void Volume Fraction Determination

C-4. Standard Error of Mean Determination

C-1. Mechanical Properties of Composite Samples

C-1.1. Tensile properties

The tensile properties were determined according to ASTM D638. Using the Instron tensile tester to perform the tensile tests on the dumb-bell shaped specimens with the dimensions as shown in Figure B-1 under the following conditions of testing:

cross-head speed = 5 mm/ min (0.2 in/ min)

gauge length = 60 mm (2.36 in.)

clip gauge caalibration = 0.5 % strain / 1 in. of chart paper.

strain rate = 8.0 % / min (i.e, cross-head speed / gauge length * 100)

C-1.2. Using a vernier caliper, to measure and record cross-sectional dimensions of the narrowest portion of all the specimens before testing. For each sample, record load - strain data on the X-Y plotter of the Instron. Record load ranges, capacity of load cell,etc.

C-1.3. Analyze load (f)-strain (ε) data for the materials as follows:

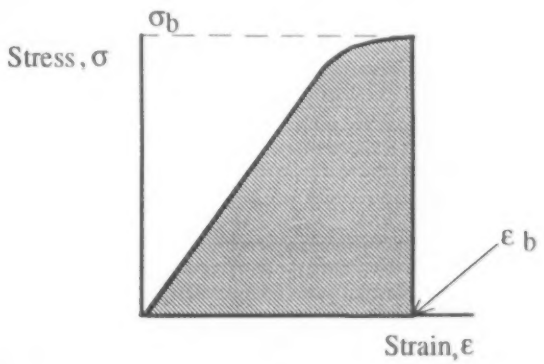

$$\text{Load, } F = \sigma A$$

$$\text{Young's modulus, } E = \left|\frac{d\sigma}{d\varepsilon}\right|_{\varepsilon \to 0}$$

		=	slope of tangent to the curve at zero limit strain
where	σ	=	stress, MPa
	ε	=	strain, %
	A	=	cross sectional area of specimen, m^2
	toughness	=	area under the curve , MPa

C-1.4. Sample calculations

C-1.4.1. Tensile stress at ultimate point, σ_b

Sample: ^{1}Untreated (tensile specimen T1), $^1U_{T1}$

F_b, load at breaking point	=	365	lb_f
	A	=	4×10^{-5} m^2
	σ_b	=	$\frac{365\ lb_f}{4\times10^{-5}\ m^2}\times 4.4482\ \frac{N}{lb_f}$
		=	40.59 x 10^6 $\frac{N}{m^2}$
		=	40.59 Pa

C-1.4.2. Strain at ultimate point, ε_b

Strain was determined by measuring distance from 0 to breaking point on x-axis, ε_b

1 inch of graph paper	=	0.5 %	strain
	=	0.005	strain
For sample $^1U_{T1}$: ε_b	=	1.5	inch of graph paper
	=	0.7×0.005	
$\therefore$ ε_b	=	0.0075	

C-1.4.3. Young's modulus, E

$$E = \left|\frac{d\sigma}{d\varepsilon}\right|_{\varepsilon \to 0}$$

= slope of tangent to the curve at limit of zero strain

For sample $^{1}U_{T1}$: $E = \frac{305 \times 4.4482}{4 \times 10^{-5} \times 0.005}$ Pa

$\therefore \quad E = 6.78 \times 10^{9}$ Pa

$= 6.78$ GPa

C-1.4.4. Toughness

Toughness is measured by measuring the area under the stress-strain curve from zero to breaking point.

Cross sectional area of the specimen, $^{1}U_{T1}$ = 4×10^{-5} m^2

From chart paper at x-axis, 1 inch = $\frac{100 \times 4.4482}{4 \times 10^{-5}}$ Pa

at y-axis, strain at 1 inch = 0.005

$\therefore$ 1 in^2 of graph paper = 55602.5 Pa

For sample $^{1}U_{T1}$:

A (area under the the curve) = 3.61 in^2

$\therefore$ toughness = 3.61×55602.5 Pa

= 200725 Pa

= 0.20 MPa

C-2. Density Determination

The density of composite was determined in accordance with ASTM D792-66 by using small wires tied the samples and weighed the samples in air and in liquid, then weighed only small wire in air and in liquid (Acetone, density of 0.7857 g/cm^3 at 25°C). Record the room temperature. The density of the samples was calculated by the following equation.

$$\rho_c = \frac{w_1}{w_1 - w_2} \cdot \rho_{liquid}$$

where w_1 = weight of tied sample in air - weight of wire in air

w_2 = weight of tied sample in liquid - weight of wire in liquid

For sample ^{1}Untreated (at position 1), $^1U_1$:

w_1 = 0.592 g

w_2 = 0.2859 g

$$\rho_c = \frac{0.592}{0.592 - 0.2859} \times 0.7857$$

= 1.520 g/cm^3

C-3. Fiber and Void Volume Fraction Determination

Fiber and void volume fraction were determined by burning the known weight of samples (using crucible as containers) in the muffle furnace at 600°C for 30 minutes, putting the crucible into a desiccator, and allowing the heated samples to cool down to room temperature before weighing.

C-3.1. Fiber volume fraction, V_f (%)

The fiber volume fraction was calculated by the following equation:

$$V_f = \frac{W_f}{\rho_f} \cdot \rho_c \times 100$$

where V_f = fiber volume fraction

W_f = fiber weight fraction

ρ_f = fiber density = 2.54 g/cm^3 (ASTM:D 2734 - 70)

Sample $^1U_1$: W_f = 0.5051

ρ_c = 1.520 g/cm^3

ρ_f = 2.54 g/cm^3

$$\therefore \quad V_f = \frac{0.5051}{2.54} \times 1.520 \times 100$$

$$= 30.23 \quad \%$$

C-3.2. Void volume fraction calculation, V_v (%)

The void volume fraction was calculated by the following equation:

$$V_v = 100 - \rho_c \left(\frac{W_m}{\rho_m} + \frac{W_f}{\rho_f} \right) \times 100$$

where W_m = weight fraction of matrix, %

ρ_m = density of matrix (nylon 6), g/cm^3

ρ_c = density of composite, g/cm^3

For Sample $^1U_1$: W_m = 0.4949

ρ_m = 1.125 g/cm^3

$$\rho_c = 1.520 \ g/cm^3$$

$$Vv = 100 - 1.520 \times \left(\frac{0.4949}{1.125} + \frac{0.5051}{2.54} \right) \times 100$$

$$= 2.907 \ \%$$

C-4. Standard Error of Mean, S.E.

y_i (i = 1,2,3,...) = set of data

n = total frequency (number of sample)

$\bar{y}$ = sample mean

s = standard deviation

$$s^2 = \frac{\sum_{i=1}^{n} (y_i - \bar{y})^2}{n-1}$$

$$S.E. = \frac{s}{\sqrt{n}}$$

APPENDIX D

Figure D-1. Stress-Strain Curve of Fibreglass/Nylon 6 Composites (Using Instron Machine)

Figure D-2. Stress-Strain Curve of Fibreglass/Nylon 6 Composites (Using Lloyds L6000R Universal Testing Machine)

Figure D-1. Stress-Strain Curve of Fiberglass/Nylon 6 Composites
(Using Instron Machine in Room 712, CME, U of A)

x axis: Load, F, lb scale: 100 lb/in. of chart paper
y axis: strain, ε scale: 0.005/in. of chart paper

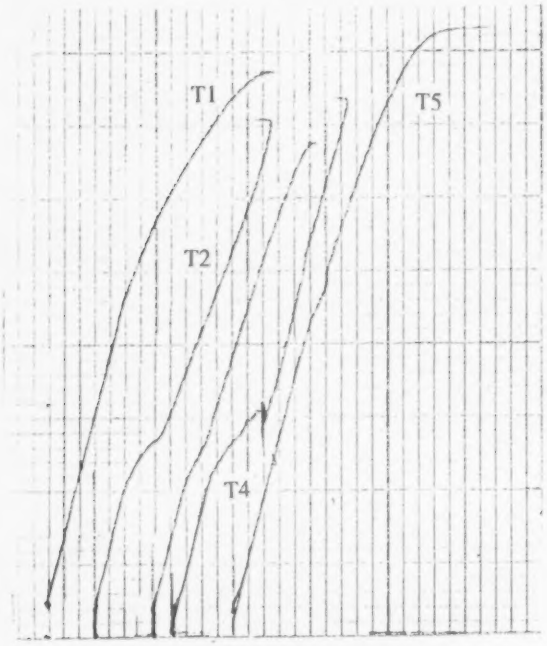

Figure D-1.1. [1]Untreated

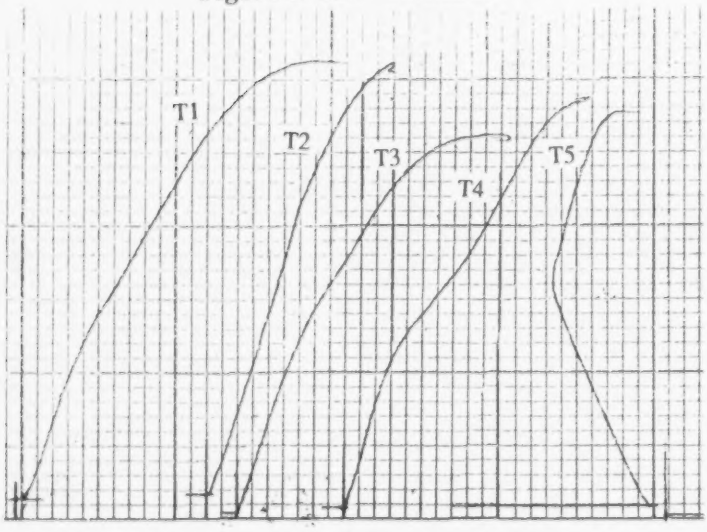

Figure D-1.2. [1]Silane I (10 %)

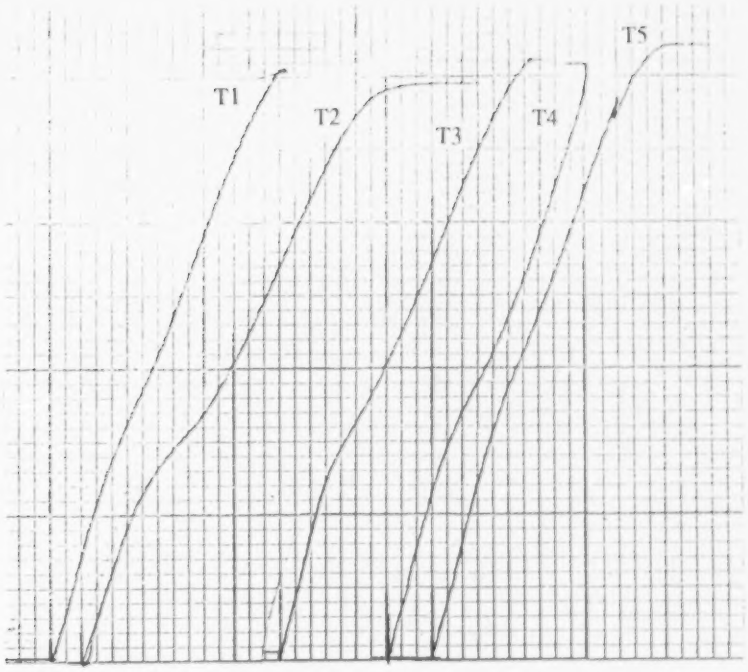

Figure D-1.3. [1]Silane II (5 %)

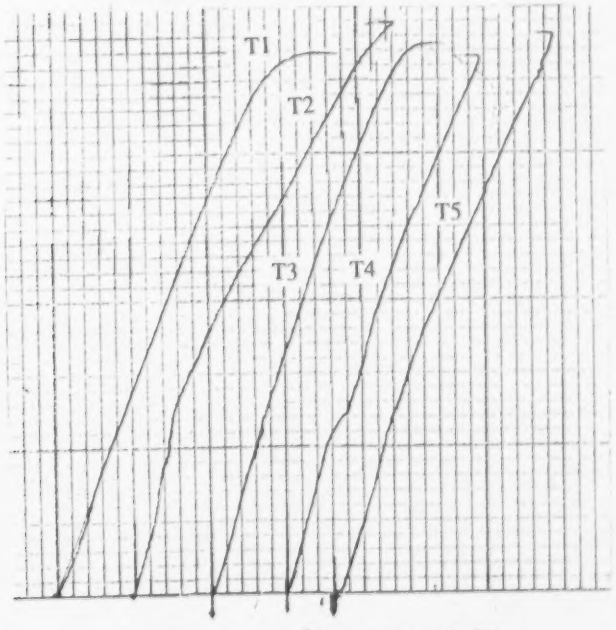

Figure D-1.4. [1]Silane II (10 %)

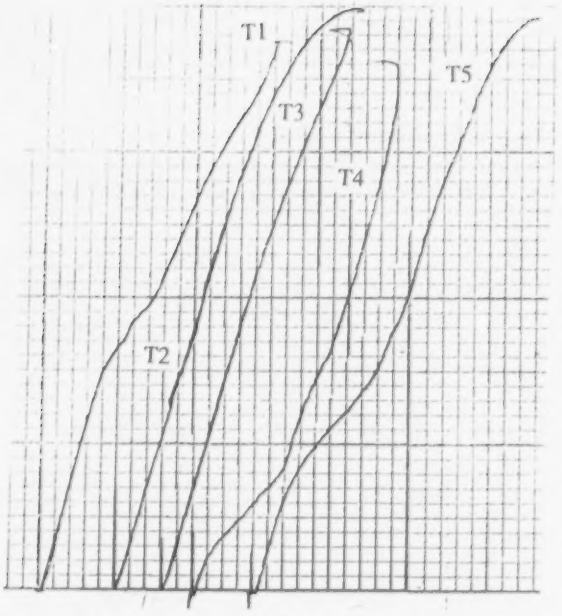

Figure D-1.5. [1]Silane III (5 %)

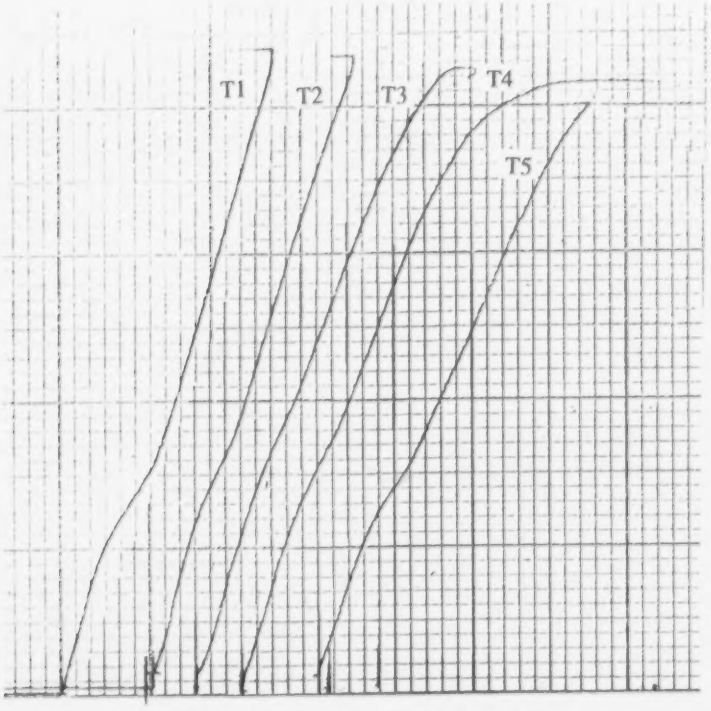

Figure D-1.6. [1]Silane III (5 %)

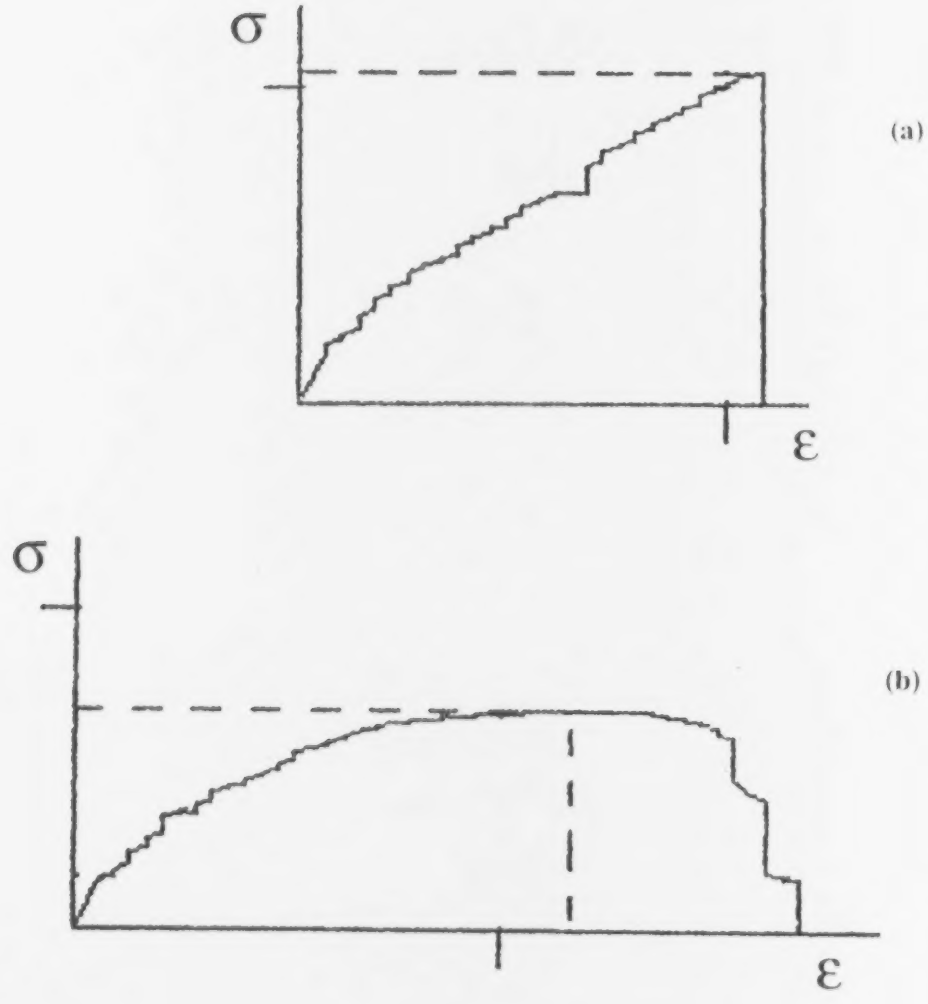

x-axis: Strain (ε), % scale: 1: 1.67
y-axis: Load (F), N scale: 1: 1500

Figure D-2. Stress-strain curve of fiberglass/nylon 6 composites (Using Lloyds L6000R Universal Testing Machine) (a) Dry specimens (b) Wet specimens

APPENDIX E

E-1. Calculation of Number of Silane Molecules (Approximately) Saturated with the Glass Fiber Surface

E-1. Calculation of number of silane molecules (approximately) reacted to glass fiber surfaces

Silane III molecule : $(CH_3)_3SiCl$

Molar mass, M = 108

$A_s = (4\mathring{A})^2 = 16\ \mathring{A}^2$ (1 molecule of silane/area 16 $\mathring{A}^2$)

$N_{s,sat} = \frac{A_{mat}}{A_s}$

where $N_{s,sat}$ = number of silane molecules saturated to glass-fiber surface

Typical surface treatment (5%): 100 ml silane/2000 ml toluene

N_s = number of silane molecules in the solution (silane/toluene)

Silane III, ρ = 0.856 g/ml

$$= 100\text{ml} \times \frac{0.856\text{g}}{\text{ml}} \times \frac{1\text{mole}}{108\text{g}} \times 6\times10^{23}\ \frac{\text{molecules}}{\text{mole}}$$

$N_s \cong 4.76\times10^{23}$ molecules ($\cong$1mole)

$A_{mat} = L_{fiber} \times D_{fiber} \pi$

where $D_{fiber} \cong 13\mu m$ (E-glass)

Mass of mat, M_{mat} = 150 g

$V_{mat} = \frac{M_{mat}}{\rho_{glass}} = \frac{\pi}{4} D^2_{fiber} \times L_{fiber}$

$L_{fiber} = \frac{M_{mat}}{\rho_{glass}} \cdot \frac{4}{\pi D^2_{fiber}}$

$A_{mat} = \left[\frac{M_{mat}}{\rho_{glass}} \cdot \frac{4}{\pi D^2_f}\right] \cdot \pi D_f = \frac{4M_{mat}}{\rho_g D_f}$

$$= \frac{4}{\left(2.56\text{g}/\text{cm}^3\right)} \cdot \frac{150\text{g}}{13\times10^{-4}\text{cm}}$$

$\cong 0.2\times10^6\text{cm}^2$

$$N_{s,sat} \cong \frac{0.2\times10^6\text{cm}^2}{16\mathring{A}^2 \times \left(10^{-8}\frac{\text{cm}}{\mathring{A}}\right)^2}$$

$\cong 1.25\times10^{20}$ molecules

$$N_s/N_{s.sat} = \frac{4.76\times10^{23}}{1.25\times10^{20}} = 3.8\times10^3$$

$\therefore$ Silane III (5 %) = 3.8×10^3 times $N_{,saturated}$

These values for $N_{s,\,sat}$ and $N_s/N_{s,sat}$ depend on the specific number chosen for A_s. Here, we chose a conservative (small) value of 16 $\mathring{A}^2$, which presumed that the molecule projected outward from the glass surface at the point of connection to the surface oxygen (hydroxyl) group. It is possible that the molecule actually collapses down onto the surface, covering a larger area (dependent on its full size), which would make A_s larger and $N_{s,sat}$ smaller. This would increase the "margin of safety" for the toluene solution concentration from 3800 to a still larger number.

APPENDIX F

Valve redesign

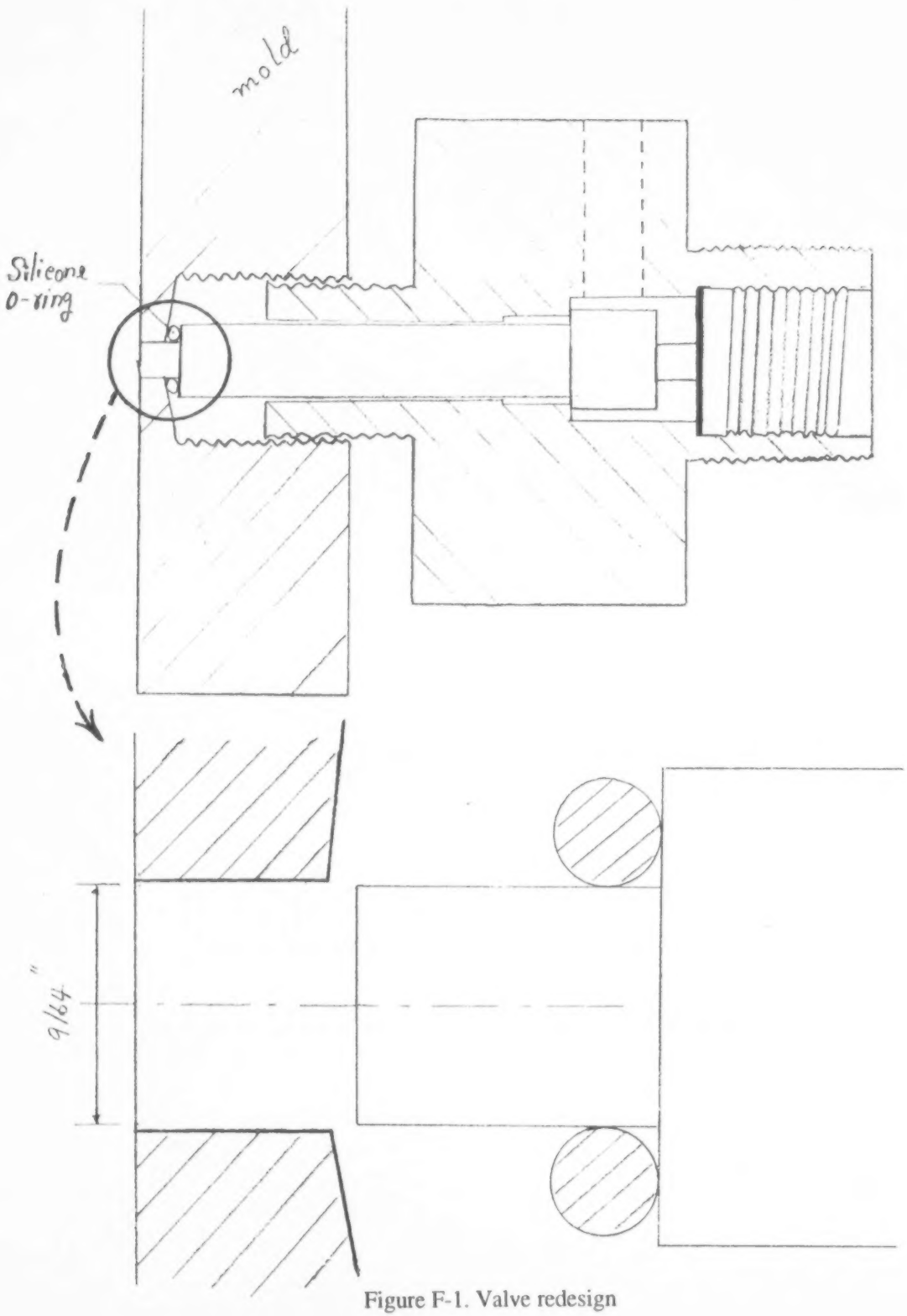

Figure F-1. Valve redesign